Chemical and Biological Oceanographic Conditions on the Scotian Shelf and in the Eastern Gulf of Maine during 2022

Benoit Casault, Lindsay Beazley, Catherine Johnson, Emmanuel Devred, and Erica Head

Fisheries and Oceans Canada
Maritimes Region
Bedford Institute of Oceanography
P.O. Box 1006
Dartmouth, Nova Scotia
B2Y 4A2

2024

Canadian Technical Report of
Fisheries and Aquatic Sciences 3589

Fisheries and Oceans Canada | Pêches et Océans Canada

Canada

Canadian Technical Report of Fisheries and Aquatic Sciences

Technical reports contain scientific and technical information that contributes to existing knowledge but which is not normally appropriate for primary literature. Technical reports are directed primarily toward a worldwide audience and have an international distribution. No restriction is placed on subject matter and the series reflects the broad interests and policies of Fisheries and Oceans Canada, namely, fisheries and aquatic sciences.

Technical reports may be cited as full publications. The correct citation appears above the abstract of each report. Each report is abstracted in the data base *Aquatic Sciences and Fisheries Abstracts*.

Technical reports are produced regionally but are numbered nationally. Requests for individual reports will be filled by the issuing establishment listed on the front cover and title page.

Numbers 1-456 in this series were issued as Technical Reports of the Fisheries Research Board of Canada. Numbers 457-714 were issued as Department of the Environment, Fisheries and Marine Service, Research and Development Directorate Technical Reports. Numbers 715-924 were issued as Department of Fisheries and Environment, Fisheries and Marine Service Technical Reports. The current series name was changed with report number 925.

Rapport technique canadien des sciences halieutiques et aquatiques

Les rapports techniques contiennent des renseignements scientifiques et techniques qui constituent une contribution aux connaissances actuelles, mais qui ne sont pas normalement appropriés pour la publication dans un journal scientifique. Les rapports techniques sont destinés essentiellement à un public international et ils sont distribués à cet échelon. II n'y a aucune restriction quant au sujet; de fait, la série reflète la vaste gamme des intérêts et des politiques de Pêches et Océans Canada, c'est-à-dire les sciences halieutiques et aquatiques.

Les rapports techniques peuvent être cités comme des publications à part entière. Le titre exact figure au-dessus du résumé de chaque rapport. Les rapports techniques sont résumés dans la base de données *Résumés des sciences aquatiques et halieutiques.*

Les rapports techniques sont produits à l'échelon régional, mais numérotés à l'échelon national. Les demandes de rapports seront satisfaites par l'établissement auteur dont le nom figure sur la couverture et la page du titre.

Les numéros 1 à 456 de cette série ont été publiés à titre de Rapports techniques de l'Office des recherches sur les pêcheries du Canada. Les numéros 457 à 714 sont parus à titre de Rapports techniques de la Direction générale de la recherche et du développement, Service des pêches et de la mer, ministère de l'Environnement. Les numéros 715 à 924 ont été publiés à titre de Rapports techniques du Service des pêches et de la mer, ministère des Pêches et de l'Environnement. Le nom actuel de la série a été établi lors de la parution du numéro 925.

Canadian Technical Report of
Fisheries and Aquatic Sciences 3589

2024

CHEMICAL AND BIOLOGICAL OCEANOGRAPHIC CONDITIONS ON THE SCOTIAN SHELF AND IN THE EASTERN GULF OF MAINE DURING 2022

by

Benoit Casault, Lindsay Beazley, Catherine Johnson, Emmanuel Devred, and Erica Head

Fisheries and Oceans Canada
Maritimes Region
Bedford Institute of Oceanography
P.O. Box 1006
Dartmouth, Nova Scotia
B2Y 4A2

© His Majesty the King in Right of Canada, as represented by the Minister of the Department of Fisheries and Oceans, 2024.

Cat. No. Fs 97-6/3589E-PDF ISBN 978-0-660-69867-0 ISSN 1488-5379

Correct citation for this publication:

Casault, B., Beazley, L., Johnson, C., Devred, E., and Head, E. 2024. Chemical and Biological Oceanographic Conditions on the Scotian Shelf and in the Eastern Gulf of Maine during 2022. Can. Tech. Rep. Fish. Aquat. Sci. 3589 : vi + 72 p.

CONTENTS

ABSTRACT

Casault, B., Beazley, L., Johnson, C., Devred, E., and Head, E. 2024. Chemical and Biological Oceanographic Conditions on the Scotian Shelf and in the Eastern Gulf of Maine during 2022. Can. Tech. Rep. Fish. Aquat. Sci. 3589 : vi + 72 p.

Chemical and biological oceanographic conditions observed in the Maritimes Region in 2022 are presented. Surface and deep inventories of nitrate and silicate were near or above normal in the eastern part of the region while the surface and deep phosphate inventories remained near or below normal across the region. Inventories of *in situ* chlorophyll-*a* have indicated important spatial and temporal variability across the region apart from the Bay of Fundy where below-normal levels have been observed since 2014. Abnormally high surface chlorophyll-*a* concentrations measured by remote sensing were observed during winter 2022. Observations in recent years suggest earlier and longer spring phytoplankton blooms with higher-than-normal amplitude and magnitude. Diatom abundance has remained lower than normal in the Bay of Fundy while reaching near-normal levels on the central Scotian Shelf in the last two years. The overall zooplankton biomass and the abundance of *Calanus finmarchicus* and Arctic *Calanus* species remained mainly below normal levels in 2022. Observations from the Continuous Plankton Recorder confirm the main regional trends observed in phyto- and zooplankton abundances. Observations in Bedford Basin in recent years have indicated generally warmer-than-normal conditions, near-normal chlorophyll-*a* concentrations, and mainly near or higher-than-normal bottom nutrient (nitrate, silicate and phosphate) concentrations.

RÉSUMÉ

Casault, B., Beazley, L., Johnson, C., Devred, E., and Head, E. 2024. Chemical and Biological Oceanographic Conditions on the Scotian Shelf and in the Eastern Gulf of Maine during 2022. Can. Tech. Rep. Fish. Aquat. Sci. 3589 : vi + 72 p.

Les conditions océanographiques chimiques et biologiques observées dans la région des Maritimes en 2022 sont présentées. Les inventaires de nitrate et de silicate en surface et en profondeur étaient proches ou supérieurs à la normale dans l'est de la région, tandis que les inventaires de phosphate en surface et en profondeur sont restés proches ou inférieurs à la normale dans toute la région. L'inventaire de chlorophylle-*a in situ* indique une importante variabilité spatiale et temporelle dans la région à l'exception de la baie de Fundy où il est resté inférieur à la normale depuis 2014. Des concentrations anormalement élevées de chlorophylle-*a* en surface mesurées par télédétection ont été enregistrées durant l'hiver 2022. Les observations des années récentes suggèrent des floraisons printanières du phytoplancton plus précoces et plus longues, avec une amplitude et une ampleur supérieures à la normale. L'abondance des diatomées est restée inférieure à la normale dans la baie de Fundy mais a atteint des niveaux normaux sur le plateau néo-écossais central au cours des deux dernières années. La biomasse totale du zooplancton ainsi que l'abondance du *Calanus finmarchicus* et des espèces de *Calanus* arctiques sont demeurées généralement sous des niveaux normaux en 2022. Les observations de l'enregistreur de plancton en continu confirment les principales tendances régionales observées dans les abondances du phyto- et du zooplancton. Les récentes observations recueillies dans le bassin de Bedford indiquent des conditions généralement plus chaudes que la normale, des concentrations de chlorophylle-*a* proches de la normale, et des concentrations de nitrate, silicate et phosphate profonds proches ou supérieures à la normale.

1. INTRODUCTION

The Atlantic Zone Monitoring Program (AZMP) was implemented in 1998 to enhance Fisheries and Oceans Canada's (DFO's) capacity to describe, understand, and forecast the state of the marine ecosystem (Therriault et al. 1998). The AZMP derives its information on the marine environment and ecosystem from data collected at a network of sampling locations (high-frequency sampling stations, cross-shelf sections, and ecosystem trawl surveys) in four DFO regions (Québec, Gulf, Maritimes, and Newfoundland), sampled at a frequency of twice-monthly to once-annually. The sampling design provides fundamental information on the variability in physical, chemical, and biological properties of the Northwest Atlantic continental shelf and slope on seasonal and inter-annual scales. Ecosystem trawl surveys and cross-shelf sections provide information about broad-scale environmental variability (Harrison et al. 2005) but are limited in their seasonal coverage. High-frequency sampling stations complement the broad-scale sampling by providing detailed information on seasonal changes in ocean properties. *In situ* sampling is also complemented by remote sensing of ocean colour measurements providing additional information on the distribution of phytoplankton in the surface layer on a broad spatio-temporal scale. In addition, the North Atlantic Continuous Plankton Recorder (CPR) survey provides monthly sampling along commercial shipping routes between Reykjavik and the New England coast via the Scotian Shelf. The CPR sampling extends a dataset started in 1960, allowing present-day plankton observations to be set within a longer time frame than the AZMP core sampling. Although not considered a core AZMP station, the Compass Buoy station located in the Bedford Basin has been sampled weekly since 1992 and a summary of its environmental and phytoplankton conditions is also presented in this report.

The Scotian Shelf is located in a transition zone influenced by both sub-polar waters, mainly flowing into the region from the Gulf of St. Lawrence and the Newfoundland Shelf, and warmer offshore waters of Gulf Stream origin. The deep-water properties of the western Scotian Shelf exhibit significant shifts in temperature in response to sustained periods of weak and strong large-scale meteorological forcing resulting in changes in the source of deep slope water to the shelf between cold, low-nutrient Labrador slope water, and warm, nutrient-rich Atlantic slope water (Petrie 2007). Temperature and salinity on the Scotian Shelf are also influenced by heat transfer between the atmosphere and ocean, local mixing, precipitation, and, to some extent, runoff from land. Physical changes in the pelagic environment influence both plankton community composition and annual biological production cycles, with implications for energy transfer to higher trophic-level production.

The objective of this report is to provide a description of the nutrient and plankton conditions across the Scotian Shelf and eastern Gulf of Maine in 2022 (2021 for the CPR data) in the context of variability in shelf conditions observed since the beginning of AZMP surveys. It complements assessments for the physical environment of the Maritimes Region (Hebert et al. 2023) and for the state of the Canadian Northwest Atlantic shelf system as a whole (DFO 2023). A set of simple metrics is used to represent important processes related to plankton production cycles and composition. These include surface and subsurface nutrient inventories, representing the availability of nutrients required for phytoplankton production, and surface layer chlorophyll-*a* inventories from *in situ* and remote sensing observations, representing phytoplankton biomass and spring bloom dynamics. Zooplankton metrics include biomass and copepod and non-copepod abundance, representing the overall quantity of zooplankton present, and abundances of taxa or groups that represent dominant species (*Calanus finmarchicus*, *Pseudocalanus* spp.) or biogeographic associations (Arctic copepods, warm offshore copepods, and warm-water shelf copepods). Copepod relative abundance patterns are used to assess community variability at the high-frequency sampling stations.

2. METHODS

Sample collection and processing conform to established standard protocols to the best extent possible (Mitchell et al. 2002). Non-standard measurements or derived variables are described below.

2.1 Missions and Sampling

Sampling was conducted on the spring and fall broad-scale surveys and on the winter and summer ecosystem trawl surveys in 2022, and on day trips to the two high-frequency sampling stations and the Compass Buoy station in Bedford Basin (Table 1, Figures 1-3). A total of 432 hydrographic station occupations were completed with plankton net samples collected at 242 of these stations (Table 1).

2.1.1 High-frequency Sampling Stations

The Halifax-2 (HL2) and Prince-5 (P5) high-frequency sampling stations (Figure 1) were sampled 17 and 11 times, respectively, in 2022.

The standard sampling suite for the high-frequency stations includes the following:

- Conductivity, Temperature, Depth (CTD) profiles with dissolved oxygen, pH (HL2), fluorescence, Photosynthetically Active Radiation (PAR) and turbidity measurements.
- Niskin water bottle samples at standard depths (see Gear Deployment) for nutrients, salinity and oxygen (for CTD data validation), chlorophyll-*a* analyses and phytoplankton enumeration. Accessory phytoplankton pigments are also measured near the surface but are not reported in this document.
- Vertical ring net tows (202-µm mesh net) for zooplankton biomass (wet and dry weights), species/group abundance, and community composition.
- Secchi depth measurement for light attenuation when possible.

2.1.2 Shelf Sections

During the spring and fall seasonal surveys, samples are collected on the four primary sections (Cabot Strait [CSL]; Louisbourg [LL]; Halifax [HL]; Browns Bank [BBL]; Figure 1) and at a number of ancillary sections/stations (black markers in Figure 2). However, results from the ancillary sections/stations are not reported in this document. During the 2022 spring survey, the primary sections were sampled between March 22nd and April 5th, which is nearly two to three weeks earlier than historical sampling time for the sections. Therefore, the estimated annual anomalies for the sections in 2022 presented below should be interpreted with this sampling time difference in mind.

The standard sampling suite for the cross-shelf section stations is the same as for the high-frequency sampling stations listed above, except for phytoplankton enumeration. In addition to the standard suite of analyses performed on water samples, particulate organic carbon is measured at standard depths but not reported in this document.

2.1.3 Ecosystem Trawl Surveys

AZMP-DFO Maritimes Region participated in two primary ecosystem trawl surveys in 2022. The winter survey on Georges Bank (GB) which took place from late March until early April, and the summer survey on the Scotian Shelf and in the eastern Gulf of Maine which took place from early July until early August (Table 1 and Figure 3). The summer survey was shortened due to vessel availability issues, and therefore, there was no sampling performed east of longitude 61°W.

The sampling suite for the ecosystem trawl survey stations includes the measurements listed above for the high-frequency sampling stations, but the standard set of water bottle sampling depths is reduced to four or five depths, and vertical ring net tows (202-µm mesh) are only collected at a subset of stations (Table 1 and Figure 3).

2.2 Gear Deployment

2.2.1 Conductivity, Temperature, Depth and Water Sampling

The CTD is lowered to a target depth within 2 m of the bottom.

Standard depths for water samples include:

- High-frequency sampling stations:
    1. HL2: 1 m, 5 m, 10 m, 20 m, 30 m, 40 m, 50 m, 75 m, 100 m, 140 m
    2. P5: 1 m, 10 m, 25 m, 50 m, 95 m
- Seasonal sections: near-surface, 10 m, 20 m, 30 m, 40 m, 50 m, 60 m, 80 m, 100 m, 250 m, 500 m, 1000 m, 1500 m, 2000 m, near-bottom (depths sampled are limited by bottom depth)
- Ecosystem trawl surveys: 5 m, 25 m, 50 m, 100 m (in water near or deeper than 200 m), and near bottom when possible.

2.2.2 Net Tows

Ring nets of a standard 202-µm mesh are towed vertically from near bottom to surface at a speed of approximately 1 $m \cdot s^{-1}$. In deep offshore waters, the maximum tow depth is 1000 m. Samples are preserved in a 4% solution of buffered formaldehyde and analyzed according to the protocol outlined in Mitchell et al. (2002).

2.3 Derived Metrics

2.3.1 Optical Properties

The optical properties of seawater (attenuation coefficient [K_d], euphotic depth [Z_{eu}]) are derived from *in situ* light attenuation measurements using a rosette-mounted PAR radiometer and Secchi disk, according to the following procedures:

1. The downward vertical attenuation coefficient for PAR ($K_{d\text{-}PAR}$) is estimated as the slope of the linear regression of $\ln(E_d(z))$ as a function of depth z (where $E_d(z)$ is the value of

downward irradiance at depth z) in the depth interval from minimum depth to around 50 m. The minimum depth is typically around 2 m although the calculation is sometimes forced below that target when near-surface PAR measurements appear unreliable.

2. The value of the light attenuation coefficient $K_{d\text{-}Secchi}$ from Secchi disc observations is found using:

$$K_{d\_secchi}\ (m^{-1}) = 1.44 / Z_{sd}$$

where Z_{sd} is the depth (in m) at which the Secchi disc disappears from view (Holmes 1970).

Estimates of the euphotic depth (Z_{eu}), defined as the depth where PAR is 1% of the surface value, are obtained using the following expression (Churilova et al. 2017):

$$Z_{eu}\ (m) = 4.6 / K_d$$

2.3.2 Vertically Integrated Variables

Integrated chlorophyll-*a* and nutrient inventories are calculated over various depth intervals (i.e., 0–100 m for chlorophyll-*a* concentration, and 0–50 m and 50–150 m for nutrients) using trapezoidal numerical integration. When the maximum depth at a given station is shallower than the lower depth limits noted above, the inventories are calculated by setting the lower integration limit to the maximum depth at that station (e.g., 95 m for P5). Data at the surface (0 m) is taken as the closest near-surface sampled value. Data at the lower depth is taken as:

1. the interpolated value when sampling occurs below the lower integration limit; or
2. the closest deep-water sampled value when sampling is shallower than the lower integration limit.

2.3.3 Phytoplankton Taxonomic Groups

Phytoplankton abundance and taxonomic composition at the high-frequency sampling stations are estimated from pooled aliquots of water collected in the upper 100 m (140 m for HL2) of the water column using the Utermöhl technique (Utermöhl 1931).

2.4 Remote Sensing of Ocean Color

Near-surface chlorophyll-*a* concentrations derived from ocean colour data collected by the Moderate Resolution Imaging Spectroradiometer (MODIS) sensor on the Aqua platform are used for the purpose of assembling time series for different sub-regions of the Maritimes Region (HL2, Cabot Strait [CS], Eastern Scotian Shelf [ESS], Central Scotian Shelf [CSS], Western Scotian Shelf [WSS], Lurcher Shoal [LS], Georges Bank [GB]; Figure 4). The MODIS time series extends from July 2002 to present. The POLY4 band-ratio algorithm (Clay et al. 2019) was used to derive the chlorophyll-*a* concentrations from remote sensing reflectance data which were downloaded from NASA's Ocean Color website (accessed on August 1, 2023). This algorithm is based on the O'Reilly et al. (1998) algorithm but with coefficients that were regionally tuned using the AZMP chlorophyll-*a* concentration database (i.e., high performance liquid chromatography [HPLC] inferred chlorophyll-*a* concentrations). The R Shiny app *PhytoFit* (accessed on August 1, 2023) (Clay et al. 2021) was used to download daily chlorophyll-*a* concentrations for the purpose of visualizing the annual cycle, calculating

weekly/monthly/annual means and anomalies, and estimating the parameters of the spring phytoplankton bloom using the shifted-Gaussian function of time model (Zhai et al. 2011). Four metrics are computed to describe the spring bloom characteristics: start date (day of year), cycle duration (days), magnitude (the integral of chlorophyll-*a* concentration under the Gaussian curve), and amplitude (maximum minus the background chlorophyll-*a* concentration).

2.5 Annual Anomaly Scorecards

Scorecards of key indices, based on normalized, seasonally-adjusted annual anomalies, represent changes in physical, chemical, and biological observations in a compact format. Annual estimates of water column inventories of nutrients, chlorophyll-*a,* zooplankton biomass, and the mean abundance of key zooplankton species or groups, at both the high-frequency sampling stations and as an overall average along each of the four standard sections, are based on general linear models of the form:

$$Density = \alpha + \beta_{YEAR} + \delta_{MONTH} + \varepsilon$$ for the high-frequency sampling stations, and

$$Density = \alpha + \beta_{YEAR} + \delta_{STATION} + \gamma_{SEASON} + \varepsilon$$ for the sections.

Density is in units of m^{-2} (or L^{-1} for microplankton abundance), α is the intercept and ε is the error. For the high-frequency sampling stations, β and δ are categorical effects for year and month, respectively. For the sections, β, δ *and* γ take into account the effect of year, station and season, respectively.

This approach is also used to calculate the seasonal estimates of zooplankton indices (i.e., zooplankton biomass and *Calanus finmarchicus* abundance) for the individual sections. In this case, a reduced model including the year and station effects is fitted to the seasonal data subsets.

Density in terms of surface chlorophyll-*a* concentration and *in situ* chlorophyll-*a* inventory is log-transformed [$log_{10}(n)$] to normalize the skewed distribution of the observations. For zooplankton and phytoplankton abundance, one is added to the log-transformed *Density* term [$log_{10}(n+1)$] to include observations for which the value equals zero. Integrated inventories of nutrients and zooplankton biomass are not log-transformed. An estimate of the least-squares means based on Type III Sums of Squares (Lenth et al. 2022) is used as the measure of the overall year effect.

The general linear model approach is also applied to the remote sensing data to calculate annual estimates of near-surface chlorophyll-*a* concentration. In this case, the model is fitted for each selected sub-region (i.e., HL2, CS, ESS, CSS, WSS, LS and GB) using year and day-of-year as categorical variables.

For the ecosystem trawl surveys, seasonal mean indices are calculated as the arithmetic mean of the zooplankton biomass or the log-transformed *C. finmarchicus* abundance data collected within each season/year and each Northwest Atlantic Fisheries Organization (NAFO) area. The reporting of the zooplankton indices based on the NAFO areas for the ecosystem trawl surveys conforms with similar reporting for the physical indices (e.g., DFO 2023) and with most fisheries stock assessment reports.

Annual anomalies are calculated as the deviation of an individual year from the mean of the annual estimates over the period 1999–2020. For the remote sensing surface chlorophyll-*a* concentrations and bloom metrics, a reference period of 2003–2020 is used due to missing data prior to 2003. The annual anomalies are expressed either in absolute units or as normalized quantities (i.e., by dividing by the standard deviation [sd] of the annual estimates over the same period). For the purpose of data interpretation, normalized anomalies are considered near

normal when within ±0.5 sd, slightly above/below normal when between ±0.5 sd and ±1 sd, and above/below normal otherwise (i.e., larger/smaller than ±1 sd).

A standard set of indices representing anomalies of nutrient availability, phytoplankton biomass, and the abundance of dominant zooplankton species and groups (*C. finmarchicus*, *Pseudocalanus* spp., total copepods, and total non-copepods) are produced in each of the AZMP regions, including the Maritimes. To visualize Northwest Atlantic shelf scale patterns of variability, a zonal scorecard including observations from all of the AZMP regions is presented in DFO's Science Advisory Report (DFO 2023).

2.6 Bedford Basin Monitoring Program

The Compass Buoy station has been occupied weekly as part of the Bedford Basin Monitoring Program since 1992 (Li 2014). Regular occupations consist of: i) a CTD cast for the measurement of pressure, temperature, conductivity, salinity, density, dissolved oxygen, pH, fluorescence, and PAR; ii) a vertical net tow for zooplankton identification and enumeration using AZMP protocols; and iii) Niskin bottle water samples collected at 1 m, 5 m, 10 m, and 60 m for the analysis of nutrients, salinity, dissolved oxygen, chlorophyll-*a*, phytoplankton pigments and absorption, particulate organic carbon and nitrogen, total inorganic carbon, total alkalinity, and cell abundance from flow cytometry. The analysis and archival of zooplankton samples in the local database is incomplete and therefore, only the CTD sensor and bottle observations are reported in this summary of 2022 conditions. For ease of interpretation, surface conditions are expressed as the arithmetic mean of data collected at 1 m, 5 m, and 10 m. There is strong seasonal agreement among these depths for the physical and chemical conditions being measured and generally a minor difference in magnitude.

2.7 Continuous Plankton Recorder

The Continuous Plankton Recorder (CPR) is an instrument towed by commercial ships that collects plankton at a depth of approximately 7 m, on a long continuous ribbon of silk (approximately 260-µm mesh). Plankton counting is performed for sections of silk representing 10 nautical miles of tow for which the location of the different sampling stations along the tow route are assigned. CPR data are analyzed to detect differences in the surface indices of phytoplankton (colour and relative numerical abundance of large taxa) and zooplankton (relative abundance) for different months, years, or decades in the Northwest Atlantic. Abundance data are expressed in numbers per sample and each sample represents approximately 3 m^3 of filtered seawater. The indices are used to indicate relative changes in concentration over time (Richardson et al. 2006). The sampling methods from the first surveys in the Northwest Atlantic (1960 for the continental shelf) have remained unchanged to date so that valid inter-annual and inter-decadal comparisons can be made.

The tow routes between Reykjavik and the Gulf of Maine are divided into eight regions: WSS, ESS, the southern Newfoundland Shelf, the Newfoundland Shelf, and four regions in the Northwest Atlantic sub-polar gyre, divided into 5 degrees of longitude bins (Figure 5). Only CPR data collected on the Scotian Shelf since 1992 are reported here, since these provide complementary information to AZMP survey results which date back to 1999 (Head et al. 2022). CPR data collected in all regions and all decades (i.e., including the four regions in the sub-polar gyre east of 45° W) are presented in annual Atlantic Zone Offshore Monitoring Program reports (e.g., Ringuette et al. 2022). In 2021, there was CPR sampling during 11 months on both the WSS and the ESS.

Monthly log-transformed abundances [$log_{10}(n+1)$] of 14 taxa and the Phytoplankton Colour Index (PCI), a semi-quantitative measure of total phytoplankton abundance, are calculated by averaging values for all individual samples collected within either the WSS or ESS region for each month and year sampled. The examined plankton taxa include: diatoms and dinoflagellates (phytoplankton), four groups of *Calanus* species/stages, three representative small copepod taxa, two macrozooplankton taxa, and three acid-sensitive taxa.

Climatological cycles are obtained by averaging monthly averages for 1992–2020 for three indices of phytoplankton abundance and for the *Calanus* I–IV and *C. finmarchicus* V–VI taxa, and these are compared with values in the months sampled in 2021. Annual abundances and their anomalies are calculated for all 14 examined taxa for years during which there are 8 or more months of sampling, with no gaps of 3 or more consecutive months, conditions that were met in both sub-regions in 2021.

3. OBSERVATIONS

3.1 Optical Properties

Oceanic waters are generally classified as Case 1 or Case 2 waters whereas optical properties of Case 1 waters are principally influenced by phytoplankton and related particles, and Case 2 waters are influenced, in addition to phytoplankton, by inorganic particles in suspension and yellow substances (IOCCG, 2000).

The euphotic depth (Z_{eu}) in Case 1 waters (e.g., HL2) is generally deepest during the winter months and after the decline of the spring phytoplankton bloom, and shallowest during the period of the bloom when light attenuation in the water column is maximal (Figure 6). In 2022 at HL2, Z_{eu} estimates based on PAR measurements were near or slightly shallower than normal throughout the year except in December when it was considerably shallower than normal. Secchi depths were only measured for four occupations at HL2 in 2022. The Secchi-based euphotic depth was slightly deeper than normal in September, but subsequently shallower than normal during the fall (Figure 6).

At P5, which is characterized by Case 2 waters, euphotic depths are relatively constant year-round since the primary attenuator is non-living suspended matter due to tidal action and continental freshwater input (Figure 6). In 2022, both the PAR-based and Secchi-based estimates of the euphotic depth were mainly near or shallower than normal at P5 (Figure 6).

3.2 Nutrients

The primary dissolved inorganic nutrients (nitrate, silicate, and phosphate) measured by the AZMP strongly co-vary in space and time (Petrie et al. 1999). For this reason, and because the availability of nitrogen is most often associated with phytoplankton growth limitation in coastal waters of the Maritimes Region (DFO 2000), this report focuses mainly on variability patterns for nitrate, with information on silicate and phosphate concentrations presented to help interpret phytoplankton taxonomic group succession at HL2 and P5.

3.2.1 High-frequency Sampling Stations

At HL2, the highest surface nitrate concentrations are typically observed in the winter when the water column is well mixed and primary production is low (Figure 7). Surface nitrate declines with the onset of the spring phytoplankton bloom, and the lowest surface nitrate concentrations

are observed in spring through early fall. Deep-water nitrate concentrations are lowest in the late fall and early winter, and increase from May to August, perhaps reflecting sinking and decomposition of the spring phytoplankton bloom (Petrie and Yeats 2000).

In 2022, the surface nitrate inventory over the 0-50 m layer at HL2 was near or above normal in spring, mainly below normal in summer, and variable during fall (Figure 8). The below-normal surface inventory during summer was associated with a deeper-than-normal nitrate-depleted layer extending from surface to ca. 40 m during the summer months (Figure 7). Overall, the surface nitrate annual inventory at HL2 was slightly below average in 2022, as mainly observed in the last seven years with the exception of 2021 (Figure 9). On the other hand, the deep nitrate inventory over the 50-150 m layer was near or above normal throughout most of the year with the exception of September when it was below normal (Figure 8). Nitrate concentrations in the bottom layer were particularly higher than normal in late June/early July and in late October (Figure 7 and Figure 8). Overall, the deep nitrate annual inventory at HL2 was above average in 2022 for a second year in a row (Figure 9). For silicate, the surface (slightly below normal) and deep (slightly above normal) annual inventories were similar to those of nitrate (Figure 9). For phosphate, both the surface and deep inventories were below or slightly below normal (Figure 9). There was no sampling at HL2 during winter when surface nitrate is typically highest and deep nitrate typically lowest, which possibly introduces bias in the annual estimates of the nitrate inventories.

The nitrate dynamics at P5 differ considerably from those at HL2 because of nutrient input from outflow of the nearby Saint John River, combined with the strong tidal mixing which contributes to a lower nitrate accumulation in the deep water while maintaining a higher overall surface inventory. The highest nitrate concentrations are observed in the winter and late fall, when the water column is well mixed from surface to bottom and phytoplankton growth is minimal due to light limitation (Figure 7). Nitrate concentrations start to decline in the upper water column when the spring phytoplankton bloom starts in April or May, and the lowest surface nitrate concentrations and corresponding inventory are typically observed from June to September (Figure 7 and Figure 8).

At P5 in 2022, both the surface and deep nitrate inventories were mainly near or below normal throughout the year (Figure 8). Nitrate concentrations were atypically low throughout the water column in February, and surface nitrate concentrations were also below normal during August and September (Figure 7) resulting in lower-than-normal surface inventory in those months (Figure 8). Overall, both the surface and deep nitrate annual inventories at P5 were below or slightly below average in 2022 as observed for the last eight or nine years (Figure 9). In parallel with the nitrate conditions, the surface and deep annual inventories for silicate and phosphate were also near or below normal at P5 in 2022, continuing the pattern of the last ten years (Figure 9).

3.2.2 Broad-scale Surveys

Sampling on the sections in spring indicated low nitrate concentrations in the upper 50 m at all stations of all sections in 2022 (Figure 10a). Despite the near-depleted nitrate conditions in the surface layer, surface nitrate anomalies in spring were positive on Cabot Strait, the shelf stations of the Louisboug section, the Halifax inshore stations (HL1 and HL2), but negative across the Browns Banks section (Figure 10a). Surface nitrate concentrations were also low at all stations of all sections in fall 2022 (Figure 10b). With the exception of CSL where surface anomalies were mainly negative across the section, surface anomalies were spatially variable within and across the other sections (Figure 10b). Overall, the annual inventory of surface nitrate in 2022 was above normal on CSL and LL, near-normal on HL, and below normal on

BBL (Figure 9). The same pattern was observed for the annual surface silicate inventory while surface phosphate was near normal on LL and below normal elsewhere (Figure 9). For CSL, LL and HL, this suggests a recent shift toward near- or above-normal levels of surface nitrate and silicate in the last two to three years despite some spatial and temporal variability observed since 2014 (Figure 9).

Nitrate concentrations in the deep 50-150 m layer were generally higher than in the surface layer in both spring and fall seasons (Figure 10a and Figure 10b). For CSL, positive anomalies were observed in spring on the east side (CSL5 and CSL6; Figure 10a) and across the entire section in fall (Figure 10b). Otherwise, nitrate anomalies in the deep layer were spatially variable within and across the other sections in both seasons (Figure 10a and Figure 10b). Overall, the annual inventory of deep nitrate in 2022 was above normal on CSL and near normal elsewhere (Figure 9). The same pattern was observed for deep silicate while deep phosphate was near normal on CSL and BBL, and slightly below or below normal on LL and HL (Figure 9). For CSL and LL, this again suggests a recent shift toward near- or above-normal levels of deep nitrate and silicate inventories in the last two to four years.

Nitrate concentration profiles collected during the 2022 summer ecosystem trawl survey were used to reconstruct bottom nitrate fields using Barnes interpolation (Kelley and Richards 2022) with parameters tuned for the Scotian Shelf. The method differs from the objective analysis tool used in previous reporting (e.g., Casault et al. 2022) and is consistent with the method used for the reporting of bottom temperature fields (Hebert et al. 2023). The results indicated predominantly higher-than-normal bottom nitrate levels in the outer Bay of Fundy, the eastern Gulf of Maine and part of the western Scotian Shelf, while mixed anomalies were obtained in the central and the eastern Scotian Shelf where sampling was performed (Figure 11). Lower-than-normal bottom nitrate levels were observed in the inner Bay of Fundy, in LaHave and Emerald basins, and on Baccaro, Emerald and Western banks (Figure 11). There was no sampling east of ca. longitude 61°W which prevents a complete description of bottom nitrate at the full scale of the Scotian Shelf.

In a similar manner, oxygen concentration profiles collected during the 2022 summer ecosystem trawl survey were used to reconstruct bottom oxygen saturation fields. The results indicated that the highest saturation levels were observed in the northeast Bay of Fundy and on Emerald and Western banks (Figure 12). Although not included in the interpolation grid, high saturation levels were also observed on eastern Georges Bank. Saturation levels near or below 60% were mainly observed along the Eastern and South shores areas, and Emerald and LaHave basins (Figure 12). Anomalies of bottom oxygen were not calculated due to insufficient quality of oxygen data collected prior to 2015 thus preventing the calculation of a representative climatology.

3.3 Phytoplankton

Although phytoplankton temporal and spatial variability is high in coastal and shelf waters, a recurrent annual pattern is observed across the Scotian Shelf, including a pronounced spring diatom-dominated phytoplankton bloom, that is followed by a small secondary summer-fall bloom. Blooms develop as phytoplankton growth outpaces losses due to grazing, sinking and other processes (Behrenfeld and Boss 2014). Spring bloom initiation is thought to be regulated by the light environment and temperature, starting when the water column stabilizes in late winter and early spring (Sverdrup 1953). Bloom magnitude is thought to be regulated largely by nutrient supply, while bloom duration is regulated by both nutrient supply and, to a lesser extent, by loss processes such as aggregation-sinking, grazing by zooplankton (Johnson et al. 2012), and lysis (Mojica et al. 2016). Phytoplankton biomass is assessed in terms of the integrated chlorophyll-*a* inventory derived from *in situ* measurements and the surface chlorophyll-*a*

concentration derived from remote sensing observations. The two indices are complementary and often present divergent patterns due to differences in the spatial and temporal extent of the signals they capture.

3.3.1 High-frequency Sampling Stations

The start of the spring bloom at HL2 in 2022 could not be inferred from *in situ* observations due to the absence of sampling prior to March 22nd. Both the *in situ* chlorophyll-*a* concentration profiles and the corresponding chlorophyll-*a* inventories (Figure 13) as well as the total phytoplankton abundance (Figure 14) all indicated lower-than-normal biomass/abundance at the time of the first sampling event which could suggest that the peak of the spring bloom had already occurred. However, the large proportion of diatoms observed in March and April could also suggest that the spring bloom occurred at normal time but with a considerably lower-than-normal amplitude (Figure 14). On the other hand, remote sensing measurements indicated increasing surface chlorophyll-*a* concentrations as early as the beginning of February, suggesting an early onset of the spring bloom (Figure 15). However, bloom metrics estimated from the shifted-Gaussian model as calculated using the *PhytoFit* application indicated a delayed onset of the spring bloom with normal amplitude (Figure 15). Overall based on the various observation methods, the 2022 spring bloom dynamics appeared to deviate markedly from the climatological pattern, presenting a challenge for estimating bloom metrics in a comparable manner to past values. Following the spring bloom, the *in situ* chlorophyll-*a* inventory (Figure 13), the total phytoplankton abundance (Figure 14) and the surface chlorophyll-*a* measured by remote sensing (Figure 15) remained near normal until December, when the phytoplankton abundance and the surface chlorophyll-*a* concentrations were above normal while the chlorophyll-*a* inventory was slightly below normal. Overall at HL2, the annual estimate of the three phytoplankton abundance/biomass indices were slightly above or above normal in 2022 (Figure 16) although the indices based on *in situ* observations could possibly be biased due to the absence of sampling prior to and during the spring bloom period when phytoplankton abundance and biomass are highest.

The other HL2 bloom metrics calculated using the *PhytoFit* application indicated a slightly shorter-than-normal duration, normal amplitude, and near-normal magnitude (Figure 15). However, estimates of the duration and magnitude are questionable as they depend strongly on an accurate estimate of the bloom onset. The phytoplankton community was dominated by diatoms during April and May, as is typical, but their relative abundance was slightly lower than normal during the summer and fall months, while that of flagellates was slightly higher than normal over the same period (Figure 14). Overall, the annual abundance of all phytoplankton groups (diatoms, dinoflagellates, ciliates and flagellates) was near or slightly above normal at HL2 in 2022 (Figure 16).

At P5 in 2022, there was no sampling in April and May, which also prevented any description of the onset of the spring bloom based on *in situ* data (Figure 13). Surface chlorophyll-*a* concentrations measured by remote sensing and their derived spring bloom metrics are not presented here as a new chlorophyll-*a* algorithm is being developed for the processing of P5 data to account for the influence of the inherent water properties (e.g., high content of suspended matter) typically encountered in the outer Bay of Fundy.

The *in situ* chlorophyll-*a* inventory at P5 was slightly lower than normal in winter when low chlorophyll-*a* concentrations were observed throughout the water column (Figure 13). Sampling at the end of May captured a higher-than-normal chlorophyll-*a* inventory before chlorophyll-*a* declined to low levels at the next station occupation in mid June, suggesting that the bloom peak likely occurred earlier than usual (Figure 13). Chlorophyll-*a* concentrations near the

surface were lower than normal during summer which translated into a lower-than-normal inventory for that period (Figure 13). The chlorophyll-*a* inventory was back to near-normal values during fall (Figure 13). Overall at P5, the *in situ* chlorophyll-*a* inventory was below normal in 2022 for a fifth consecutive year (Figure 16).

The phytoplankton community at P5 was mostly dominated by diatoms throughout the year with slightly higher-than-normal contribution of ciliates during winter and dinoflagellates during fall (Figure 14). Overall at P5, the total abundance of phytoplankton and that of diatoms were slightly lower than normal in 2022, while the abundance of dinoflagellates and ciliates was higher than normal. For diatoms, dinoflagellates and ciliates, this continues respective trends observed over the last 12 to 14 years (Figure 16). Flagellate abundance was near normal in 2022 and has shown more variability during the last decade (Figure 16).

3.3.2 Broad-scale Surveys

Annual estimates of the integrated *in situ* chlorophyll-*a* inventories during the seasonal surveys indicated above-normal levels on CSL and BBL, near-normal level on HL, and slightly lower-than-normal level on LL in 2022 (Figure 17). The time series of the *in situ* chlorophyll-*a* inventory annual anomalies indicates considerable short-term variability (ca. one to three years) within each section, as well as important spatial variability within specific years (Figure 17).

Annual estimates of surface chlorophyll-*a* concentrations measured by remote sensing were higher than normal across the region with the exception of GB where it was normal (Figure 17). Record-high levels were reached for the shelf sub-regions (ESS, CSS and WSS) and for LS (Figure 17). With the exception of GB, surface chlorophyll-*a* levels have remained mainly above normal for the last three to four years (Figure 17).

Contradictory patterns between the *in situ* integrated chlorophyll-*a* inventory and the remotely sensed surface chlorophyll-*a* concentrations such as those observed in 2022 for LL and ESS or HL and CSS (Figure 17) are not uncommon. They are due in part to the inherent differences between the two indices, including the vertical extent of the signal they capture (i.e., surface vs. water column integrated), the temporal resolution of the observations (i.e., daily vs. semi-annual), and the spatial extent they represent (i.e., averaging over sub-regions vs. section means).

The remote sensing mean weekly surface chlorophyll-*a* concentrations for 2022 indicated evidence of relatively intense spring bloom conditions for most sub-areas of the region with the exception of ESS and GB (Figure 18a and Figure 18b). Peak surface concentrations during spring were much higher than their corresponding climatological values for the sub-regions CS, CSS, WSS and LS, which translated into positive anomalies of the bloom amplitude and magnitude (except for magnitude for CS) for these sub-regions (Figure 19). Following the spring bloom, surface chlorophyll-*a* concentrations remained consistently near normal from late-spring and through the summer in all sub-regions with GB showing the most variability (Figure 18b and Figure 18b). During fall, surface chlorophyll-*a* concentrations were higher than normal and indicative of fall bloom conditions in the CS, ESS, LS and GB sub-regions, with CS and GB displaying the largest amplitude of the fall bloom (Figure 18a and Figure 18b). Spring bloom metrics derived from the remote sensing chlorophyll-*a* observations indicated later-than-normal initiation for CS, ESS and GB, and considerably earlier-than-normal bloom initiation for CSS, WSS and LS (Figure 19). Spring bloom duration was shorter than normal on CS and ESS, and slightly longer or longer than normal elsewhere (Figure 19).

For the CS sub-region in 2022, the bloom initiation derived from the shifted-Gaussian model appears doubtful due to the lack of surface chlorophyll-*a* concentrations from mid-March until

mid-April (Figure 18a), with consequences on the associated duration and magnitude. In general, inaccurate predictions of the timing of the spring bloom in one or multiple years can introduce important bias in the anomalies of the initiation, duration and magnitude for a given sub-region.

3.4 Zooplankton

Zooplankton include a broad variety of small animals (ca. 0.2 to 20 mm in length) that feed primarily on phytoplankton and hence, are a critical link between primary producers and larger organisms. Zooplankton includes copepods, which are the most abundant zooplankton organisms in the Northwest Atlantic, and the less abundant non-copepods which consist mostly of larval stages of benthic invertebrates, carnivorous groups that feed on other zooplankton, and small-particle feeders. *Calanus finmarchicus* is a large, energy-rich, and broadly distributed copepod species across the region and represents an important prey for planktivorous consumers such as herring and mackerel, North Atlantic right whales, and other pelagic species. *Pseudocalanus* spp. are smaller and less energy-rich than *Calanus* spp, but they are also important prey for small fish due to their high abundance and wide spatial distribution. Zooplankton is primarily assessed here in terms of the abundance of copepods, non-copepods, *C. finmarchicus* and *Pseudocalanus* spp., and biomass of the mesozooplankton size class (i.e., in the range of 0.2 to 10 mm).

3.4.1 High-frequency Sampling Stations

At HL2, the total abundance of zooplankton is lowest in January and February, and increases to maximum values in April, similar to the spring phytoplankton bloom peak timing, before declining to low levels again in the fall (Figure 20). In 2022, the total zooplankton abundance was slightly below normal in early spring, near normal in late spring, well below normal during the summer, and normal or slightly below normal during fall (Figure 20). The zooplankton community at HL2 was dominated by copepods, similar to climatological conditions, with copepods representing roughly 90% or more of the total zooplankton abundance throughout the year (Figure 20). Overall at HL2, the annual mean abundances of copepods and non-copepods in 2022 were below and slightly below normal, respectively (Figure 21).

At P5, the total abundance of zooplankton is typically lowest from January through May and increases to maximum values between July and October, lagging the increase in phytoplankton by about a month, before declining to low levels again in the late fall (Figure 20). In 2022, zooplankton abundance was low but normal during winter, and variable during summer and fall with a transient peak abundance observed in November (Figure 20). Copepods also represented a large proportion of 80% or more of the total zooplankton abundance at P5 (Figure 20). In July, a larger-than-normal proportion of appendicularians and a lower-than-normal proportion of bivalves were observed (Figure 20). Overall at P5, the annual mean abundance of copepods was above average and that of non-copepods was normal in 2022 (Figure 21).

Because copepods generally dominate the local zooplankton community at both stations, their seasonal abundance pattern closely follows that of total zooplankton abundance (Figure 20, Figure 22a and Figure 22b). Therefore, total copepod abundance at HL2 in 2022 was slightly below normal in early spring, near normal in late spring, well below normal during the summer, and normal or slightly below normal during fall (Figure 22a). Among the eleven most abundant copepod taxa, nearly all were below normal in abundance, with the exception of *Microcalanus* sp. and *Paracalanus* sp. (Figure 23). Record-low anomalies were recorded for *Metridia lucens*, *C. hyperboreus* and *M. longa* (Figure 23). The dominant copepods *Oithona similis*, *C. finmarchicus* and *Pseudocalanus* spp. represented a combined proportion of roughly 60% of the

total copepod abundance from late March until September with the relative contribution of *C. finmarchicus* slightly higher than normal during July and August (Figure 22a). During the fall, the copepod community was mostly composed of the species *O. similis*, *Centropages* spp., and *Paracalanus* sp. (Figure 22a).

At P5, the total copepod abundance in 2022 was low during the winter, and variable during summer and fall with a transient peak abundance observed in November (Figure 22b). Annual average abundance anomalies of the top nine copepod taxa were mixed, with slightly positive anomalies for the three most abundant taxa, *Oithona similis*, *Pseudocalanus* sp., and *Centropages* sp., and negative anomalies for the next three most abundant taxa, *C. finmarchicus*, *Acartia* spp., and *Temora longicornis* (Figure 23). Copepod community composition was variable and diverged substantially from climatological conditions at times in 2022. The relative abundance of *O. similis* was particularly high in winter and late fall, when total copepod abundance was low (Figure. 22b). Relative abundance of *Pseudocalanus* spp. was above normal in July but low in much of the rest of the year, while *Centropages* sp. relative abundance was unusually high from August until December (Figure 22b). The relative abundance of *C. finmarchicus* was lower than normal in all sampled months (Figure 22b). *Acartia* spp. relative abundance was unusually high during February, when total copepod abundance was low, but nearly absent thereafter (Figure 22b)

The abundance of *C. finmarchicus* at HL2 in 2022 was near or lower than normal throughout the year except in early-May and early-July (Figure 24). The first generation of *C. finmarchicus*, characterized by a higher abundance of early stages, appeared to have peaked at the normal time in April/May, and a second generation, albeit with low abundance, developed later in late-July/early-August (Figure 24). The *C. finmarchicus* population during fall was dominated by stage CV with a transient peak of CIV in mid-October, and early stages (CI–CII) were absent from early-September until December (Figure 24). Overall at HL2, the abundance of *C. finmarchicus* was slightly lower than normal in 2022, continuing a 12-year period of mainly near- or below-normal abundances (Figure 21 and Figure 23).

At P5, the abundance of *C. finmarchicus* in 2022 was particularly low during winter and composed exclusively of stages CV and CVI, with a complete absence in the sample collected in February (Figure 24). The highest *C. finmarchicus* abundances were observed at the normal time in late-May/mid-June, and abundances returned to low levels from July to December (Figure 24). The *C. finmarchicus* population during early summer was dominated by the early stages CI–CIV, and by stage CV during late summer and fall (Figure 24). Overall at P5, the abundance of *C. finmarchicus* was below normal in 2022 and continuing an 8-year sequence of mainly near- or below-normal abundances (Figure 21 and Figure 23).

Zooplankton biomass typically peaks around April-May at HL2 and around August-September at P5 (Figure 25). There is strong similarity in the annual variability pattern of dry and wet biomass at both the HL2 and P5 stations (Figure 25). The dry biomass estimates are a close representation of the mesozooplankton size class (i.e. 0.202 mm to 10 mm) while the wet biomass estimates can represent both mesozooplankton and microzooplankton (i.e. larger than 0.202 mm), including gelatinous plankton. In 2022, mesozooplankton dry biomass at HL2 was mainly near or lower than normal throughout the year with the exception of the early-July and early-October sampling events (Figure 25). The spring peak of zooplankton biomass was observed in early May and reached its normal level, but overall zooplankton dry biomass was slightly below normal at HL2 during 2022 (Figure 21). At P5, mesozooplankton dry biomass was low during winter and variable around normal levels during summer and fall with above normal biomass in October (Figure 25). Overall, the annual mean mesozooplankton dry biomass was slightly above normal at P5 in 2022 (Figure 21) owing in part to the above-normal biomass observed in October (Figure 25).

3.4.2 Broad-scale Surveys

The abundance of *C. finmarchicus* and mesozooplankton dry biomass during the 2022 winter ecosystem trawl survey in area 5Ze were both near normal (Figure 26 and Figure 27). However, those averages were based on only six samples which were all collected in the northeast part of area 5Ze (Figure 26 and Figure 27). The abundance of *C. finmarchicus* during the 2022 summer ecosystem trawl survey was near normal in area 4W and below normal in area 4X (Figure 26) while the mesozooplankton biomass was below normal in both areas (Figure 27). The summer seasonal means for area 4W were also based on only six samples collected on the western side of the area and fewer than normally sampled (Figure 26 and Figure 27). Estimates for area 4V were not available due to the absence of sampling in that area.

The abundance of *C. finmarchicus* during the 2022 seasonal surveys was slightly below or below normal during spring, and mainly near or below normal during fall (Figure 28). The annual estimates of *C. finmarchicus* abundance were near (CSL and BBL) or below (LL and HL) normal in 2022, with HL reporting a record-low anomaly value (Figure 21). The mesozooplankton dry biomass was below normal on all sections during spring 2022, and slightly below or below normal during fall (Figure 29). Consequently, the annual estimates of mesozooplankton biomass were below normal for all sections in 2022 (Figure 21).

On the core sections, the annual abundance of *Pseudocalanus* spp. in 2022 was slightly below or near normal in 2022 with anomalies gradually increasing from negative values in the east (CSL) to positive values in the west (BBL) (Figure 21). For BBL, this represents a 5-year sequence of near- or above-normal abundances of *Pseudocalanus* spp. Total copepod abundance was near normal or below normal for each section in 2022 (Figure 21). For CSL, this represents an 8-year sequence of near- or below-normal abundances whereas for BBL, total copepod abundance has been near or above normal in the last four years (Figure 21).

The abundance of non-copepods in 2022 was above normal for CSL but near normal for the other sections (Figure 21). Except for ostracods, the abundance of non-copepod groups was either near normal, or slightly above or slightly below normal (Figure 30). Apart from ostracods, which have been nearly absent since 2016, there is considerable inter-annual variability during recent years within the other non-copepod groups such that trends in their abundances are not apparent (Figure 30).

3.4.3 Indicator Species

The Arctic *Calanus* species (*Calanus hyperboreus* and *Calanus glacialis*) were less abundant than normal across the region in 2022, consistent with the general pattern observed since 2012 (Figure 31). Record-low abundances of Arctic *Calanus* were observed on the LL and BBL sections, and at HL2 (Figure 31). With the exception of CSL, the abundances of warm offshore species (*Clausocalanus* spp., *Mecynocera clausi*, and *Pleuromamma borealis*) were near or slightly above normal in 2022 (Figure 31). For CSL, a time series record-low anomaly of those species was registered in 2022. By contrast, the abundances of warm-shelf copepod species (the summer-fall copepods *Paracalanus* sp. and *Centropages typicus*) were near or above normal across the region in 2022 and similar to 2021 (Figure 31). The abundances of warm offshore and shelf species have shown considerable spatial and temporal variability across the region during the last decade.

3.5 Bedford Basin Monitoring Program

The Bedford Basin Monitoring Program (BBMP) was fully operational during 2022, and the Compass Buoy station was sampled on a total of 48 occasions (Table 1). Sampling was

cancelled on four occasions due either to the unavailability of science staff from conflicts with other surveys, inclement weather, or from the impacts of hurricane Fiona in September 2022 and loss of power at the Bedford Institute of Oceanography.

3.5.1 Physical Conditions

Annual sea surface temperature (SST) in Bedford Basin in 2022 was above normal (+1.23 sd; Figure 32) compared to the 1999-2020 reference period, marking a continuation of the above-normal conditions in sea surface temperatures noted in 2021. Monthly anomalies in SST in 2022 (Figure 33) were either slightly above or above normal for all months of the year with the exception of December, when SST reverted to normal conditions (+0.06 sd). The month of September showed the second-highest SST anomaly (+2.60 sd) recorded since the start of the time series in 1992 (Figure 33).

Annual average bottom temperature (60 m) was also above normal in 2022 (+1.12 sd; Figure 34). Similar to SST, monthly bottom temperature anomalies were all slightly above or above normal across the year (Figure 35) and reached a maximum during the month of December with an anomaly value of +2.61 sd. This represents the highest anomaly in bottom temperature observed in December in Bedford Basin since 2012, a record year for anomalously warm ocean temperatures across the Scotian Shelf and Gulf of Maine (Hebert et al. 2013), and when the highest anomaly (+2.75 sd) in bottom temperature was observed in Bedford Basin during the month of September (Figure 35).

Monthly bottom salinities (Figure 36) were negative for the entirety of 2022 with the exception of December, when salinities suddenly increased to above normal conditions (+1.43 sd). This coincided with the sudden increase in bottom temperature, suggesting the occurrence of an intrusion event of warm saline waters of shelf origin. Section plots of temperature, salinity, and density and their anomalies relative to the 1999-2020 reference period (Figure 37) showed the presence of anomalously-high temperatures and salinities in the bottom 40 m during the month of December relative to November, which also supports the occurrence of an intrusion event. These events are typical of the fall season and are responsible for discrete, episodic replenishment of bottom oxygen levels in Bedford Basin (Platt et al. 1972; Petrie et al. 1987; Rakshit et al. 2023).

3.5.2 Nutrients and Plankton Conditions

Surface nitrate, phosphate, and silicate were near normal while surface nitrite and ammonium were slightly below normal in 2022 (Figure 32). At the bottom, nitrate, ammonium and silicate were near normal while phosphate and nitrite were slightly above and slightly below normal, respectively (Figure 34). During the month of December when the shelf-water intrusion event occurred, monthly anomalies in bottom nitrate (Figure 38), phosphate, silicate, and ammonium (figures not shown) all decreased compared to November, while bottom nitrite (not shown) showed no change between November and December. In contrast, December anomalies for surface nitrate, phosphate, and silicate increased to above-normal values (figures not shown).

Annual anomalies in surface and bottom chlorophyll, particulate organic carbon (POC) and nitrogen (PON) were near normal but negative in 2022 (Figure 32 and Figure 34). Similarly, metrics describing the phytoplankton community (e.g., HPLC and plankton pigments) at the surface and the bottom were all near normal in 2022 (Figure 32 and Figure 34).

3.6 Continuous Plankton Recorder

Observations of the abundance of a variety of planktonic taxa are made at monthly intervals in the near surface layer (0–10 m) on the Scotian Shelf by means of the Continuous Plankton Recorder (CPR). However, data are only available with a year's lag compared with AZMP observations so that reporting in this section is for 2021.

3.6.1 Phytoplankton

Average monthly values of the phytoplankton colour index (PCI) and diatom abundances (1992–2020) on the ESS and WSS show the spring bloom occurring in March–April, with low values in summer (Figure 39). In fall and winter, the PCI is low, but diatom abundance increases over the fall, remaining relatively high in winter. Dinoflagellate abundance indicates a slight increase following the peak in diatom abundance and remains relatively stable for the remainder of the year. In 2021, PCI values were generally close to normal, although higher than normal in April on the ESS (Figure 39). For the WSS, the PCI appeared to have peaked earlier than normal in March (Figure 39). Monthly diatom abundances were generally close to normal in both sub-regions, but below normal in December on the WSS and in May and September on the ESS, and above normal in November on the ESS (Figure 39). Monthly dinoflagellate abundances were slightly below or below normal during the first half of the year on the WSS, and near normal during the second half although absent in December (Figure 39). On the ESS, dinoflagellates were absent in March and December, less abundant than normal in August, and otherwise close to normal levels (Figure 39).

Annual mean PCI was above or slightly above normal in ESS and WSS, respectively, while diatom abundance was near normal and dinoflagellates abundance was below normal in both regions in 2021 (Figure 40). Annual diatom abundance has been mainly near or below normal since the early- to mid-2000's similar to the trend observed from *in situ* samples collected at HL2 and P5. PCI has been consistently near or above normal since 2016 on the ESS but more variable on the WSS over the same period (Figure 40). In contrast, dinoflagellate abundance has been consistently near or below normal on the WSS since 2016 but variable on the ESS over the same period (Figure 40).

3.6.2 Zooplankton

CPR-derived climatological (1992–2020) seasonal cycles for *Calanus* I–IV (mostly *C. finmarchicus*) and *C. finmarchicus* CV–VI have broad spring–summer (April–July) peaks in abundance on the WSS (Figure 41). On the ESS, *Calanus* CI–IV abundance has a similar, lower magnitude peak, but *C. finmarchicus* CV–VI does not. On the WSS in 2021, monthly abundances for *Calanus* I–IV were mainly near normal throughout the year with the exception of April when it was below normal, while abundances of *C. finmarchicus* V–VI were near or slightly above normal during the winter, and mainly near or slightly below normal for the rest of the year (Figure 41). On the ESS, *Calanus* I–IV abundances were mainly near or below normal throughout the year with the exception of higher or slightly higher-than-normal levels in January and June (Figure 41). Monthly abundances of *C. finmarchicus* V–VI followed a temporal pattern similar to *Calanus* I–IV while remaining with ±1 sd throughout the year (Figure 41). Both *Calanus* I–IV and *C. finmarchicus* V–VI were absent in August in both the WSS and the ESS (Figure 41).

On the WSS, the annual abundance anomaly for *Calanus* I–IV in 2021 was slightly negative and negative for *C. finmarchicus* V–VI and continuing the pattern of mainly negative anomalies since 2016. On the ESS, the anomaly was near normal but weakly positive for *Calanus* I–IV and weakly negative for *C. finmarchicus* V–VI (Figure 40). The annual abundances of the Arctic *Calanus* taxa (*C. glacialis*, *C. hyperboreus*) were slightly below normal in both Scotian Shelf

sub-regions in 2021, which is consistent with net samples collected across the region in 2021 (Figure 40 and Figure 31). The abundances of the three small copepod taxa (copepod nauplii, *Para/Pseudocalanus*, *Oithona* spp.) were also near or slightly below normal in both sub-regions in 2021 (Figure 40). The abundances of each of the two large taxa (euphausiids, hyperiid amphipods) was below normal on the WSS in 2021 but above normal for euphausiids and below normal for hyperiids on the ESS (Figure 40). For the hyperiid amphipods, this breaks a sequence of mainly positive anomalies observed since 2012-13 in both sub-regions, while for euphausiids, this extends a sequence of mainly positive anomalies since 2017 on the ESS and negative anomalies since 2010 on the WSS (Figure 40).

3.6.3 Acid-Sensitive Organisms

In 2021, the abundances of all three acid-sensitive taxa (coccolithophores, foraminifera, *Limacina* spp.) were near or slightly below normal on the WSS. On the ESS, the abundances were slightly below normal for coccolithophores, slightly above normal for foraminifera, and above normal for *Limacina* spp. (Figure 40).

4. DISCUSSION

In the Maritimes Region, the Scotian Shelf (SS) is characterized by a strong annual cycle of temperature and stratification, and spatial variability in the form of longitudinal and cross-shelf gradients. While the temperature annual cycle and its perturbations are mostly driven by meteorological forcing, spatial gradients are mostly the result of the varying contributions of the dominant source water originating from the Gulf of St. Lawrence, the Labrador Current and the Gulf Stream. The interaction between the Labrador Current and the Gulf Stream at the tail of the Grand Banks is particularly relevant in this context as it leads to the creation of anomalous warm/salty (or cold/fresh) eddies that travel east-to-west along the shelf-break (Brickman et al. 2018) having direct impacts on the spatial variability of temperature and salinity. In addition, the complex bathymetry of the SS contributes to local circulation patterns, which combined with the temporal and spatial hydrographic patterns, have direct and indirect influences on the distribution and dynamics of plankton and nutrients in the region.

Ocean temperatures on the SS and in the eastern GoM have exhibited strong inter-decadal variability since the 1950s, with recent years (2010 and onward) being generally warmer than the long-term averages. A composite index of several *in situ* ocean temperature time series from surface to bottom indicated warmer-than-normal conditions across most of the region in 2022, with record-high temperatures observed at multiple locations on the SS and in the eastern GoM (Figure 52 in Hebert et al. 2023). The warmer subsurface conditions observed over the period 2010-2020 are associated with an increased contribution of Gulf Stream source water being advected onto the shelf as suggested by Lehmann et al. (2023). Although slightly lower than normal in 2022, stratification on the SS was consistent with the general increasing trend resulting from the combined warming and freshening of surface waters (Hebert et al. 2023). The combination of warmer ocean temperatures and increased stratification observed in recent years may be directly or indirectly linked to changes observed in the nutrient and lower trophic level conditions presented in this report.

The nutrient environment on the SS is influenced directly or indirectly by water inputs from upstream, for example, the Labrador Current and the outflow from the Gulf of St. Lawrence, as well as by intrusions of nutrient-rich slope water and Gulf Stream meanders (Pepin et al. 2013). The major advective source of nitrate and silicate for the Scotian Shelf is the Gulf of St. Lawrence outflow during winter, while the contribution of on-shelf transport during summer can

be almost as strong in some areas (Petrie and Yeats, 2000). Surface nutrients display strong seasonality linked to phytoplankton production, with surface nutrient depletion typically associated with high production during spring and summer, followed by surface nutrient replenishment during late fall and winter when phytoplankton production is low and vertical mixing is high. On the other hand, deep nutrients, especially nitrate, provide a better representation of the nutrient pool available for new primary production. In addition to changes in shelf circulation, deep nitrate concentrations are also dependent on changes in the export of surface particulate nitrogen and its remineralisation at depth, and on the vertical transport toward the surface via mixing and/or upwelling. Nutrient-poor subsurface conditions on the SS have been reported over the period 2010-2020 despite evidence of Gulf Stream dominated water source (Lehmann et al. 2023). The general pattern of below-normal deep nutrient levels observed on LL, CSL and BBL between ~2015 and 2020 (Figure 9) is consistent with the corresponding decreasing trend observed at the scale of the ESS, CSS and WSS, respectively (Figure 4 in Lehmann et al. 2023). However, near or above-normal levels of deep nitrate and silicate observed on LL and HL in 2021 and 2022 appear to be linked to corresponding positive anomalies observed in the central Gulf of St. Lawrence and Cabot Strait area (Blais et al. 2023). This recent change in nutrient conditions in the central and eastern SS and upstream in the central Gulf and Cabot Strait area could be temporary but could also be indicative of a shift in the source water advected onto the SS. Although the deep nutrient inventories were near or above normal in 2021 and 2022, the general pattern of lower-than-normal levels observed in the recent period coupled with the increase in stratification observed on the SS (Hebert et al. 2023) could imply lower primary productivity, with potential impacts on the structure and functioning of the food web.

In ocean regions where annual-scale environmental variability is a dominant frequency, plankton life history, behavior, and physiology provide adaptations that focus reproductive effort on favorable times of year and minimize exposure to risk at unfavorable times of year. However, unpredictable perturbations in the range of environmental seasonality and in seasonal timing can disrupt these adaptations (Greenan et al. 2008, Mackas et al. 2012). Large-scale shifts in water mass boundaries also influence local plankton community composition (e.g., Keister et al. 2011). The main recurring feature of the phytoplankton dynamics on the SS and in the GoM is the spring bloom, which generally develops under favourable conditions of increased insolation, warming water temperatures, and water column stratification. However, Ross et al. (2017) observed spring blooms on the SS when stratification was at its lowest, water temperature at its coldest, and when the surface mixed layer was still much deeper than the euphotic depth, in apparent contradiction with the critical-depth hypothesis. Similar observations of phytoplankton blooms in the absence of vertical stratification have also been reported in the GoM (Townsend et al. 1992). Remote sensing observations revealed an unusual pattern of winter phytoplankton biomass on the Scotian Shelf in 2022. Abnormally large anomalies of surface chlorophyll-*a* were recorded during the month of February in sub-regions of the Scotian Shelf and on Lurcher Shoal (Figure A.1). At the same time, sea surface temperatures across the region were +2 to +3 sd higher than normal across the region in February 2022 (Figure A.2). Temperature affects phytoplankton growth following an exponential relationship (Eppley 1972). However, temperature effects are not solely responsible for controlling the seasonal evolution of phytoplankton populations since nutrient supply, light history, and other ecosystem-linked processes (e.g. grazing) all play prominent roles (Moisan et al. 2002). The premature surge in phytoplankton biomass observed in February across the shelf in 2022 occurred when zooplankton biomass is typically lowest and hence during a period of low grazing pressure. The early increase in phytoplankton bimass could also possibly be linked to intermittent events of mixed layer restratification, typically associated with sufficiently long periods, at timescales of

days, of reduced surface wind and cooling, allowing phytoplankton growth before the vernal restratification (Lacour et al. 2017).

The period of 2011 to present has been characterized by a persistent change in the zooplankton assemblage on the SS, marked most notably by the decline in the abundance of *C. finmarchicus*, the biomass-dominant member of the zooplankton assemblage, and an associated decline in mesozooplankton biomass. The year 2011 marked a regime shift to lower biomass of *Calanus* spp. on the SS which also coincided with a shift to warmer temperatures (Sorochan et al. 2019). The winter abundance level of *C. finmarchicus* is an indicator of initial conditions for production, while the late-fall abundance level is an indicator of the overwintering stock for production in the following year. Low winter abundances of *C. finmarchicus* at the time series stations in recent years suggest that initial conditions for production have been poor. This may reflect both lower abundances of *C. finmarchicus* entering diapause, indicated by low abundance in fall, and increased mortality during diapause in warmer than average deep waters. The decline in *C. finmarchicus* abundance is particularly significant because copepods of the genus *Calanus* are an important food source for the endangered North Atlantic right whale (Pershing and Stamieszkin 2020), and the decline in *C. finmarchicus* abundance observed in the last decade has been linked to changes in the foraging environment and habitat use of right whales (Meyer-Gutbrod et al. 2021). During the same period, CPR and *in situ* observations also suggest changes in the phytoplankton community characterized by a higher abundance of smaller taxa to the detriment of the larger diatoms with possible effects on the zooplankton assemblage.

While warmer temperatures are typically associated with a smaller average sized copepod community (Campbell et al. 2021), the abundance of nearly all major copepod taxa were lower than average at HL2 in 2022, with the exception of *Pseudocalanus* spp., *Microcalanus* sp., and *Paracalanus* sp. However, at P5, the three most abundant small copepod species were more abundant than normal in 2022, more consistent with a shift in average copepod size. Along with the overall decline in the abundance of *C. finmarchicus* and zooplankton biomass, continued lower-than-normal abundances of Arctic *Calanus* species and higher-than-normal abundances of warm shelf species are consistent with expected responses to the warm temperatures observed on the SS in 2022. After a period from 2012 to 2019 during which warm offshore copepod species were mainly higher than normal on the shelf, in 2020 to 2022 their abundance anomalies have been more variable around normal values, suggesting that *in situ* warming on the shelf may have a greater influence on the zooplankton community in the last three years than on-shelf transport of warm water.

The year 2022 was marked with the passage of hurricane Fiona, which made landfall in eastern Nova Scotia on September 24 bringing high winds and heavy rainfall along much of the coast. The physical effects of hurricanes include deepening of the mixed layer and decreasing of the sea surface temperature, together with increasing surface chlorophyll concentrations within the cool wakes of the hurricanes, apparently in response to the injection of nutrients and/or biogenic pigments near the surface (Babin et al. 2004). CTD casts collected in Bedford Basin prior and after the passage of Fiona indicated cooling and freshening of surface water (Figure A.3) possibly as a result, among other processes, of strong wind-induced vertical mixing and higher-than-normal freshwater outflow of the nearby Sackville river. A similar but weaker pattern in the surface conditions was also observed at HL2 although profiles were more distant in time (Figure A.3). In terms of chemical and biological conditions, the impacts of hurricane Fiona were rather unclear from *in situ* sampling alone. However, remote sensing observations indicated a transient increase in surface chlorophyll-*a* in late September in the eastern Scotian Shelf sub-region (Figure 18a) possibly in response to the passage of the hurricane.

The relationships among environmental and plankton conditions are complex and their interpretation from a deterministic perspective requires a comprehensive analysis that is beyond the scope of this report. However, observations in recent years provide increasing evidence of warmer ocean conditions and changes in deep-nutrient availability, coupled with a shift in both phytoplankton and zooplankton communities away from the dominance of large phytoplankton cells and large, energy-rich copepods like *C. finmarchicus* toward smaller phytoplankton and copepod species. Since "classical" food webs, dominated by diatoms and *C. finmarchicus,* are associated with more efficient transfer of energy to higher trophic level pelagic animals than are food webs dominated by small phytoplankton cells and small zooplankton taxa, this shift may indicate a change to less-productive conditions for planktivorous fish, North Atlantic Right Whales, and planktivorous or piscivorous seabirds in the Maritimes Region.

5. SUMMARY

- In 2022, the surface nitrate inventory was above normal in the ESS (CSL and LL), near or slightly below normal in the CSS (HL and HL2), and below normal in the WSS and outer Bay of Fundy (BBL and P5). A similar spatial pattern was observed for surface silicate while surface phosphate was mainly below normal across the region.
- The deep nitrate inventory in 2022 was near or above normal across the region with the exception of P5. Deep silicate was above normal on CSL and at HL2 and near normal elsewhere while deep phosphate was mainly near or below normal across the region.
- The inventory of chlorophyll-*a* over the 0–100 m layer was variable across the region in 2022 with slightly above or above normal levels on CSL, BBL and at HL2, and near or below normal levels on LL, HL and at P5. For HL2 and P5, the annual estimates could be biased due to the absence of sampling during the spring period. On the other hand, with the exception of GB, surface chlorophyll-*a* as measured by remote sensing was higher than normal across the region with time series record-high values observed for ESS, CSS, WSS, LS and at HL2.
- Remote sensing observations indicated that the spring phytoplankton bloom was later, shorter, and had a near or lower than normal magnitude for the CS, ESS and GB sub-regions in 2022. In contrast, in the CSS, WSS and LS sub-regions the spring bloom was earlier, longer and with higher than normal amplitude and magnitude in 2022, with time series extreme values for the initiation and magnitude for those sub-regions. At HL2 and P5, the spring bloom could not be accurately described from *in situ* measurements due to the absence of sampling during the spring period.
- Observations at HL2 indicated near- or slightly-above-normal abundance of diatoms, dinoflagellates, flagellates and ciliates in 2022. At P5, the pattern of lower-than-normal abundance of diatoms and higher-than-normal abundance of dinoflagellates and ciliates continued as in the last 12–14 years. Overall, the total abundance of phytoplankton was slightly above normal at HL2 and slightly below normal at P5 in 2022, and consistent with the phytoplankton biomass (i.e., the chlorophyll-*a* inventory) observed at each station.
- In 2022, the abundance of *C. finmarchicus* was mainly near or lower than normal across the region, with a record-low value observed for HL. *Pseudocalanus* spp. and total copepod abundances were mainly near or below normal in the eastern part of the region (CSL, LL, HL and HL2), and mainly near or above normal in the western part of the region (BBL and P5). Non-copepod abundance was spatially variable with time series

record-high value observed on CSL. Mesozooplankton biomass was lower than normal across most of the region with the exception of P5.

- The abundance of Arctic *Calanus* and warm shelf copepod species were, respectively, lower and mainly higher than normal across the region in 2022. The abundance of warm offshore copepod species was below normal on CSL but mainly near or slightly above normal elsewhere. The copepod community at HL2 was characterized by record-low abundances of *Calanus hyperboreus*, *Metridia lucens* and *M. longa*. At P5, the abundances of *Acartia* spp. and *Temora longicornis* were also below normal while the abundance of *Paracalanus* sp. was above normal.
- Average surface and bottom temperatures in Bedford Basin were above normal in 2022. Average concentrations of the main nutrients (nitrate, silicate and phosphate) at the surface were near normal, while nitrate and phosphate in the bottom layers of Bedford Basin (60 m) were slightly above normal. Indices of phytoplankton abundance were all near normal in 2022.
- There was evidence of an intrusion event in Bedford Basin during December 2022. The intrusion event translated into warmer and saltier than normal conditions at the bottom, with lower than normal nitrate and silicate concentrations but slightly higher than normal phosphate.
- CPR observations indicated that in 2021, the annual PCI value was slightly above or above normal in both the WSS and ESS sub-regions, while the diatom abundance was near or slightly above normal for the ESS and WSS, respectively, and the dinoflagellate abundance was below normal in both sub-regions.
- CPR observations indicated that in 2021, the abundances of *Calanus* I-IV and *C. finmarchicus* CV-VI were near normal on the ESS, and slightly below (*Calanus* I-IV) or below (CV-VI) normal on the WSS. The abundances of two arctic *Calanus* species (*C. glacialis* and *C. hyperboreus*) and the small copepods (*Para/Pseudocalanus* and *Oithona* spp.) were mainly slightly below or below normal in both sub-regions. Euphausiids abundance was above (slightly below) normal on the ESS (WSS) while hyperiid amphipods abundance was below normal in both sub-regions. The abundances of acid-sensitive taxa (coccolithophores, foraminifera, *Limacina* spp.) were slightly below or below normal on the WSS, and near or above normal on the ESS.

6. ACKNOWLEDGEMENTS

The authors thank the personnel at the Bedford Institute of Oceanography and St. Andrews Biological Station who contributed to sample collection, sample analysis, data analysis, data management, and data sharing. We also thank the officers and crews of the Canadian Coast Guard Ships *Capt. Jacques Cartier, Teleost,* S*igma-T*, *Viola M. Davidson,* the US R/V *Atlantis,* and the British RRS *James Cook,* for their assistance in the collection of oceanographic data during 2022. Thanks to Stephanie Clay for the calculation of the spring bloom metrics using the *PhytoFit* application. Reviews by David Bélanger and Marjolaine Blais improved the manuscript.

7. REFERENCES

Babin, S.M., Carton, J.A., Dickey, T.D., and Wiggert, J.D. 2004. Satellite evidence of hurricane-induced phytoplankton blooms in an oceanic desert. J. Geophys. Res. 109: C03043.

Behrenfeld, M.J., and Boss, E.S. 2014. Resurrecting the Ecological Underpinnings of Ocean Plankton Blooms. Annu. Rev. Mar. Sci. 6: 167–194.

Blais, M., Galbraith, P.S., Plourde, S. and Lehoux, C. 2023. Chemical and Biological Oceanographic Conditions in the Estuary and Gulf of St. Lawrence during 2022. Can. Tech. Rep. Hydrogr. Ocean Sci. 357 : v + 70 p.

Brickman, D., Hebert, D., and Wang, Z. 2018. Mechanism for the recent ocean warming events on the Scotian Shelf of eastern Canada. Cont. Shelf Res. 156: 11–22.

Campbell, M. D. et al. 2021. Testing Bergmann's rule in marine copepods. Ecography. 44: 1283–1295.

Casault, B., Johnson, C., Devred, E., Head, E., Beazley, L., and Spry, J. 2022. Optical, Chemical, and Biological Oceanographic Conditions on the Scotian Shelf and in the eastern Gulf of Maine during 2020. DFO Can. Sci. Advis. Sec. Res. Doc. 2022/018. v + 82 p.

Churilova, T., Suslin, V., Krivenko, O., Efimova, T., Moiseeva, N., Mukhanov, V., and Smirnova L. 2017. Light Absorption by Phytoplankton in the Upper Mixed Layer of the Black Sea: Seasonality and Parametrization. *Frontiers in Mar. Sci.* 4: 90.

Clay, S., Peña, A., DeTracey, B., and Devred, E. 2019. Evaluation of Satellite-Based Algorithms to Retrieve Chlorophyll-a Concentration in the Canadian Atlantic and Pacific Oceans. *Remote Sens. 11(22)*: 2609.

Clay, S., Layton, C., and Devred, E. 2021. BIO-RSG/PhytoFit: First release (Version v1.0.0). Zenodo.

DFO. 2000. Chemical and Biological Oceanographic Conditions in 1998 and 1999 – Maritimes Region. DFO Sci. Stock Status Rep. G3-03 (2000).

DFO. 2023. Oceanographic Conditions in the Atlantic Zone in 2022. DFO Can. Sci. Advis. Sec. Sci. Advis. Rep. 2023/019.

Eppley, R.W. 1972. Temperature and phytoplankton growth in the sea. Fishery Bull. 70(4): 1063–1085.

Greenan B.J.W., Petrie B.D., Harrison W.G., Strain P.M. 2008. The onset and evolution of a spring bloom on the Scotian Shelf. Limnol. Oceanogr. 53(5): 1759-1775.

Harrison, G., Colbourne, E., Gilbert, D., and Petrie, B. 2005. Oceanographic Observations and Data Products Derived from Large-scale Fisheries Resource Assessment and Environmental Surveys in the Atlantic Zone. AZMP/PMZA Bull. 4: 17–23.

Head, E.J.H., Johnson, C.L., and Pepin, P. 2022. Plankton monitoring in the Northwest Atlantic: a comparison of zooplankton abundance estimates from vertical net tows and Continuous Plankton Recorder sampling on the Scotian and Newfoundland shelves, 1999–2015. ICES J. Mar. Sci. 79(3): 901-916.

Hebert, D., Pettipas, R., Brickman, D., and Dever M. 2013. Meteorological, Sea Ice and Physical Oceanographic Conditions on the Scotian Shelf and in the Gulf of Maine during 2012. DFO Can. Sci. Advis. Sec. Res. Doc. 2013/058. v + 46 p.

Hebert, D., Layton, C., Brickman, D., and Galbraith, P.S. 2023. Physical Oceanographic Conditions on the Scotian Shelf and in the Gulf of Maine during 2022. Can. Tech. Rep. Hydrogr. Ocean Sci. 359: vi + 81 p.

Holmes, R.W. 1970. The Secchi Disk in Turbid Coastal Waters. Limnol. Oceanogr. 15(5): 688–694.

IOCCG. 2000. Remote Sensing of Ocean Colour in Coastal, and Other Optically-Complex, Waters. Sathyendranath, S. (ed.), Reports of the International Ocean-Colour Coordinating Group, No. 3, IOCCG, Dartmouth, Canada.

Johnson, C., Harrison, G., Head, E., Casault, B., Spry, J., Porter, C., and Yashayaev, I. 2012. Optical, Chemical, and Biological Oceanographic Conditions in the Maritimes Region in 2011. DFO Can. Sci. Advis. Sec. Res. Doc. 2012/071.

Keister, J.E., Di Lorenzo, E., Morgan, C.A., Combes, V., and Peterson, W.T. 2011. Zooplankton species composition is linked to ocean transport in the Northern California Current. Global Change Biol. 17: 2498–2511.

Kelley, D., and Richards, C. 2022. oce: Analysis of Oceanographic Data. R package version 1.7-10.

Lacour, L., Ardyna, M., Stec, K., Claustre, H., Prieur, L., Poteau, A., Ribera D'Alcala, M., and Iudicone, D. 2017. Unexpected winter phytoplankton blooms in the North Atlantic subpolar gyre. Nature Geosci. 10: 836–839.

Lehmann, N., Reed, D.C., Buchwald, C., Lavoie, D., Yeats, P.A., Mei, Z.-P., and Johnson, C.L. 2023. Decadal Variability in Subsurface Nutrient Availability on the Scotian Shelf Reflects Changes in the Northwest Atlantic Ocean. J. Geophys. Res.: Oceans. 128: e2023JC019928.

Lenth, R., Singmann, H., Love, J., Buerkner, P., and Herve, M. 2022. emmeans: Estimated Marginal Means, aka Least-Squares Means. R package version 1.7.5.

Li, W.K.W. 2014. The state of phytoplankton and bacterioplankton at the Compass Buoy Station: Bedford Basin Monitoring Program 1992–2013. Can. Tech. Rep. Hydrogr. Ocean Sci. 304.

Mackas, D.L., Greve, W., Edwards, M., Chiba, S., Tadokoro, K., Eloire, D., Mazzocchi, M.G., Batten, S., Richardson, A.J., Johnson, C., Head, E., Conversi, A., and Pelosi, T. 2012. Changing zooplankton seasonality in a changing ocean: Comparing time series of zooplankton phenology. Progr. Oceanogr. 97–100: 31–62.

Meyer-Gutbrod, E.L., Greene, C.H., Davies, K.T.A., and Johns, D.G. 2021. Ocean regime shift is driving collapse of the north atlantic right whale population. Oceanography 34: 22–31.

Mitchell, M., Harrison, G., Pauley, K., Gagné, A., Maillet, G., and Strain, P. 2002. Atlantic zonal monitoring program sampling protocol. Can. Tech. Rep. Hydrogr. Ocean Sci. 223.

Moisan, J.R., Moisan, T.A., and Abbott, M.R. 2002. Modelling the effect of temperature on the maximum growth rates of phytoplankton populations. Ecol. Model. 153: 197–215.

Mojica, K.D.A., Huisman, J., Wilhelm, S.W., and Brussaard, C.P.D. 2016. Latitudinal variation in virus-induced mortality of phytoplankton across the North Atlantic Ocean. ISME J. 10: 500–513.

O'Reilly, J.E., Maritorena, S., Mitchell, B. G., Siegel, D. A., Carder, K. L., Garver, S. A., Kahru, M., and McClain, C. R. 1998. Ocean color chlorophyll algorithms for SeaWiFS. J. Geophys. Res. 103: 24937–24953.

Pepin, P., Maillet, G.L., Lavoie, D., and Johnson, C. 2013. Temporal trends in nutrient concentrations in the Northwest Atlantic basin. Ch. 10 (pp. 127–150) In: Aspects of climate change in the Northwest Atlantic off Canada [Loder, J.W., G. Han, P.S. Galbraith, J. Chassé and A. van der Baaren (Eds.)]. Can. Tech. Rep. Fish. Aquat. Sci. 3045: x + 190 p.

Pershing, A.J. and Stamieszkin, K. 2020. The North Atlantic Ecosystem, from Plankton to Whales. Annu. Rev. Mar. Sci. 12(1): 339–359.

Petrie, B. 2007. Does the north Atlantic oscillation affect hydrographic properties on the Canadian Atlantic continental shelf? Atmos. Ocean 45(3): 141–151.

Petrie, B., and Yeats, P. 2000. Annual and interannual variability of nutrients and their estimated fluxes in the Scotian Shelf - Gulf of Maine region. Can. J. Fish. Aquat. Sci. 57: 2536–2546.

Petrie, B., Topliss, B.J., and Wright, D.G. 1987. Coastal upwelling and eddy development off Nova Scotia. J. Geophys. Res. 92 (C12), pp. 12979-12991.

Petrie, B., Yeats, P., and Strain, P. 1999. Nitrate, Silicate and Phosphate Atlas for the Scotian Shelf and the Gulf of Maine. Can. Tech. Rep. Hydrogr. Ocean Sci. 203.

Platt T., Prakash, A., and Irwin, B. 1972. Phytoplankton nutrients and flushing of inlets on the coast of Nova Scotia, Nat. Can. 99, pp. 253– 261.

Rakshit, S., Dale, A.W., Wallace, D.W., and Algar, C.K. 2023. Sources and sinks of bottom water oxygen in a seasonally hypoxic fjord. Front. Mar. Sci., 10.

Richardson, A.J., Walne, A.W., John, A.W.G., Jonas, T.D., Lindley, J.A., Sims, D.W., Stevens, D., and Witt, M. 2006. Using continuous plankton recorder data. Progr. Oceanogr. 68: 27–74.

Ringuette, M., Devred, E., Azetsu-Scott, K., Head, E., Punshon, S., Casault, B., and Clay, S. 2022. Optical, Chemical, and Biological Oceanographic Conditions in the Labrador Sea between 2014 and 2018. DFO Can. Sci. Advis. Sec. Res. Doc. 2022/021. v + 38 p.

Ross, T., Craig, S.E., Comeau, A., Davis, R., Dever, M., and Beck, M. 2017. Blooms and subsurface phytoplankton layers on the Scotian Shelf: Insights from profiling gliders. J Marine Syst. 172: 118–127.

Sorochan, K.A., Plourde, S., Morse, R., Pepin, P., Runge, J., Thompson, C., and Johnson, C.L. 2019. North Atlantic right whale (Eubalaena glacialis) and its food: (II) interannual variations in biomass of Calanus spp. on western North Atlantic shelves. J. Plankton Res. 41(5): 687–708.

Sverdrup, H.U. 1953. On Conditions for the Vernal Blooming of Phytoplankton. J. Cons. Perm. Int. Explor. Mer. 18: 287–295.

Therriault, J.-C., Petrie, B., Pepin, P., Gagnon, J., Gregory, D., Helbig, J., Herman, A., Lefaivre, D., Mitchell, M., Pelchat, B., Runge, J., and Sameoto, D. 1998. Proposal for a Northwest Atlantic Zonal Monitoring Program. Can. Tech. Rep. Hydrogr. Ocean Sci. 194.

Townsend, D.W., Keller, M.D., Sieracki, M.E., and Ackleson, S.G. 1992. Spring phytoplankton blooms in the absence of vertical water column stratification. Nature. 360: 59–62.

Utermöhl, von H. 1931. Neue Wege in der quantitativen Erfassung des Plankton.(Mit besonderer Berücksichtigung des Ultraplanktons.). Verh. Int. Verein. Theor. Angew. Limnol. 5**:** 567–595.

Zhai, L., Platt, T., Tang, C., Sathyendranath, S., and Hernández Walls, R. 2011. Phytoplankton Phenology on the Scotian Shelf. ICES J. Mar. Sci. 68: 781–791.

8. TABLES

Table 1. Atlantic Zone Monitoring Program sampling missions in the Maritimes Region in 2022.

Group	Location	Mission ID	Dates	# Hydro Stations	# Net Stations
Ecosystem Trawl Survey - Winter	Georges Bank	CAR2022-102	Mar 28–Apr 12	53	7
Ecosystem Trawl Survey - Summer	Scotian Shelf	TEL2022-010	Jul 5–Aug 6	153	25
Seasonal Sections - Spring	Scotian Shelf	AT48-02	Mar 22–Apr 5	79	68
Seasonal Sections - Fall	Scotian Shelf	JC24301	Oct 2–19	72	66
High-frequency Stations	Halifax-2	BCD2022-666	Mar 22–Dec 5	17(6)[1]	17(6)[1]
High-frequency Stations	Prince-5	BCD2022-669	Jan 13–Dec 19	10	11
Bedford Basin	Compass Buoy Station	BCD2022-667	Jan 7–Dec 21	48	48
			Total:	432	242

[1]Total station occupations, including occupations during trawl surveys and seasonal sections (dedicated occupations with mission ID as listed at left are in parentheses).

9. FIGURES

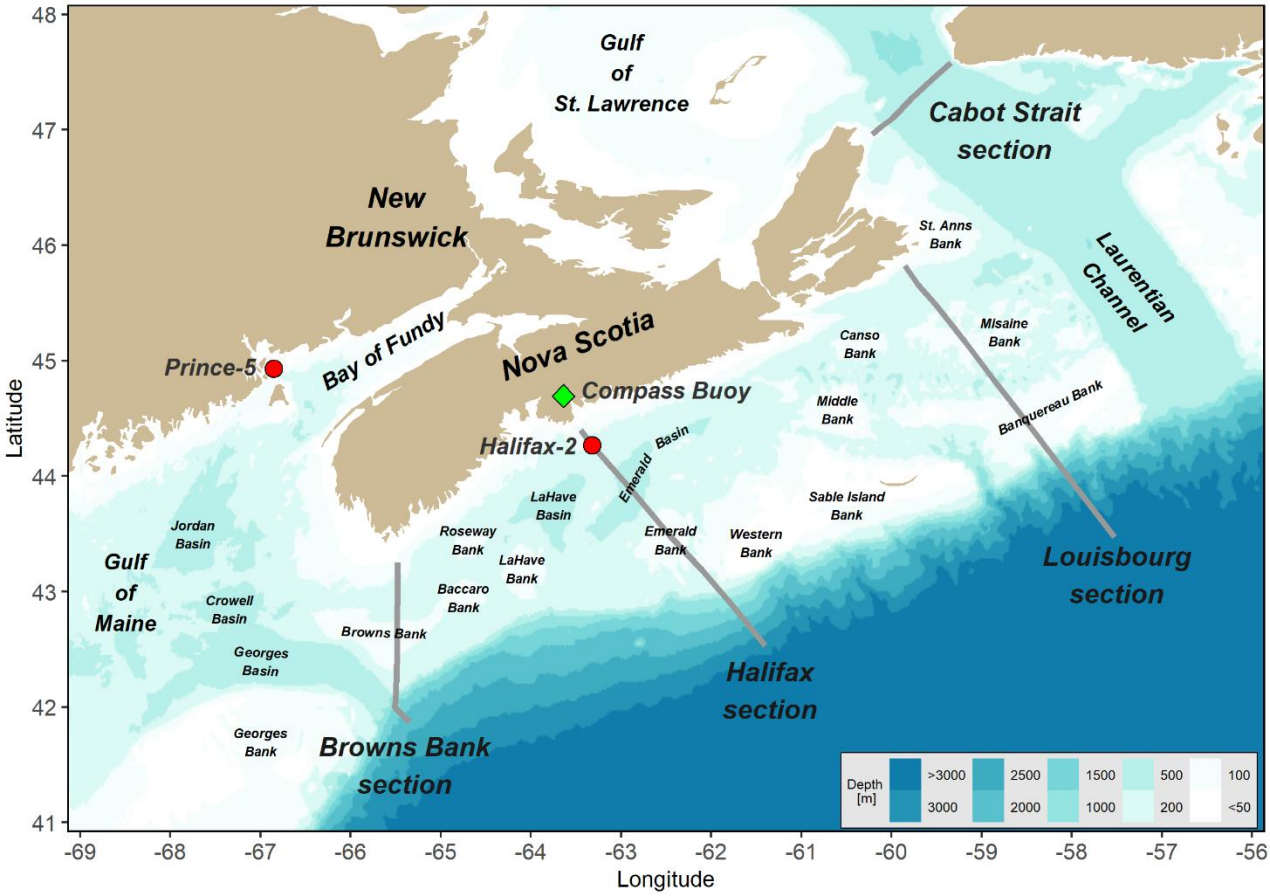

Figure 1. Map of primary sections (Cabot Strait [CSL]; Louisbourg [LL]; Halifax [HL]; Browns Bank [BBL]) and high-frequency sampling stations (Halifax-2 [HL2]; Prince-5 [P5]) sampled in the DFO Maritimes Region. The Compass Buoy station is sampled as part of the Bedford Basin Monitoring Program.

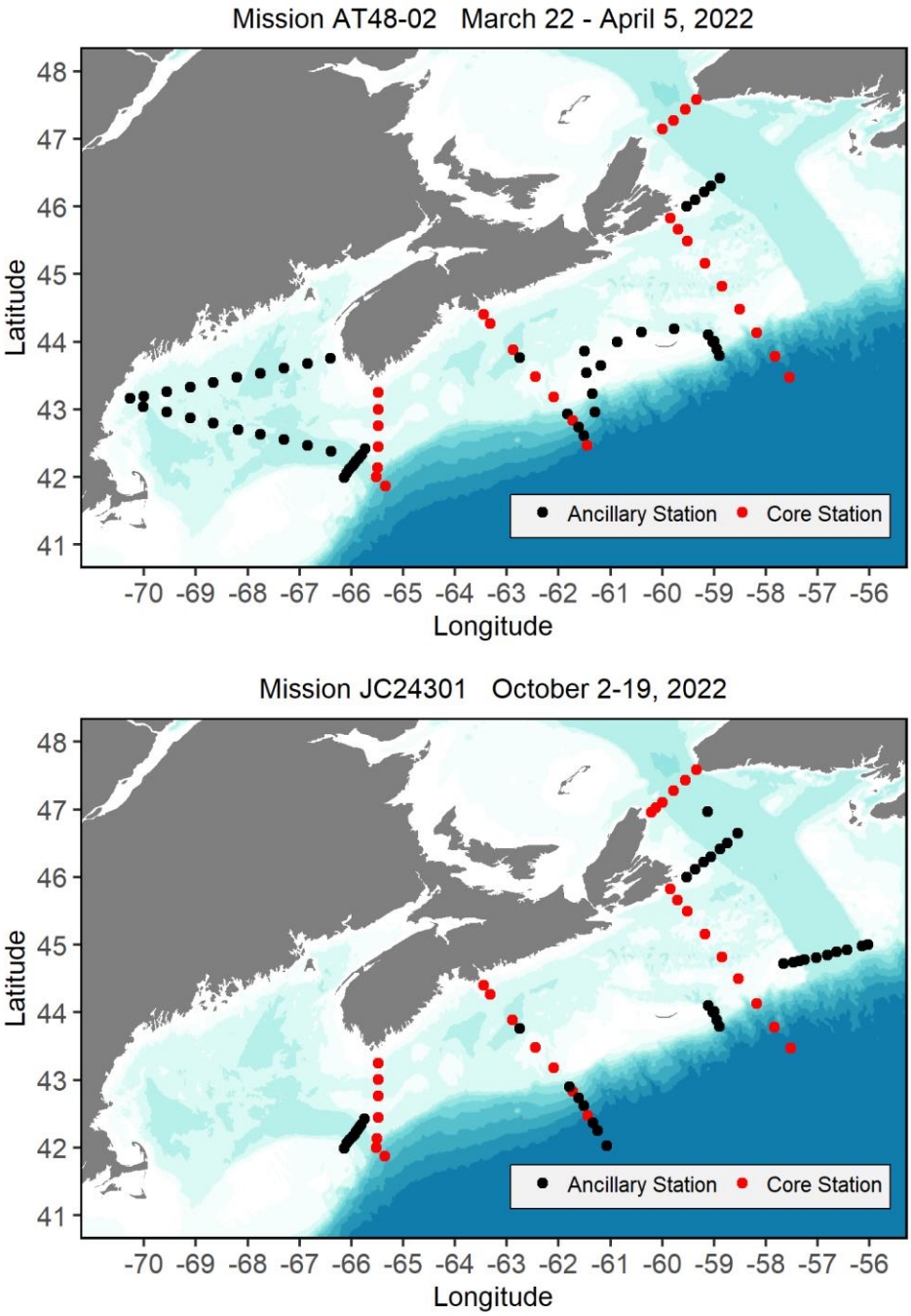

Figure 2. Stations sampled during the 2022 spring (top panel) and fall (bottom panel) surveys. Red markers indicate core stations, and black markers indicate stations sampled for ancillary programs.

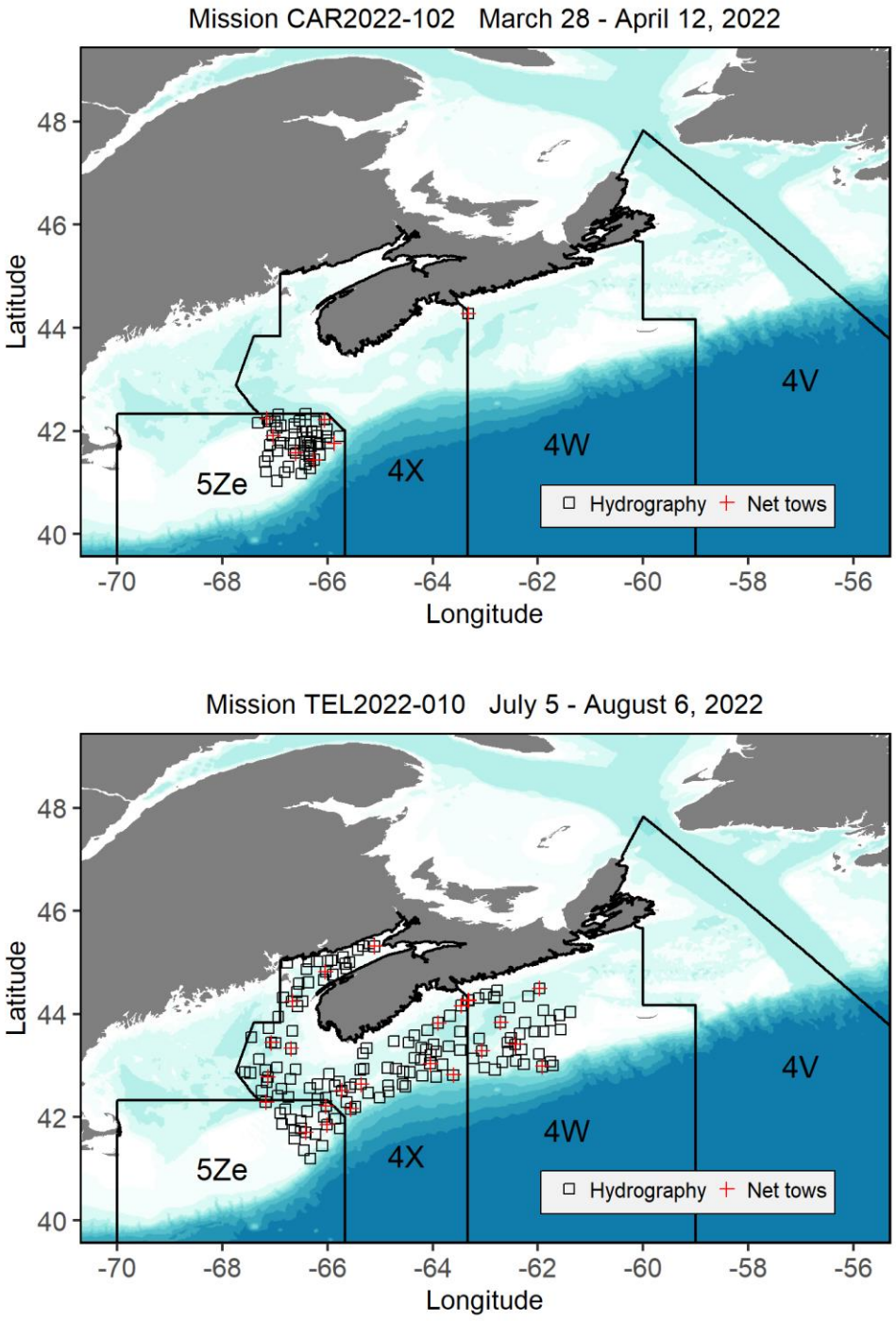

Figure 3. Stations sampled during the 2022 winter (top panel) and summer (bottom panel) ecosystem trawl surveys. Station locations are superimposed on NAFO areas.

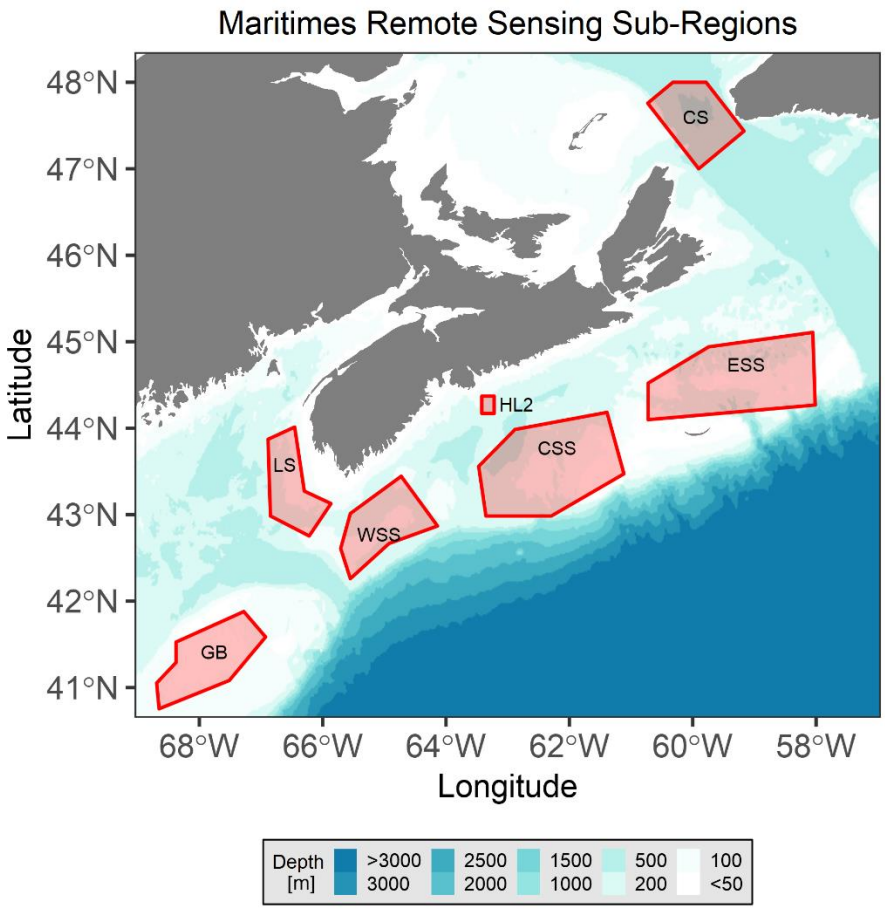

Figure 4. Sub-regions in the Maritimes Region identified for spatial/temporal analysis of satellite ocean colour data. Halifax-2 [HL2]; Cabot Strait [CS]; Eastern Scotian Shelf [ESS]; Central Scotian Shelf [CSS]; Western Scotian Shelf [WSS]; Lurcher Shoal [LS]; Georges Bank [GB].

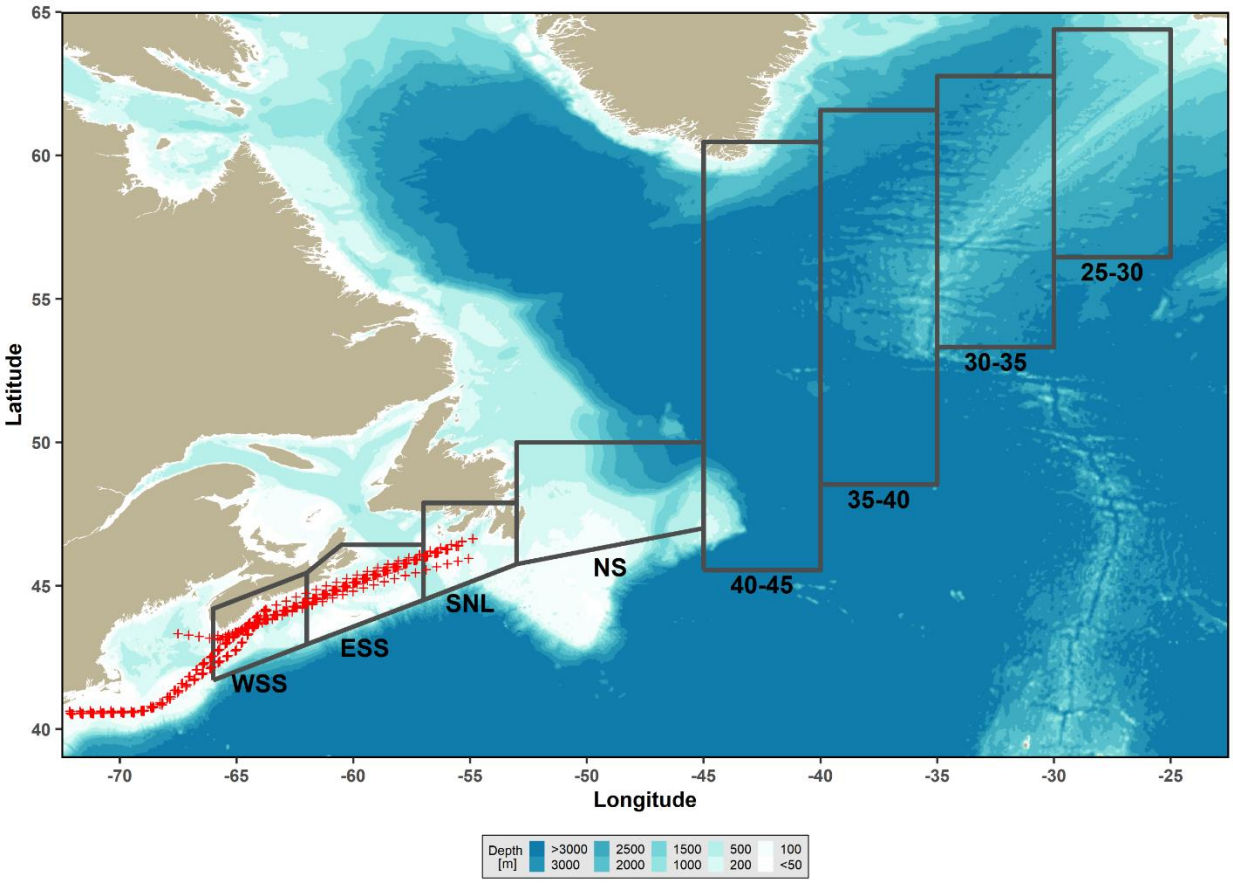

Figure 5. Continuous Plankton Recorder (CPR) lines and stations sampled in 2021 (red markers). Data are analysed by region. Regions are: Western Scotian Shelf (WSS), Eastern Scotian Shelf (ESS), South Newfoundland Shelf (SNL), Newfoundland Shelf (NS), and between longitudes 40–45°W, 35–40°W, 30–35°W, 25–30°W.

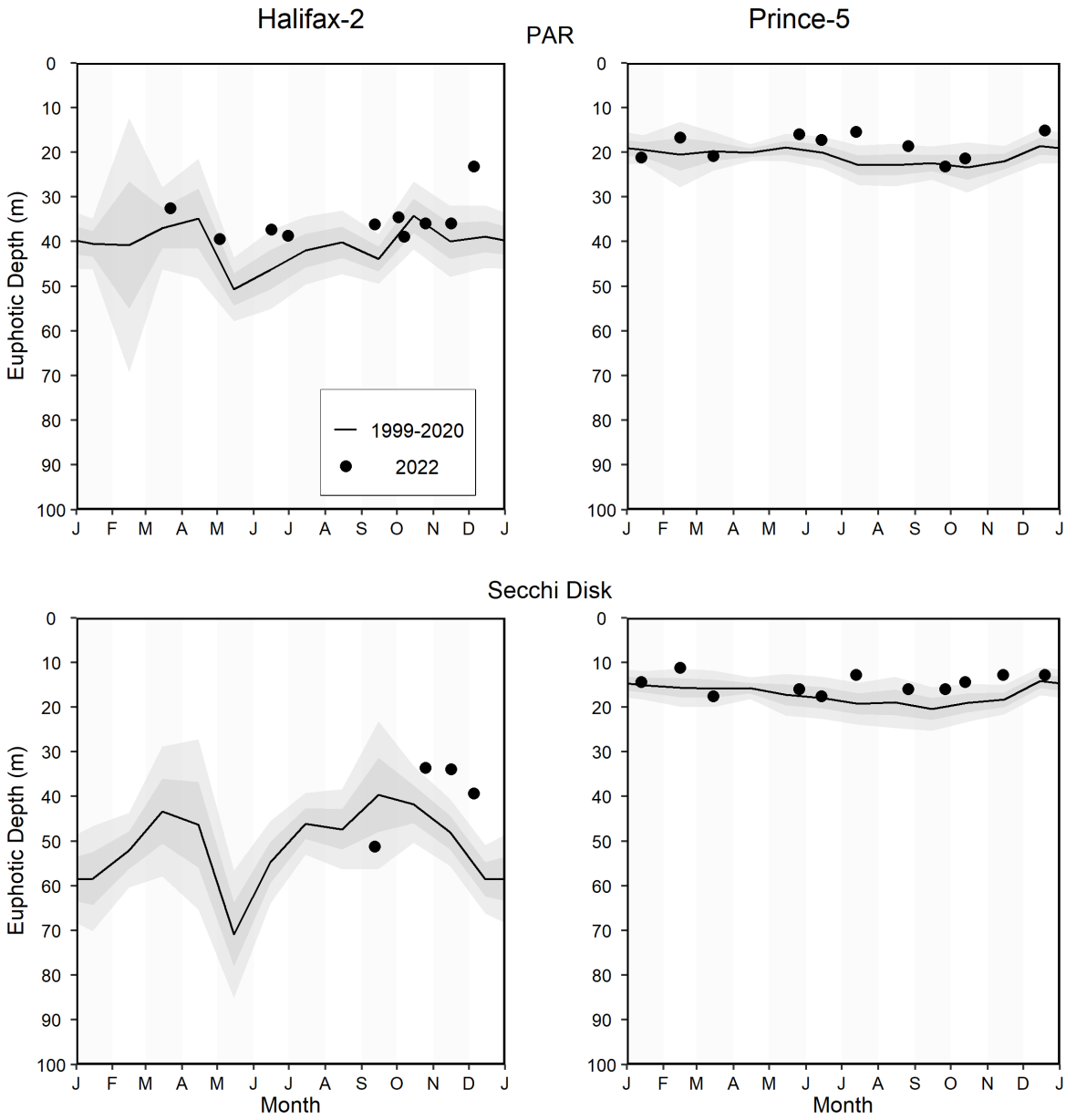

Figure 6. Euphotic depth at the Maritimes high-frequency sampling stations. Top panels: Euphotic depth calculated from PAR irradiance meter. Bottom panels: Euphotic depth calculated from Secchi disc measurements. The solid circles represent the 2022 data; the solid line represent the monthly climatological means for the reference period 1999-2020 (except 2001–2020 for euphotic depth from PAR at Prince-5); the gray shaded ribbons represent the standard deviation (±0.5 and ±1 sd) of the monthly means. Tick marks on the horizontal axes indicate the 1st day of the month.

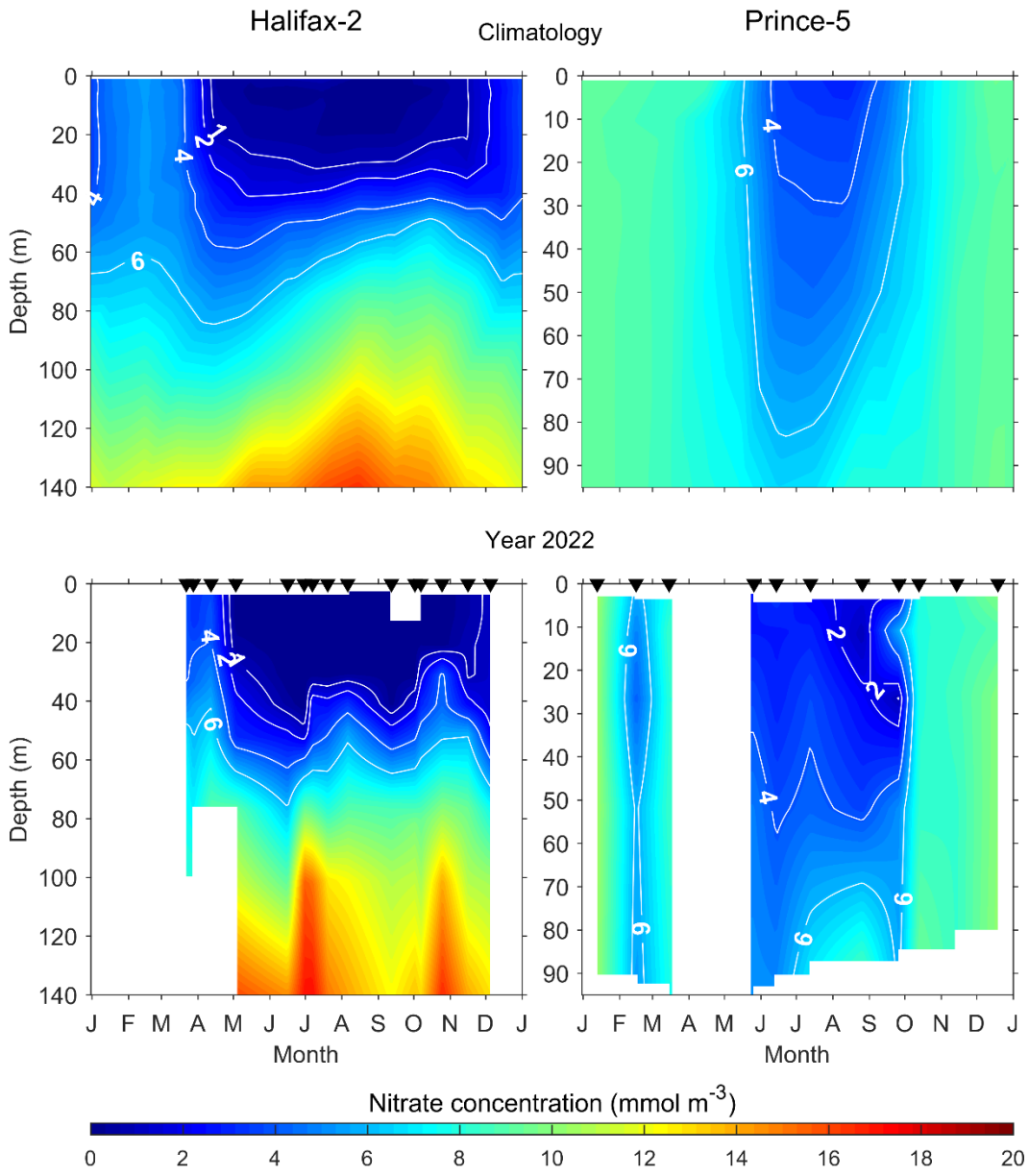

Figure 7. Nitrate concentrations at the Maritimes high-frequency sampling stations. Top panels: Climatological mean vertical structure of nitrate concentrations for the reference period 1999-2020. Bottom panels: Vertical structure of nitrate concentrations in 2022. Black triangles in the bottom panels indicate sampling dates. Tick marks on the horizontal axes indicate the 1st day of the month. White areas indicate no data.

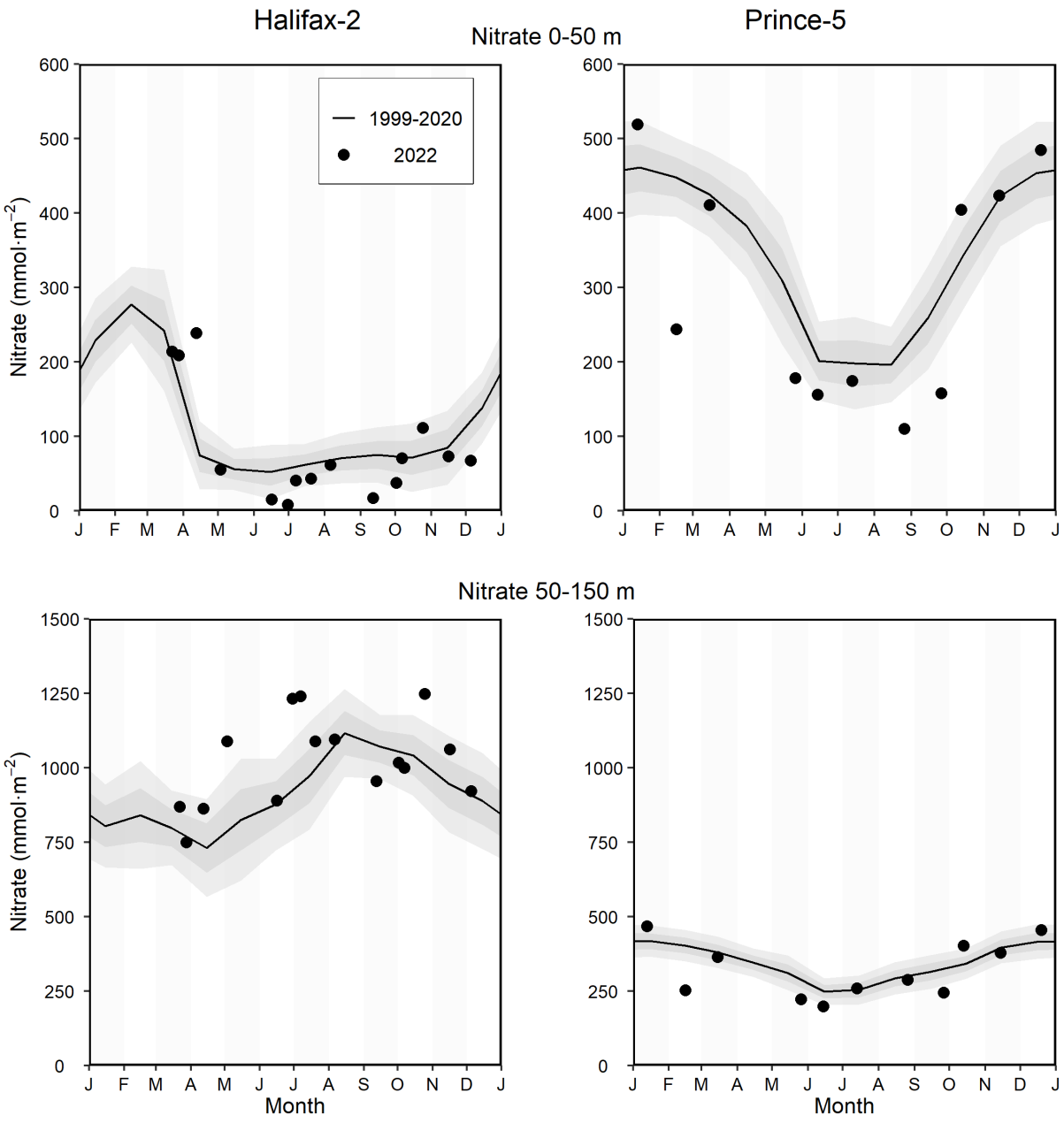

Figure 8. Nitrate inventories at the Maritimes high-frequency sampling stations. Top panels: Surface (0–50 m) nitrate inventory. Bottom panels: Deep (50–150 m for Halifax-2 and 50–95 m for Prince-5) nitrate inventory. The solid circles represent the 2022 data; the solid line represent the monthly climatological means for the reference period 1999-2020; the gray shaded ribbons represent the standard deviation (±0.5 and ±1 sd) of the monthly means. Tick marks on the horizontal axes indicate the 1st day of the month.

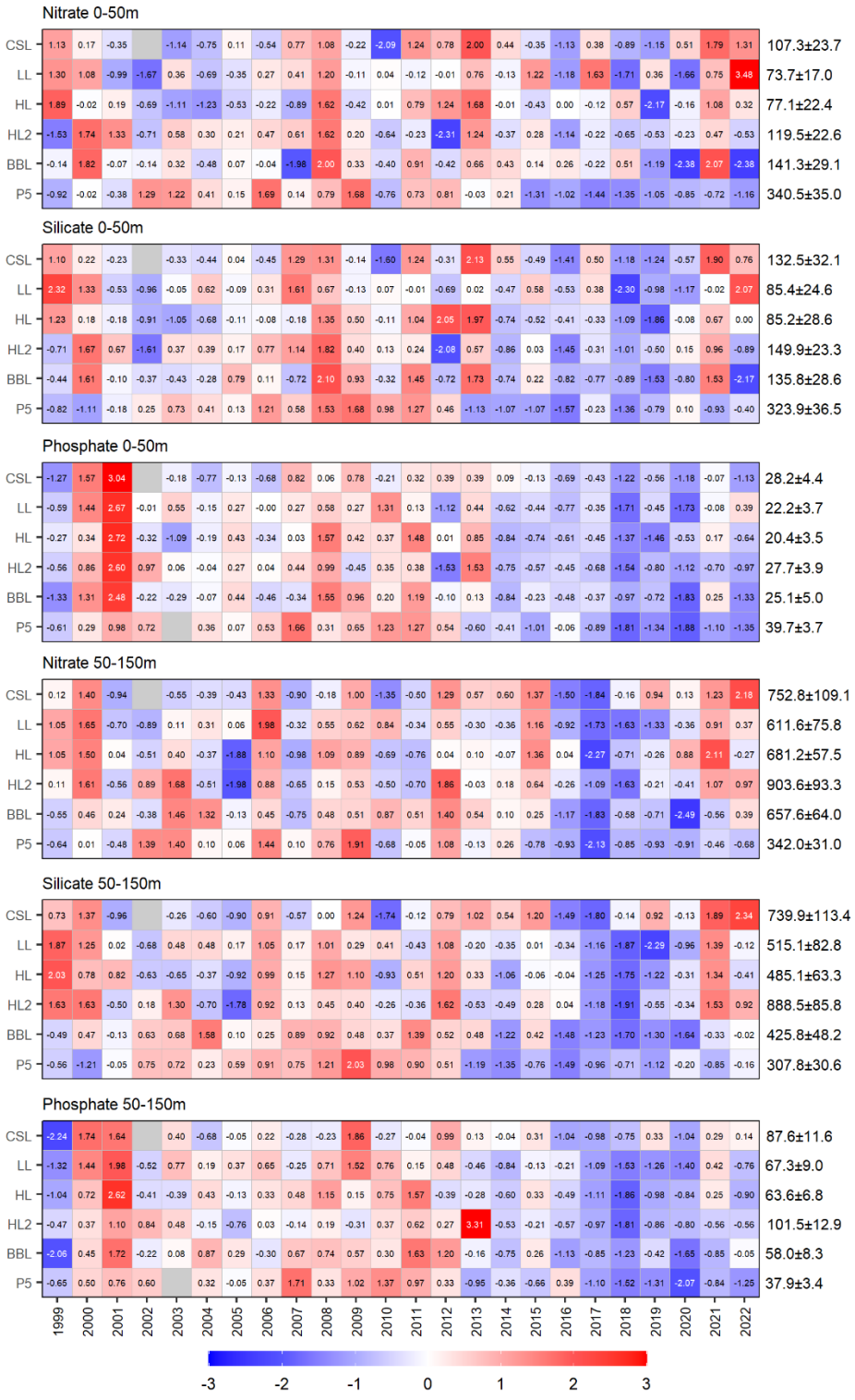

Figure 9. Annual anomaly scorecards for surface (0–50 m) and deep (50–150 m) nitrate, silicate, and phosphate inventories. Values in each cell are anomalies from the mean for the reference period 1999–2020, in standard deviation (sd) units (mean and sd listed at right in units of mmol·m^{-2}). Red (blue) cells indicate higher- (lower-) than-normal nutrients. Gray cells indicate missing data. CSL: Cabot Strait section; LL: Louisbourg section; HL: Halifax section; HL2: Halifax-2; BBL: Browns Bank section; P5: Prince-5.

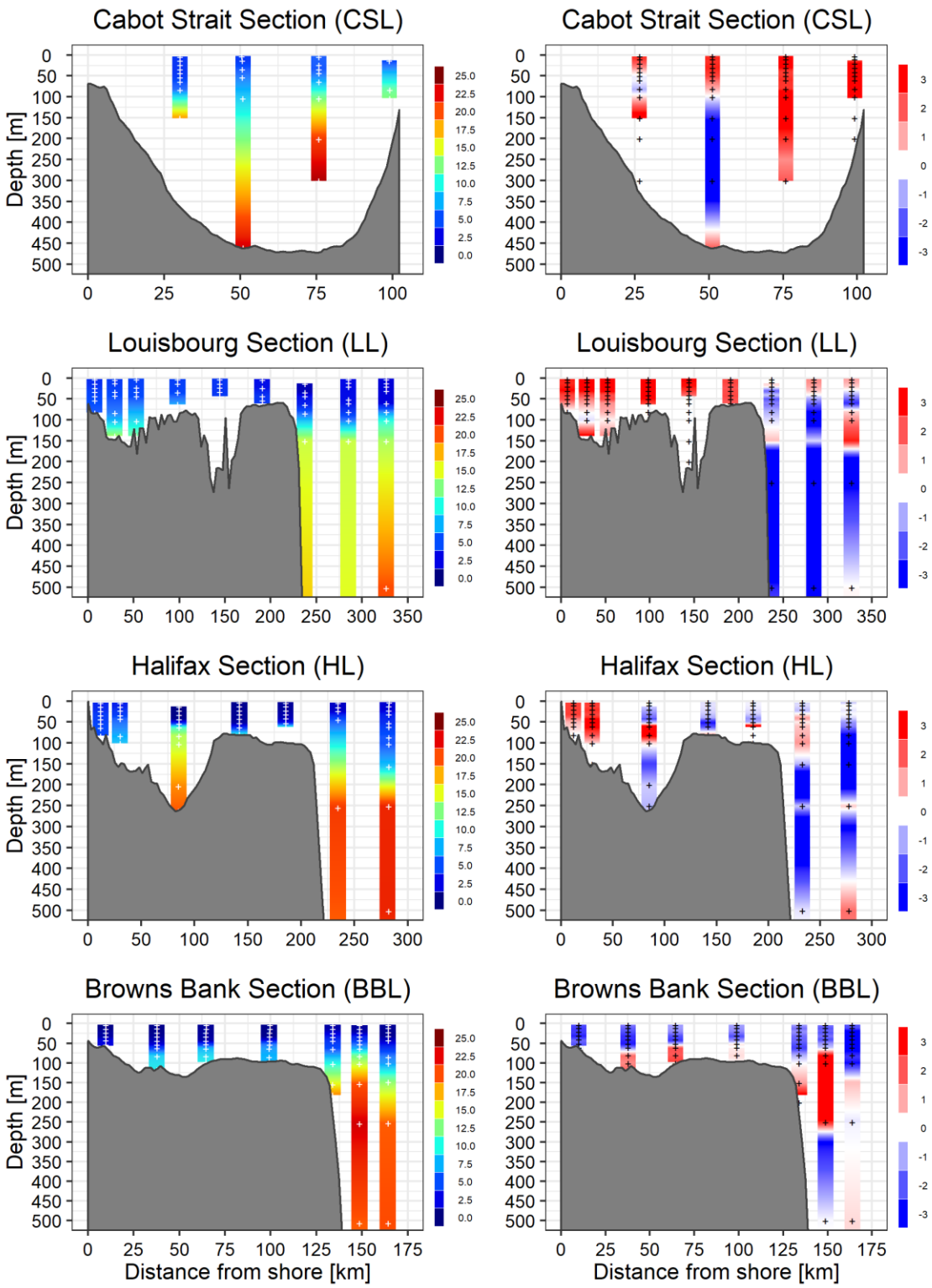

Figure 10a. Nitrate concentrations on the core sections in spring 2022. Left panels: Nitrate concentration profiles (mmol·m^{-3}) measured in spring 2022. Right panels: Nitrate concentration anomalies (mmol·m^{-3}) from the climatological means for the reference period 1999–2020. White markers on the left panels indicate the actual sampling depths. Black markers on the right panels indicate the depths at which station-specific climatological values were calculated.

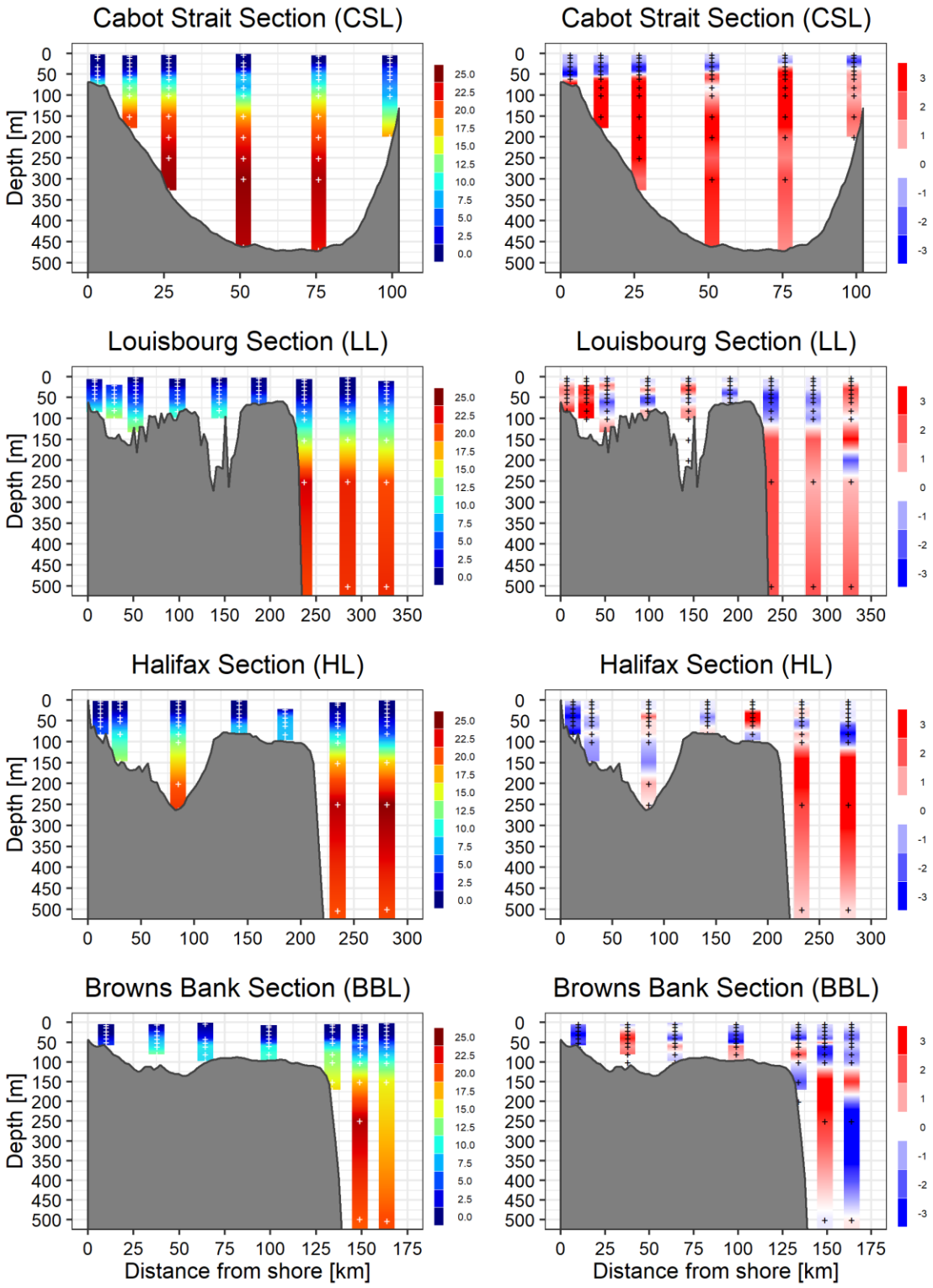

Figure 10b. Nitrate concentrations on the core sections in fall 2022. Left panels: Nitrate concentration profiles (mmol·m^{-3}) measured in fall 2022. Right panels: Nitrate concentration anomalies (mmol·m^{-3}) from the climatological means for the reference period 1999–2020. White markers on the left panels indicate the actual sampling depths. Black markers on the right panels indicate the depths at which station-specific climatological values were calculated.

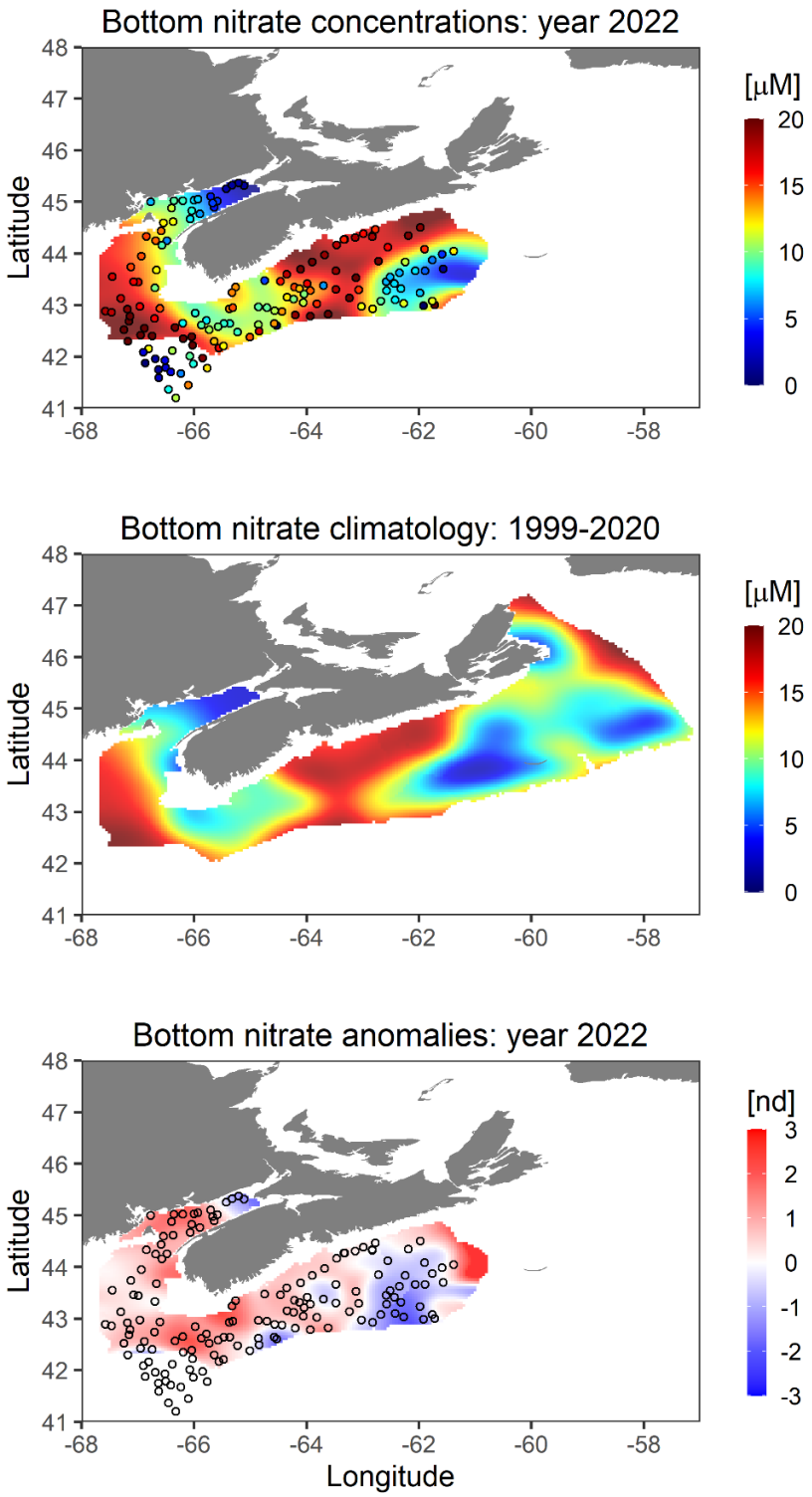

Figure 11. Bottom nitrate concentrations during the summer ecosystem trawl survey. Top panel: Nitrate concentrations during 2022. Middle panel: Climatological mean spatial structure of nitrate concentrations for the reference period 1999-2020. Bottom panel: Normalized anomalies of bottom nitrate concentrations. Markers in the top and bottom panels represent the 2022 sampling locations. Refer to Figure 1 for location of major banks and basins.

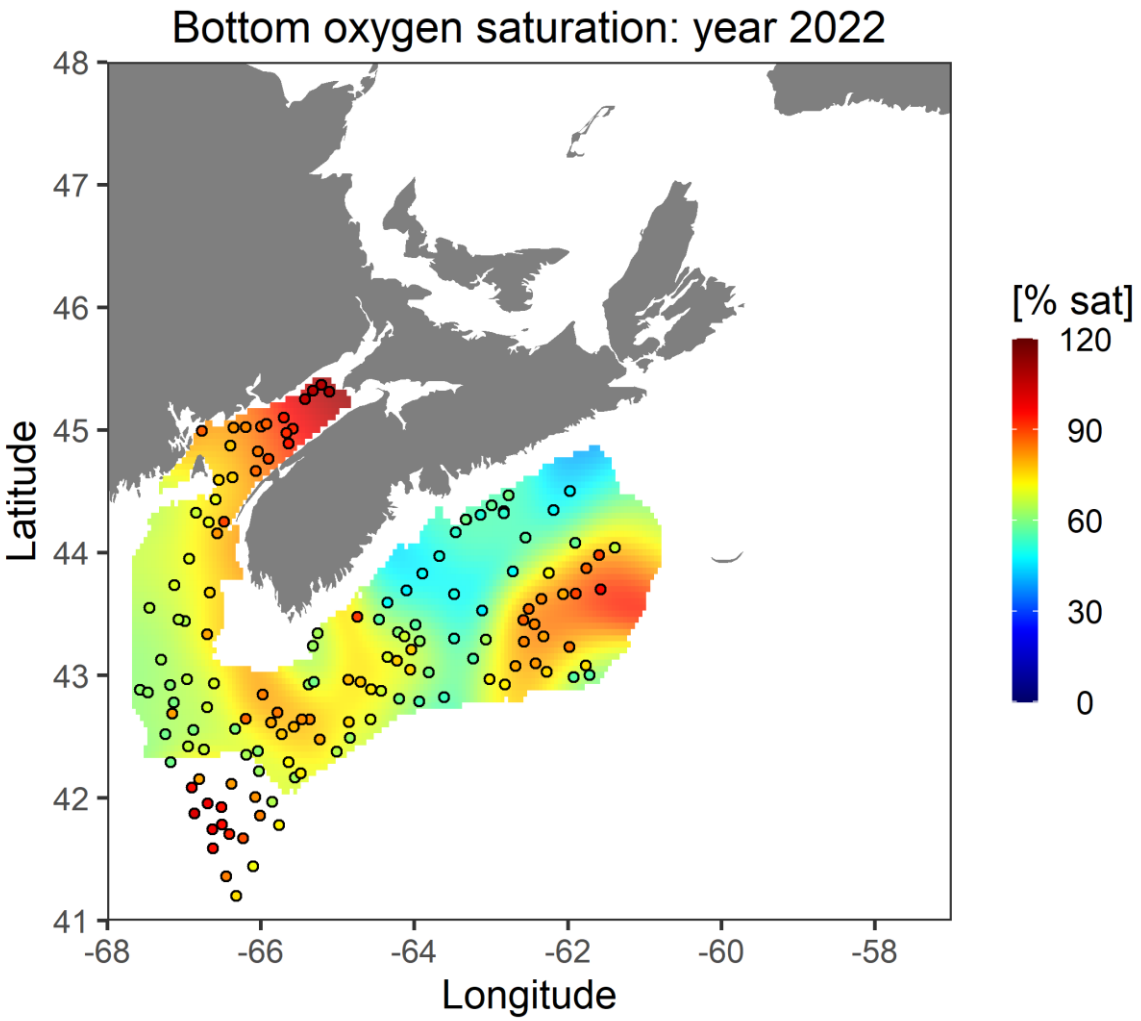

Figure 12. Bottom oxygen saturation levels during the summer ecosystem trawl survey. Markers represent the 2022 sampling locations. Refer to Figure 1 for location of major banks and basins

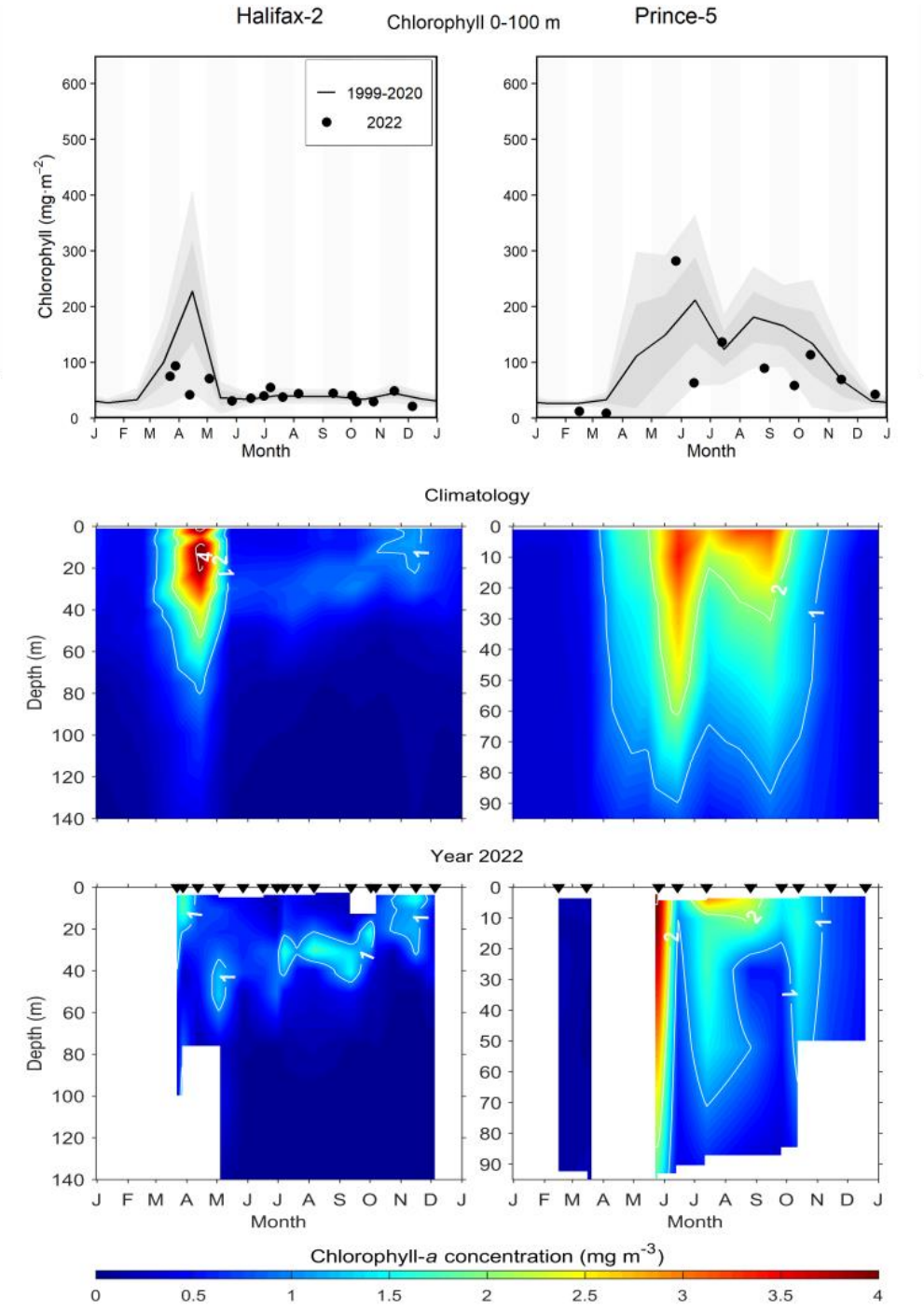

Figure 13. Chlorophyll-a inventory and concentrations at the Maritimes high-frequency sampling stations. Top panels: Chlorophyll-a inventory (0–100 m for Halifax-2 and 0–95 m for Prince-5); the solid circles represent the 2022 data; the solid line represent the monthly climatological means for the reference period 1999-2020; the gray shaded ribbons represent the standard deviation (±0.5 and ±1 sd) of the monthly means. Middle panels: Monthly climatological mean vertical structure of chlorophyll-a concentrations for the reference period 1999-2020. Bottom panels: Vertical structure of chlorophyll-a concentrations in 2022. Black triangles in the bottom panels indicate sampling dates. Tick marks on the horizontal axes indicate the 1st day of the month. White areas indicate no data.

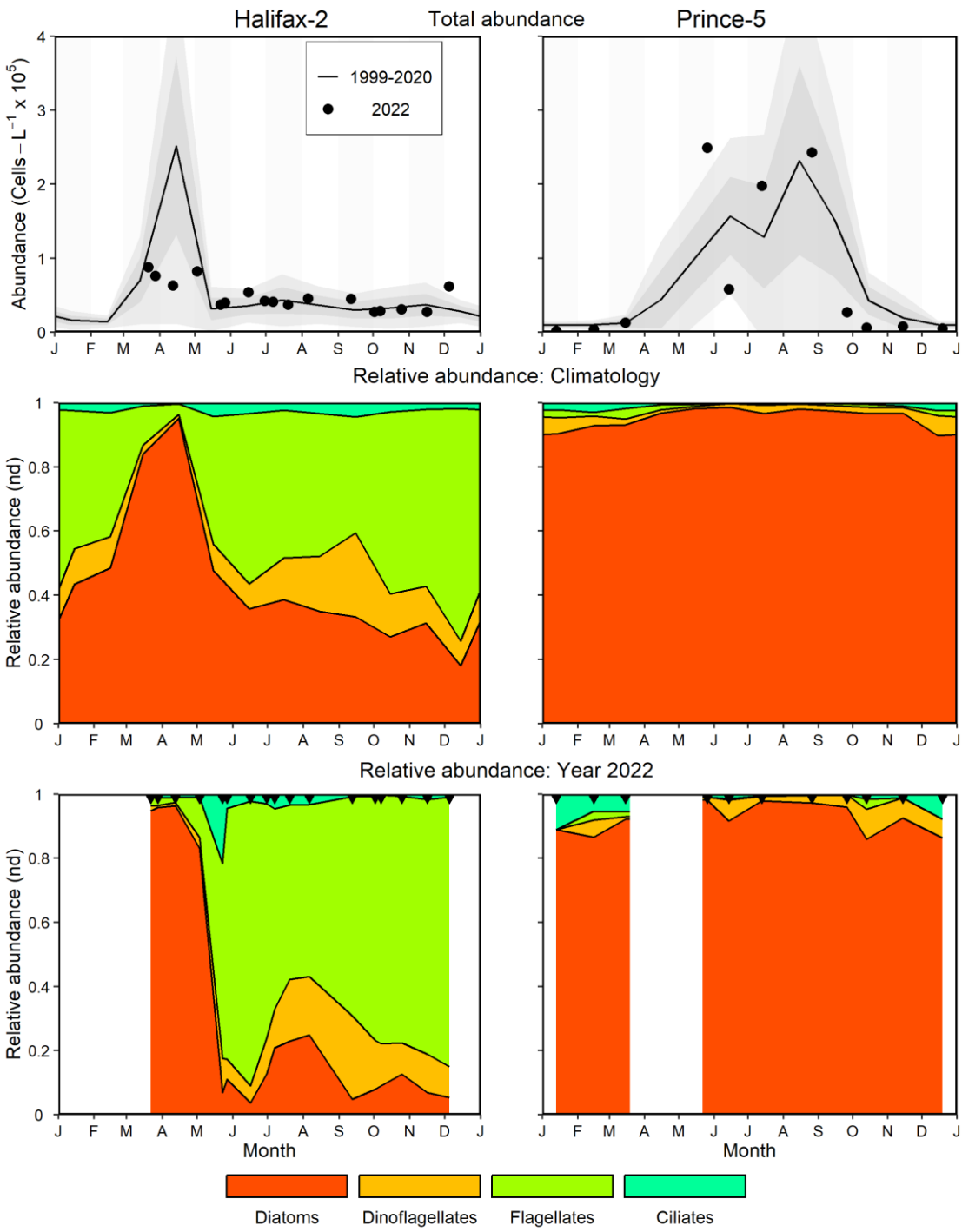

Figure 14. Phytoplankton abundance and community composition at the Maritimes high-frequency sampling stations. Top panels: Phytoplankton abundance; the solid circles represent the 2022 data; the solid line represent the monthly climatological means for the reference period 1999-2020; the gray shaded ribbons represent the standard deviation (±0.5 and ±1 sd) of the monthly means. Middle panels: Climatological mean phytoplankton relative abundance for the reference period 1999-2020. Bottom panels: Phytoplankton relative abundance in 2022. Black triangles in the bottom panels indicate sampling dates. Tick marks on the horizontal axes indicate the 1st day of the month. White areas indicate no data.

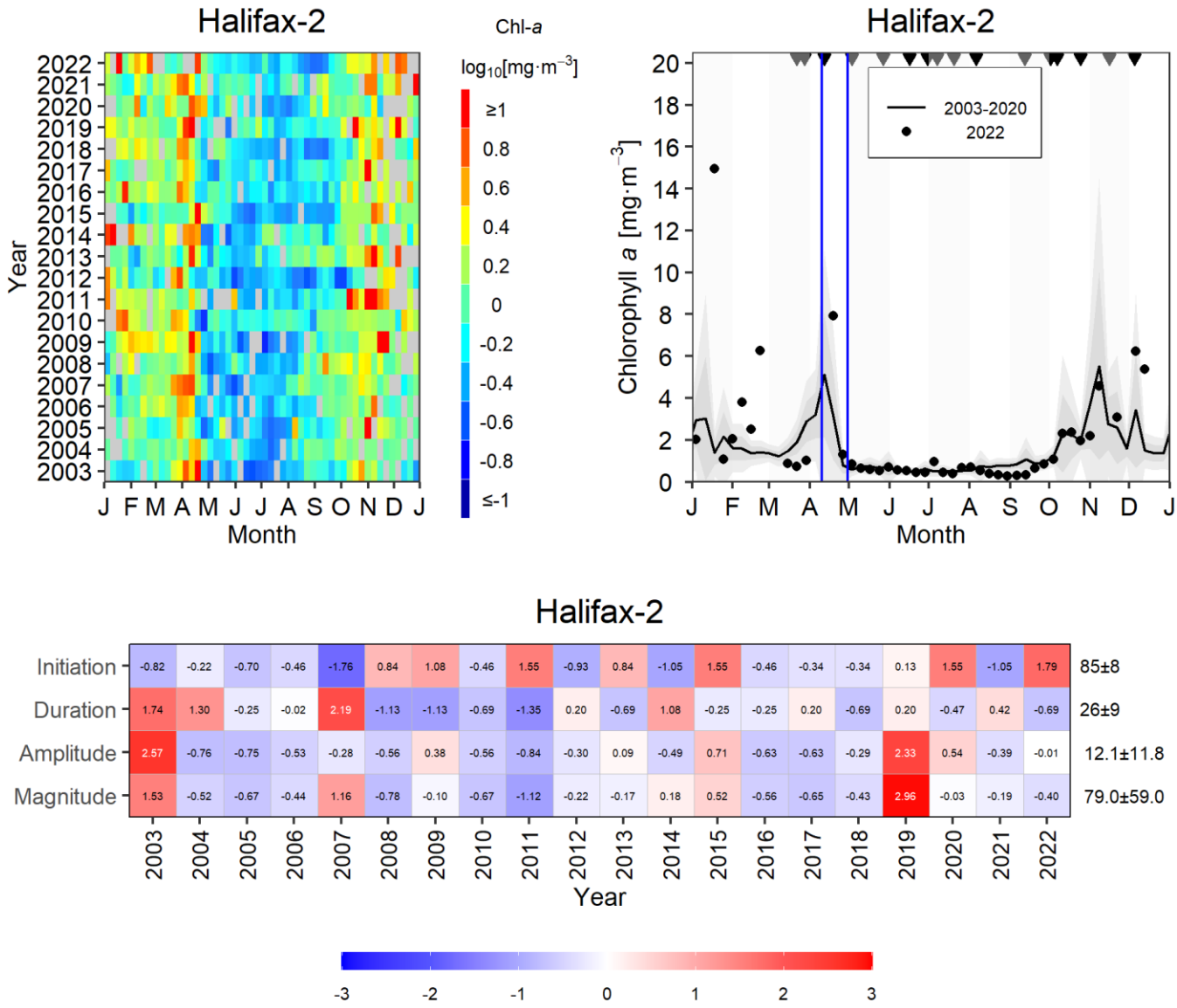

Figure 15. Surface chlorophyll-a concentrations and spring phytoplankton bloom metrics derived from remote sensing ocean colour data for Halifax-2 sub-region. Top left panel: Time series of weekly mean surface chlorophyll-a concentrations; gray pixels indicate missing data. Top right panel: Weekly mean surface chlorophyll-a concentrations; the solid circles represent the 2022 data; the solid line represent the weekly climatological means for the reference period 2003-2020; the gray shaded ribbons represent the standard deviation (±0.5 and ±1 sd) of the weekly means; the vertical blue lines delimit the period of the spring bloom as calculated by the PhytoFit application; black triangles indicate in situ chlorophyll-a sampling dates; tick marks on the horizontal axes indicate the 1st day of the month. Bottom panel: Annual anomaly scorecard for the spring phytoplankton bloom metrics; values in each cell are anomalies from the mean for the reference period 2003–2020, in standard deviation (sd) units (mean and sd listed at right in units of Day-of-Year for initiation, Days for duration, $mg_{chl} \cdot m^{-3}$ for amplitude, and mg chl·m^{-3}·d for magnitude); red (blue) cells indicate later (earlier) initiation, longer (shorter) duration or higher- (lower-) than-normal amplitude or magnitude.

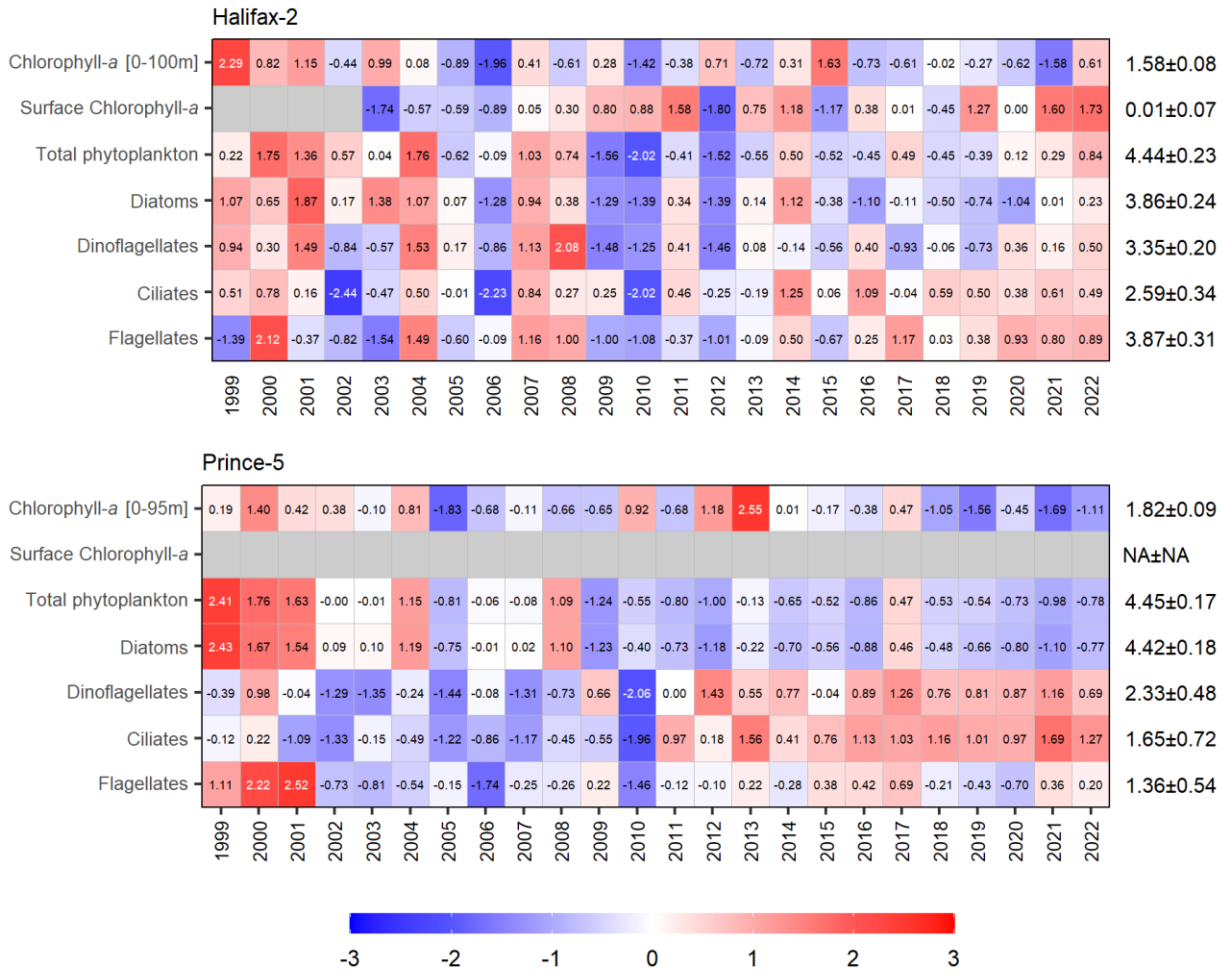

Figure 16. Annual anomaly scorecards for in situ chlorophyll-a inventory, remote sensing surface chlorophyll-a concentration, and phytoplankton abundance at the Maritimes high-frequency sampling stations. Values in each cell are anomalies from the mean for the reference period 1999–2020 for in situ chlorophyll-a inventory and phytoplankton abundance, and 2003–2020 for remote sensing surface chlorophyll-a, in standard deviation (sd) units (mean and sd listed at right in units of $log_{10}(mg \cdot m^{-2})$ for chlorophyll-a inventory, $log_{10}(mg \cdot m^{-3})$ for chlorophyll-a concentration, and $log_{10}(cells \cdot L^{-1}+1)$ for phytoplankton abundance). Red (blue) cells indicate higher- (lower-) than-normal chlorophyll-a inventories/concentrations or phytoplankton abundances. Gray cells indicate missing data.

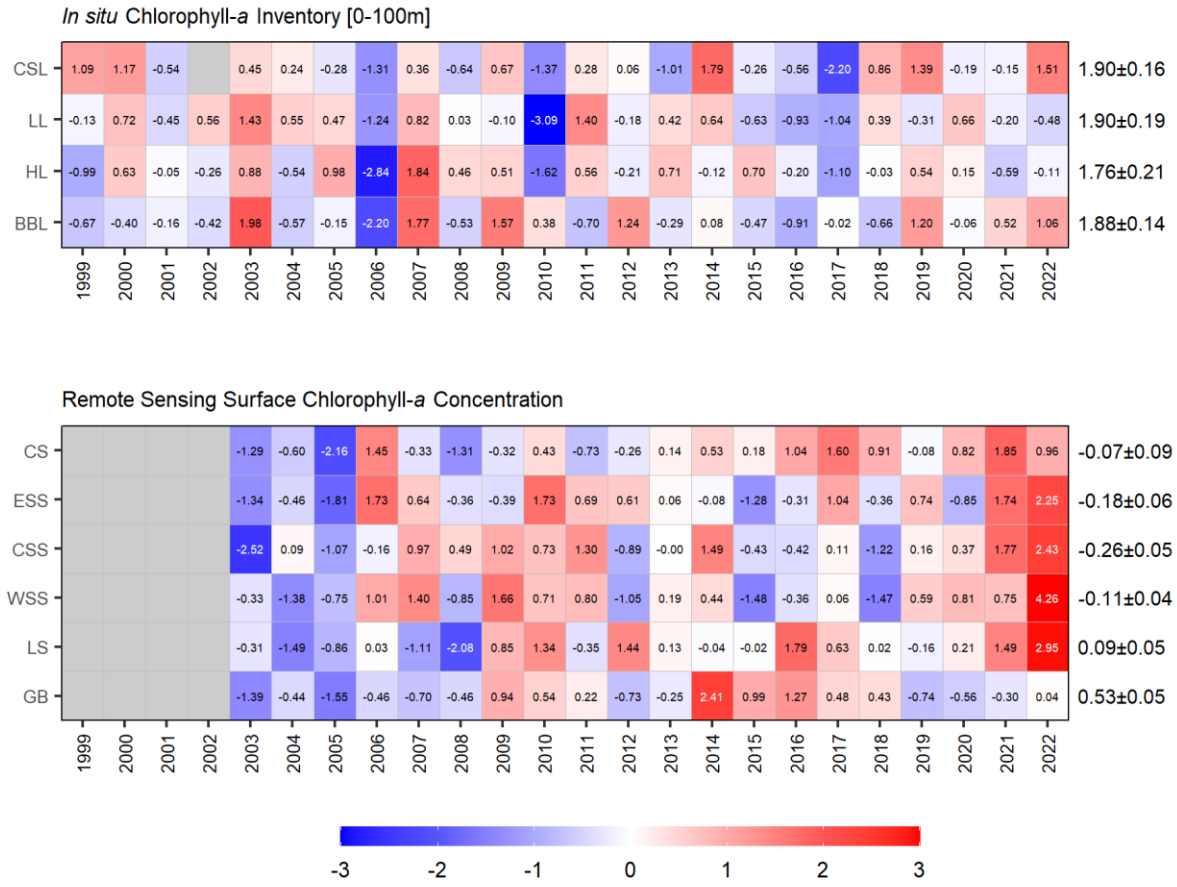

Figure 17. Annual anomaly scorecards for in situ chlorophyll-a inventory (0–100 m) on the Cabot Strait [CSL], Louisbourg [LL], Halifax [HL] and Browns Bank [BBL] sections (top panel) and for remote sensing surface chlorophyll-a concentrations on the Cabot Strait [CS], Eastern Scotian Shelf [ESS], Central Scotian Shelf [CSS], Western Scotian Shelf [WSS], Lurcher Shoal [LS], and Georges Bank [GB] sub-regions (bottom panel). Values in each cell are anomalies from the mean for the reference period 1999–2020 for in situ chlorophyll-a inventory, and 2003–2020 for remotely sensed surface chlorophyll-a, in standard deviation (sd) units (mean and sd listed at right in units of $log_{10}(mg \cdot m^{-2})$ for chlorophyll-a inventory and $log_{10}(mg \cdot m^{-3})$ for chlorophyll-a concentration). Red (blue) cells indicate higher- (lower-) than-normal chlorophyll-a inventories or surface chlorophyll-a concentrations. Gray cells indicate missing data.

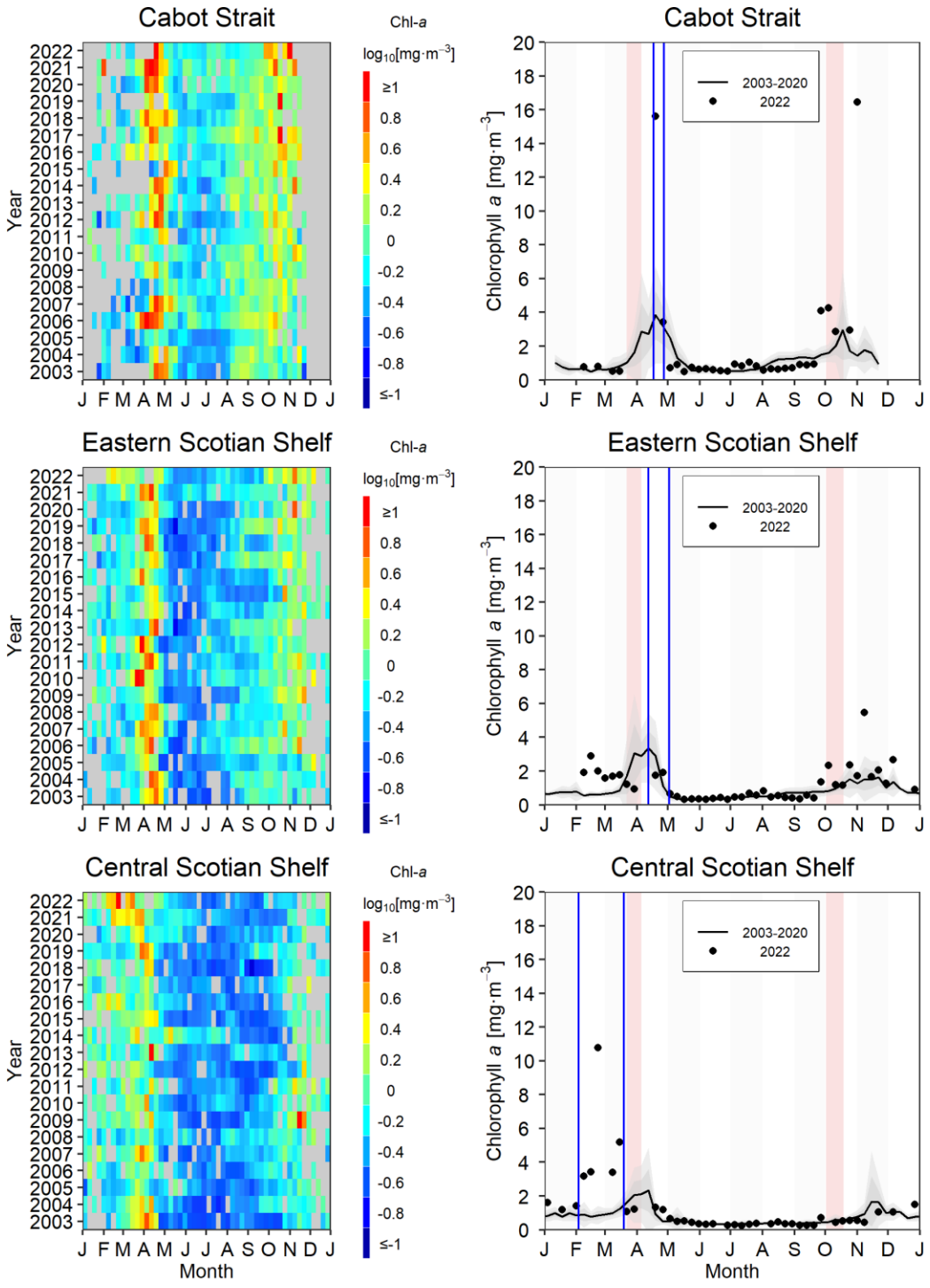

Figure 18a. Surface chlorophyll-a concentrations from remote sensing ocean colour data in the Maritimes sub-regions. Left panels: Time series of weekly mean surface chlorophyll-a concentrations; gray pixels indicate missing data. Right panels: Weekly mean surface chlorophyll-a concentrations; the solid circles represent the 2022 data; the solid line represent the weekly climatological means for the reference period 2003-2020; the gray shaded ribbons represent the standard deviation (±0.5 and ±1 sd) of the weekly means; the vertical blue lines delimit the period of the spring bloom as calculated by the PhytoFit application; the pink vertical stripe indicates the timing of the spring and fall missions. Tick marks on the horizontal axes indicate the 1st day of the month.

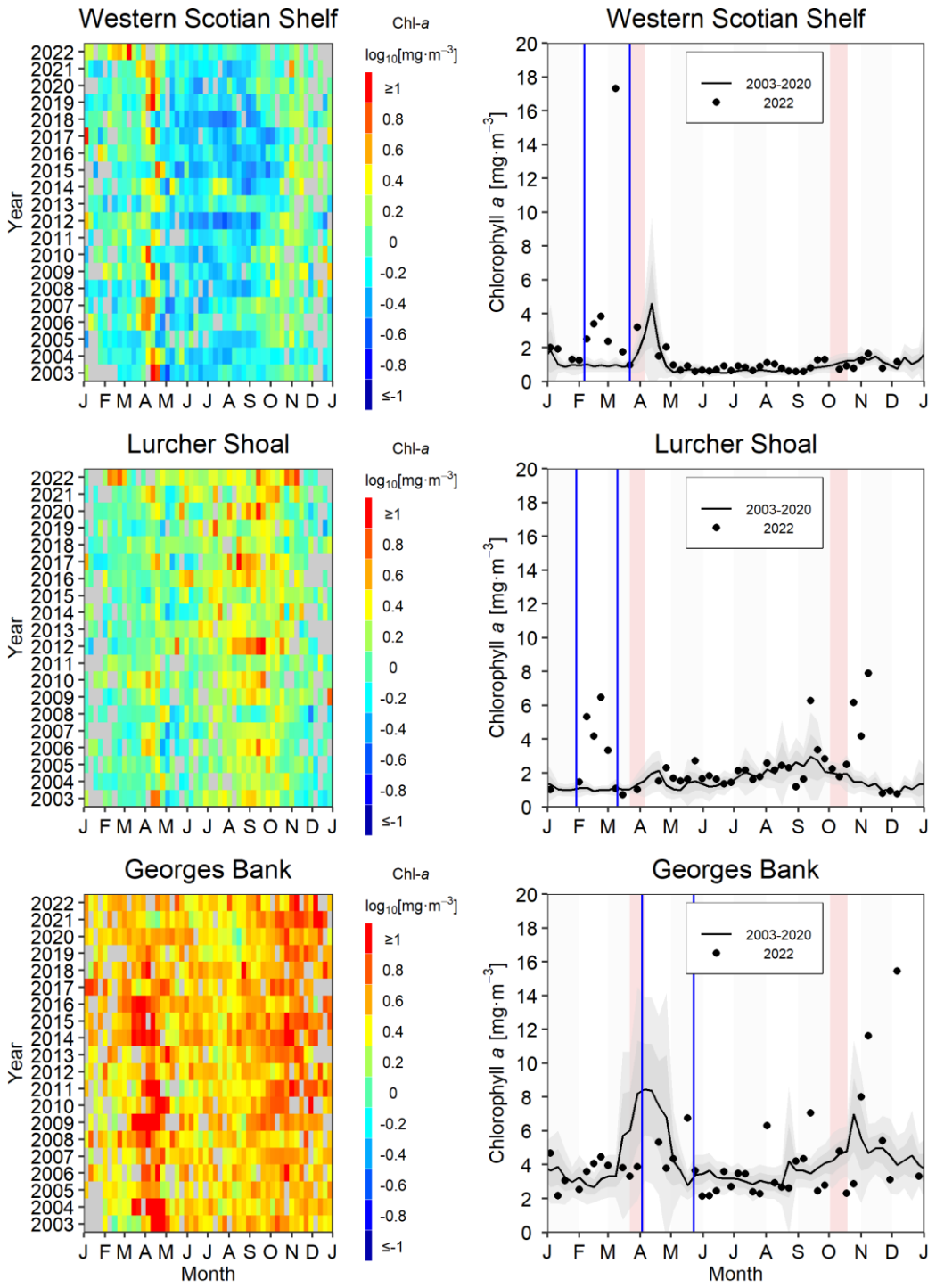

Figure 18b. Surface chlorophyll-a concentrations from remote sensing ocean colour data in the Maritimes sub-regions. Left panels: Time series of weekly mean surface chlorophyll-a concentrations; gray pixels indicate missing data. Right panels: Weekly mean surface chlorophyll-a concentrations; the solid circles represent the 2022 data; the solid line represent the weekly climatological means for the reference period 2003-2020; the gray shaded ribbons represent the standard deviation (±0.5 and ±1 sd) of the weekly means; the vertical blue lines delimit the period of the spring bloom as calculated by the PhytoFit application; the pink vertical stripe indicates the timing of the spring and fall missions. Tick marks on the horizontal axes indicate the 1st day of the month.

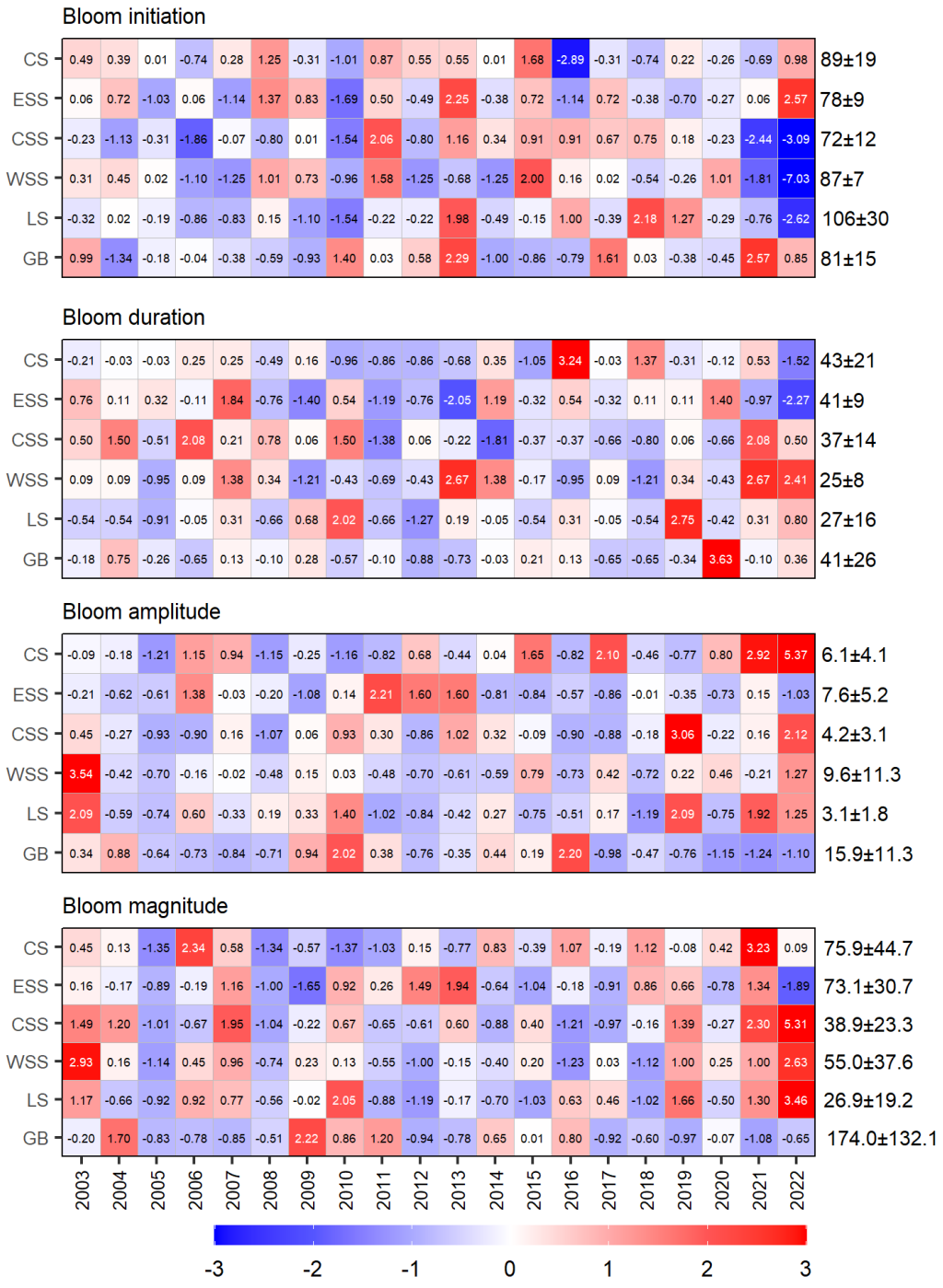

Figure 19. Annual anomaly scorecards for spring phytoplankton bloom metrics. Values in each cell are anomalies from the mean for the reference period 2003–2020, in standard deviation (sd) units (mean and sd listed at right in units of Day-of-Year for initiation, Days for duration, $mg_{chl} \cdot m^{-3}$ for amplitude, and $mg_{chl} \cdot m^{-3} \cdot d$ for magnitude). Red (blue) cells indicate later (earlier) initiation, longer (shorter) duration or higher- (lower-) than-normal amplitude or magnitude.

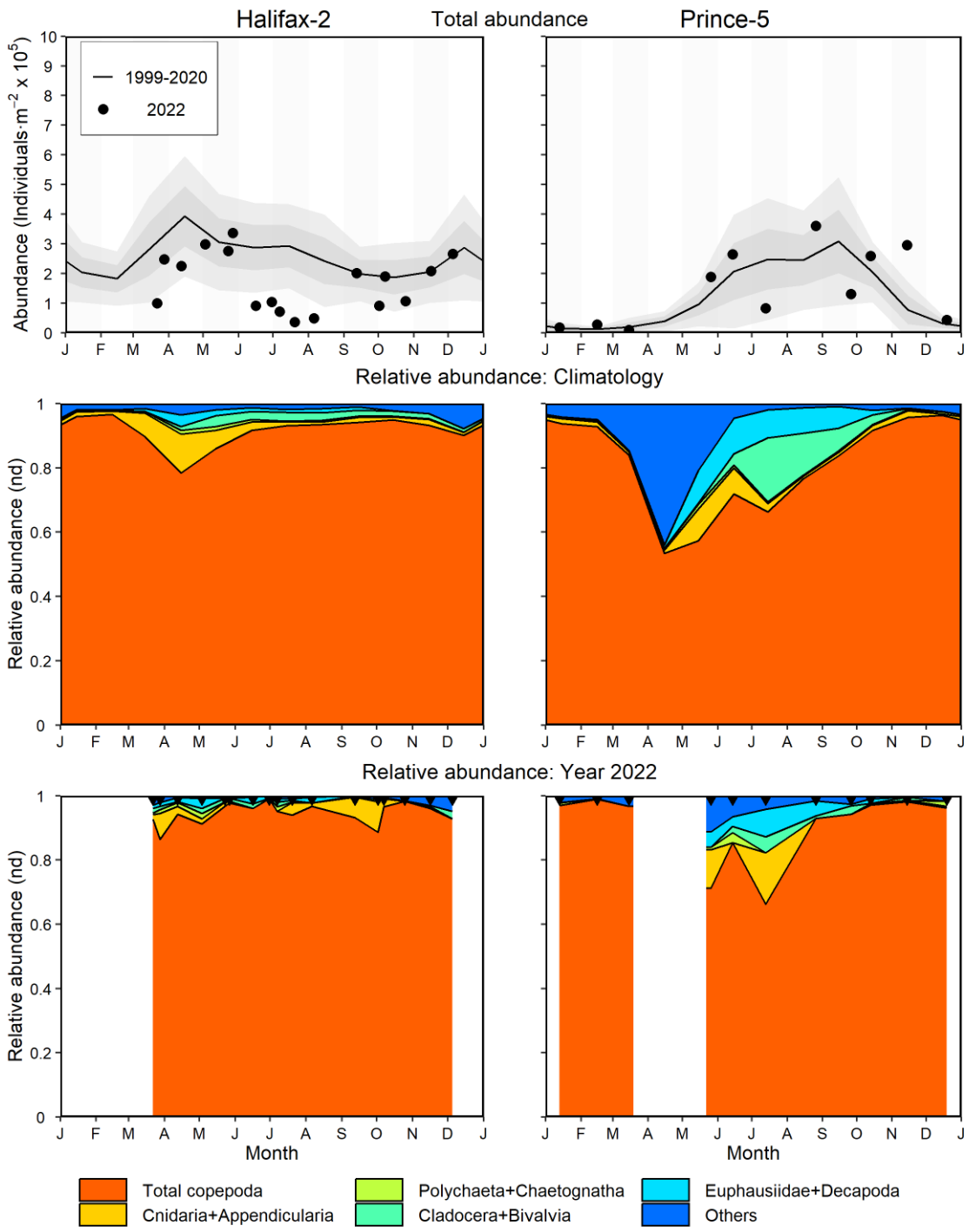

Figure 20. Zooplankton (> 200 µm) abundance and community composition at the Maritimes high-frequency sampling stations. Top panels: Zooplankton abundance; the solid circles represent the 2022 data; the solid line represent the monthly climatological means for the reference period 1999-2020; the gray shaded ribbons represent the standard deviation (±0.5 and ±1 sd) of the monthly means. Middle panels: Climatological mean zooplankton relative abundance for the reference period 1999-2020. Bottom panels: Zooplankton relative abundance in 2022. Black triangles in the bottom panels indicate sampling dates. Tick marks on the horizontal axes indicate the 1st day of the month. White areas indicate no data.

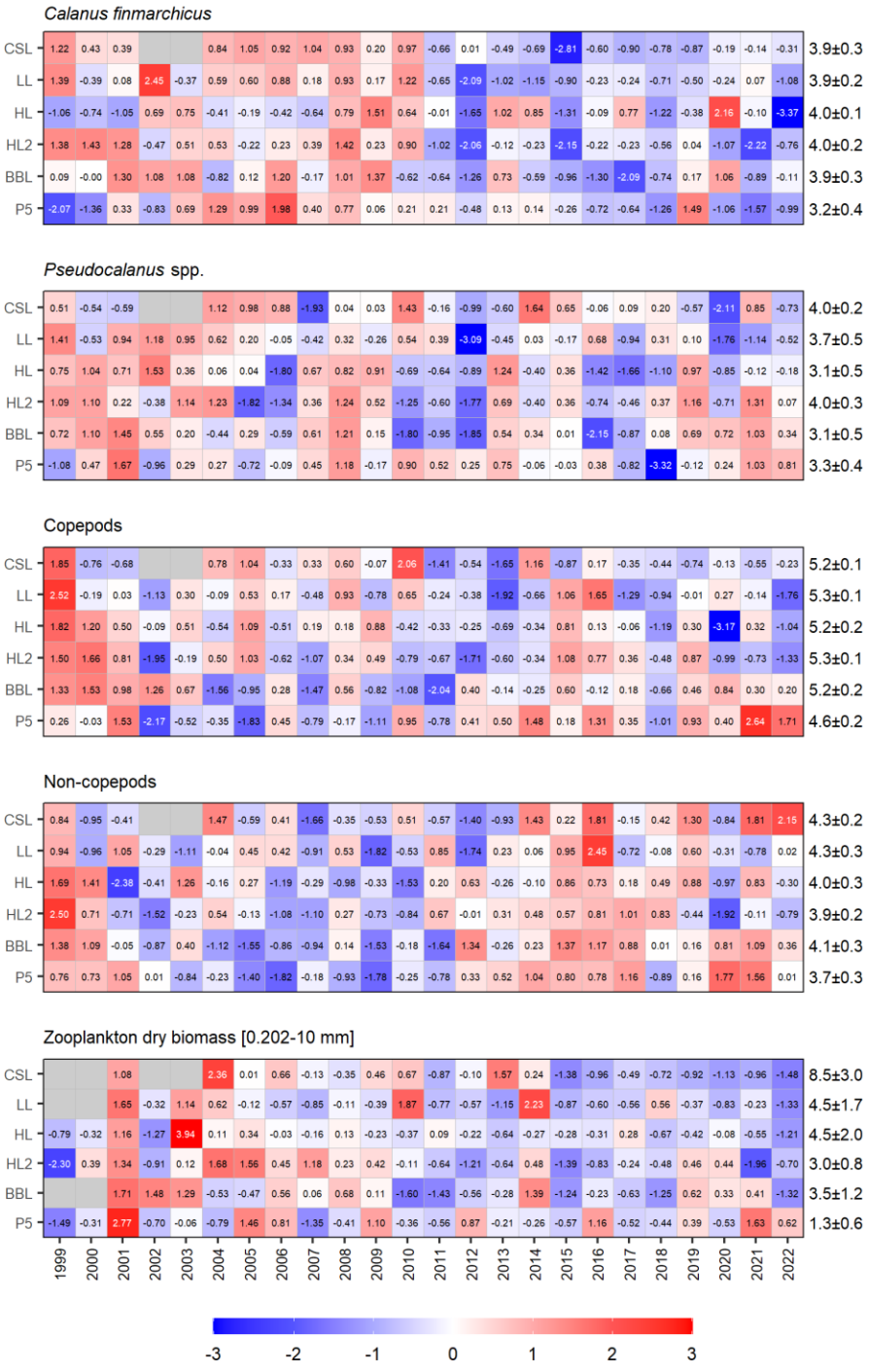

Figure 21. Annual anomaly scorecards for zooplankton abundance and biomass. Values in each cell are anomalies from the mean for the reference period 1999–2020, in standard deviation (sd) units (mean and sd listed at right in units of log_{10}(individuals·m^{-2}+1) for abundance and g·m^{-2} for biomass). Red (blue) cells indicate higher- (lower-) than-normal abundances or biomass. Gray cells indicate missing data. CSL: Cabot Strait section; LL: Louisbourg section; HL: Halifax section; HL2: Halifax-2; BBL: Browns Bank section; P5: Prince-5.

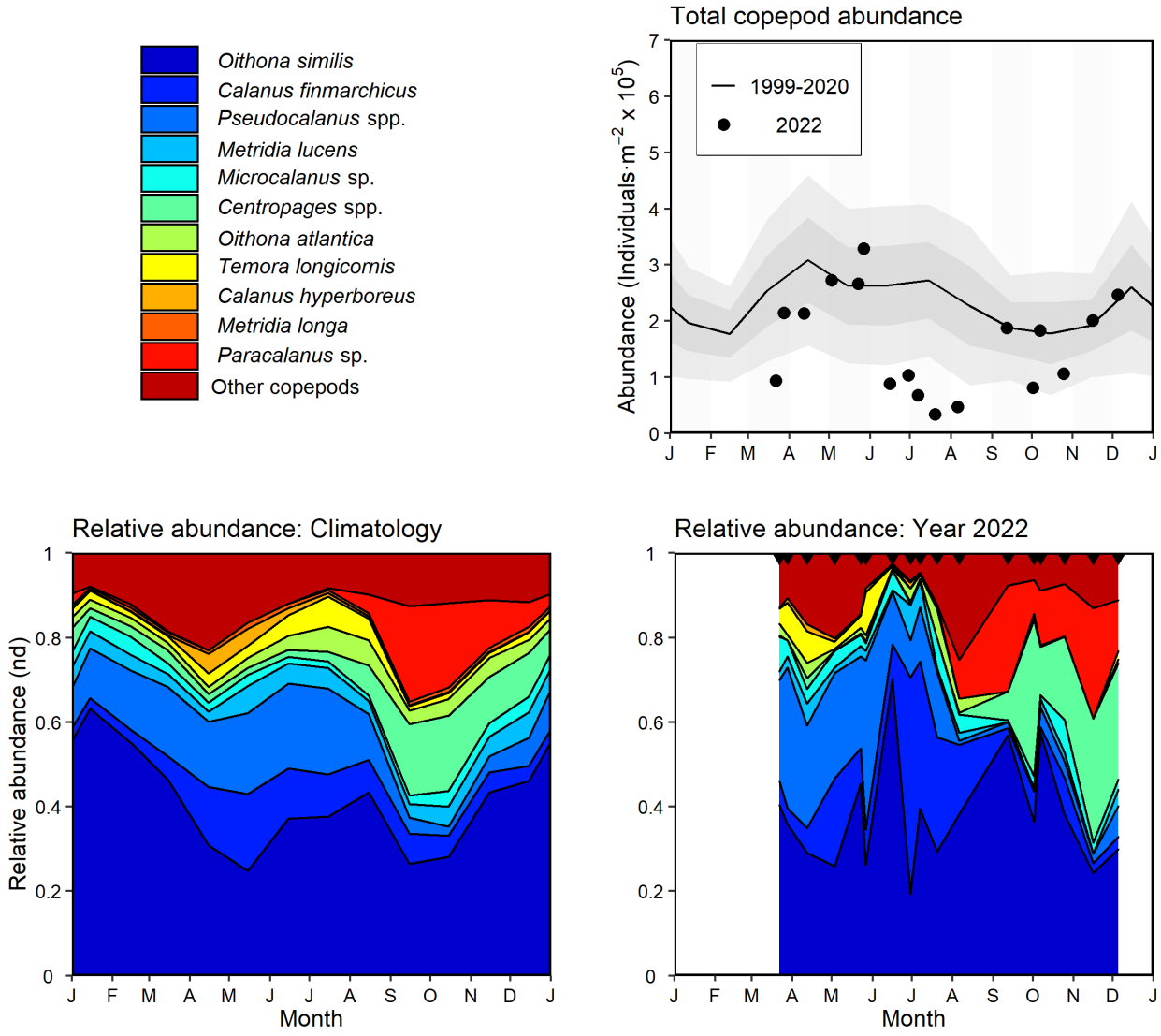

Figure 22a. Copepod abundance and composition at Halifax-2; the top 95% copepod taxa by abundance (ordered from most to least abundant) are shown individually; unidentified copepods (mostly nauplii) are grouped as "others". Top right panel: Copepod abundance; the solid circles represent the 2022 data; the solid line represent the monthly climatological means for the reference period 1999-2020; the gray shaded ribbons represent the standard deviation (±0.5 and ±1 sd) of the monthly means. Bottom left panel: Climatological mean copepod relative abundance for the reference period 1999-2020. Bottom right panel: Copepod relative abundance in 2022. Black triangles in the bottom right panel indicate sampling dates. Tick marks on the horizontal axes indicate the 1st day of the month. White areas indicate no data.

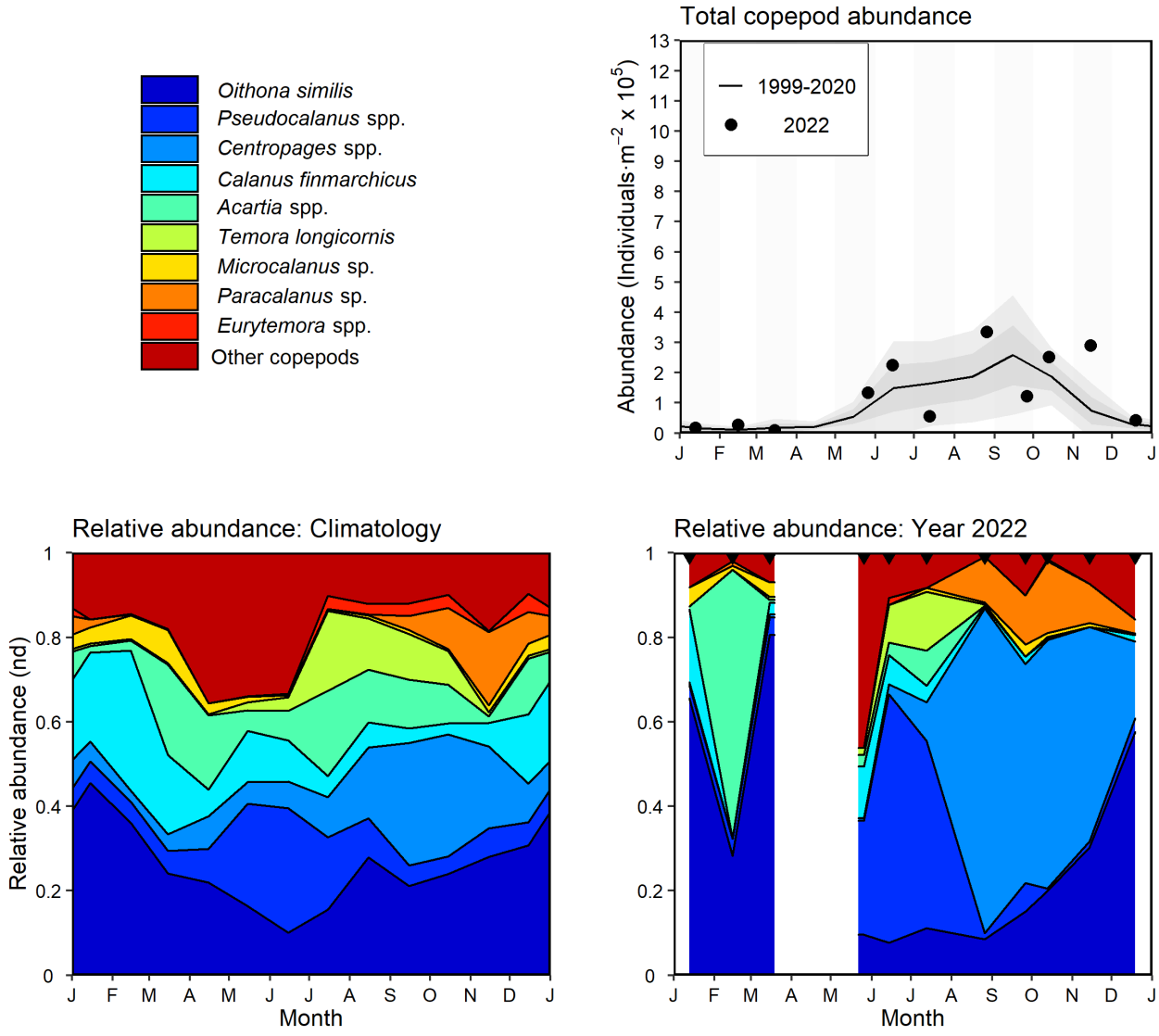

Figure 22b. Copepod abundance and composition at Prince-5; the top 95% copepod taxa by abundance (ordered from most to least abundant) are shown individually; unidentified copepods (mostly nauplii) are grouped as "others". Top right panel: Copepod abundance; the solid circles represent the 2022 data; the solid line represent the monthly climatological means for the reference period 1999-2020; the gray shaded ribbons represent the standard deviation (±0.5 and ±1 sd) of the monthly means. Bottom left panel: Climatological mean copepod relative abundance for the reference period 1999-2020. Bottom right panel: Copepod relative abundance in 2022. Black triangles in the bottom right panel indicate sampling dates. Tick marks on the horizontal axes indicate the 1st day of the month. White areas indicate no data.

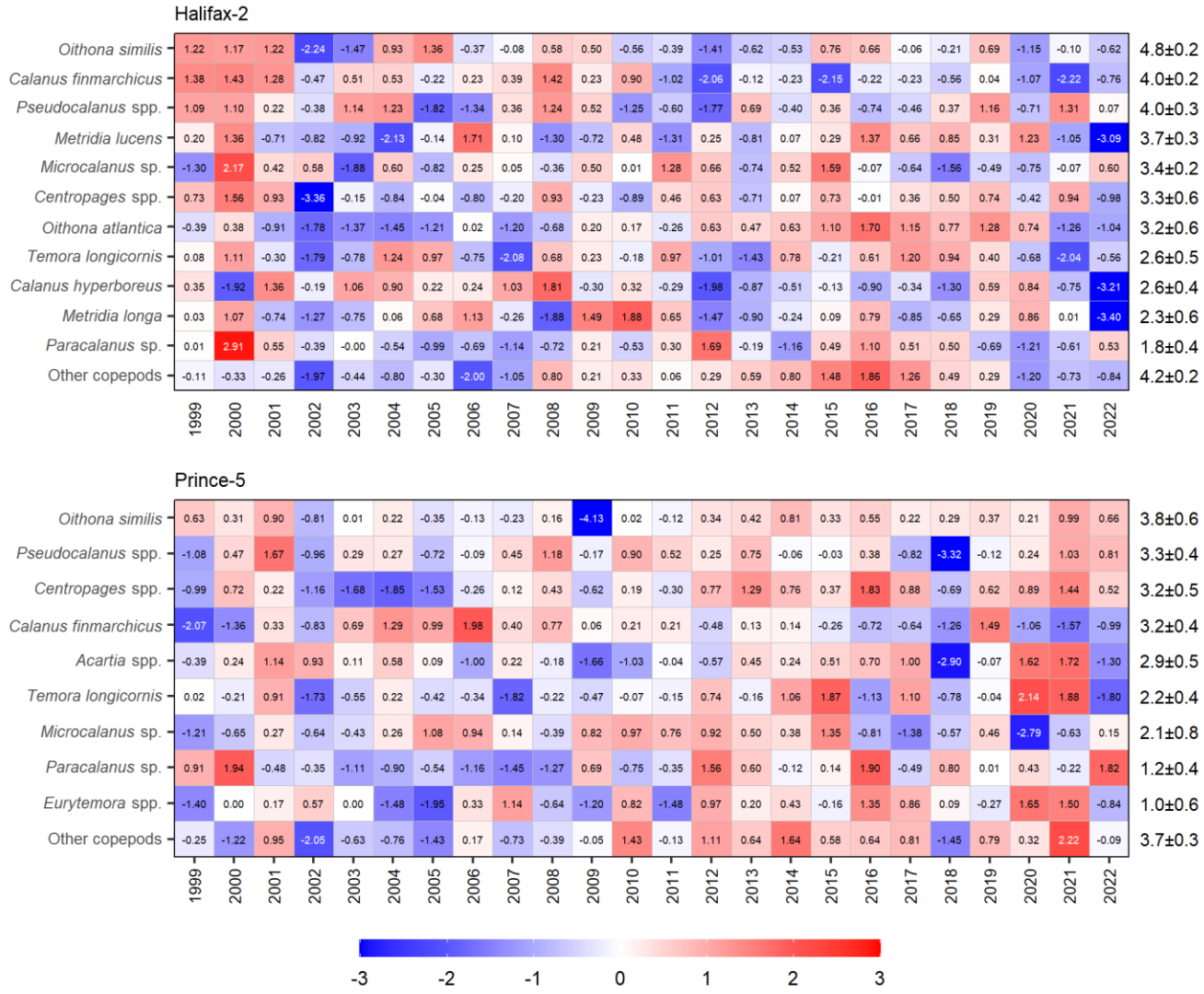

Figure 23. Annual anomaly scorecards for the top 95% of copepod taxa by abundance (ordered from most to least abundant) at the Maritimes high-frequency sampling stations. Values in each cell are anomalies from the mean for the reference period 1999–2020, in standard deviation (sd) units (mean and sd listed at right in units of log_{10}(individuals·m^{-2}+1)). Red (blue) cells indicate higher- (lower-) than-normal abundances.

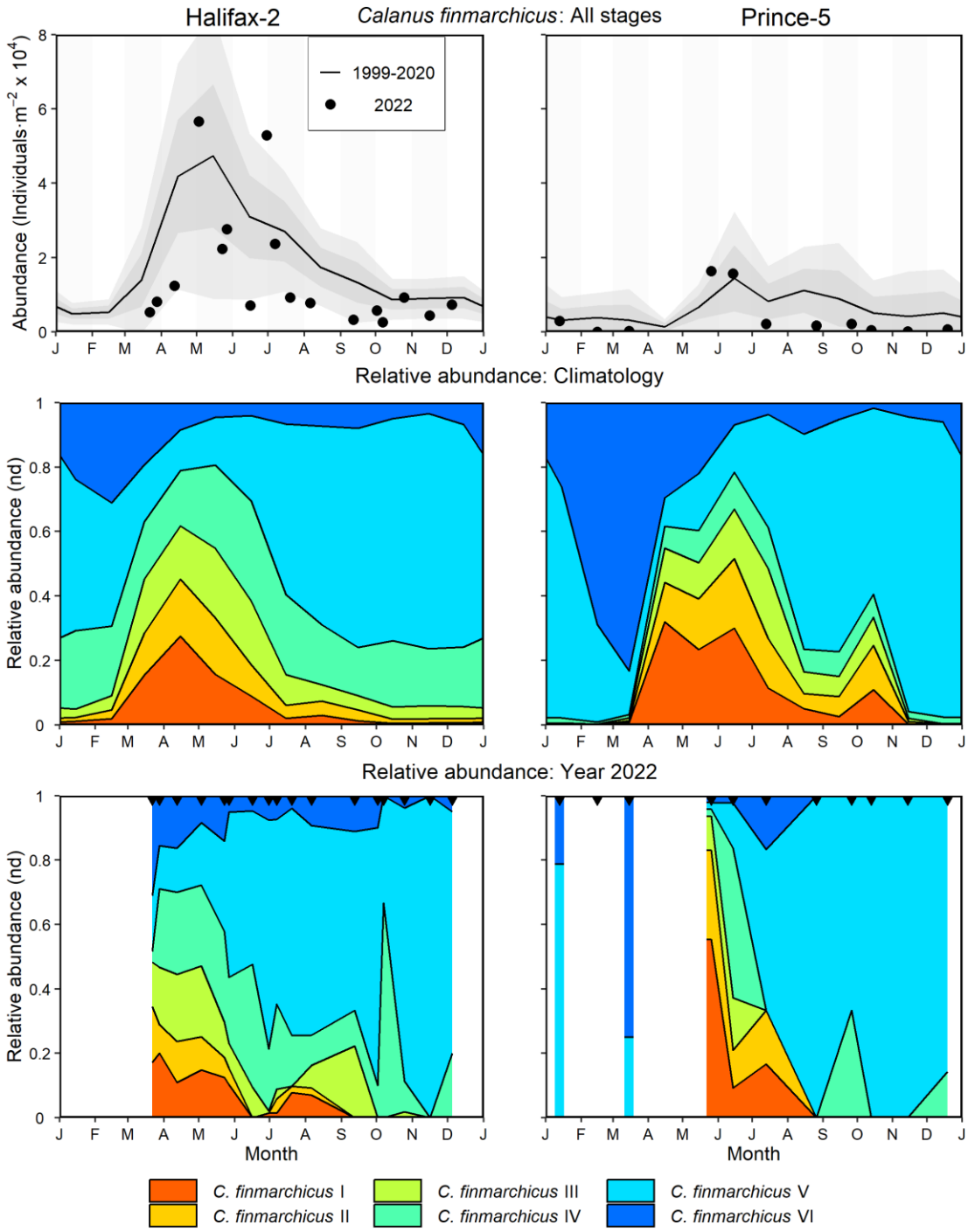

Figure 24. Calanus finmarchicus abundance and developmental stage distribution at the Maritimes high-frequency sampling stations. Top panels: C. finmarchicus abundance; the solid circles represent the 2022 data; the solid line represent the monthly climatological means for the reference period 1999-2020; the gray shaded ribbons represent the standard deviation (±0.5 and ±1 sd) of the monthly means. Middle panels: Climatological mean C. finmarchicus stage relative abundance for the reference period 1999-2020. Bottom panels: C. finmarchicus stage relative abundance in 2022. Black triangles in the bottom panels indicate sampling dates. Tick marks on the horizontal axes indicate the 1st day of the month. White areas indicate no data.

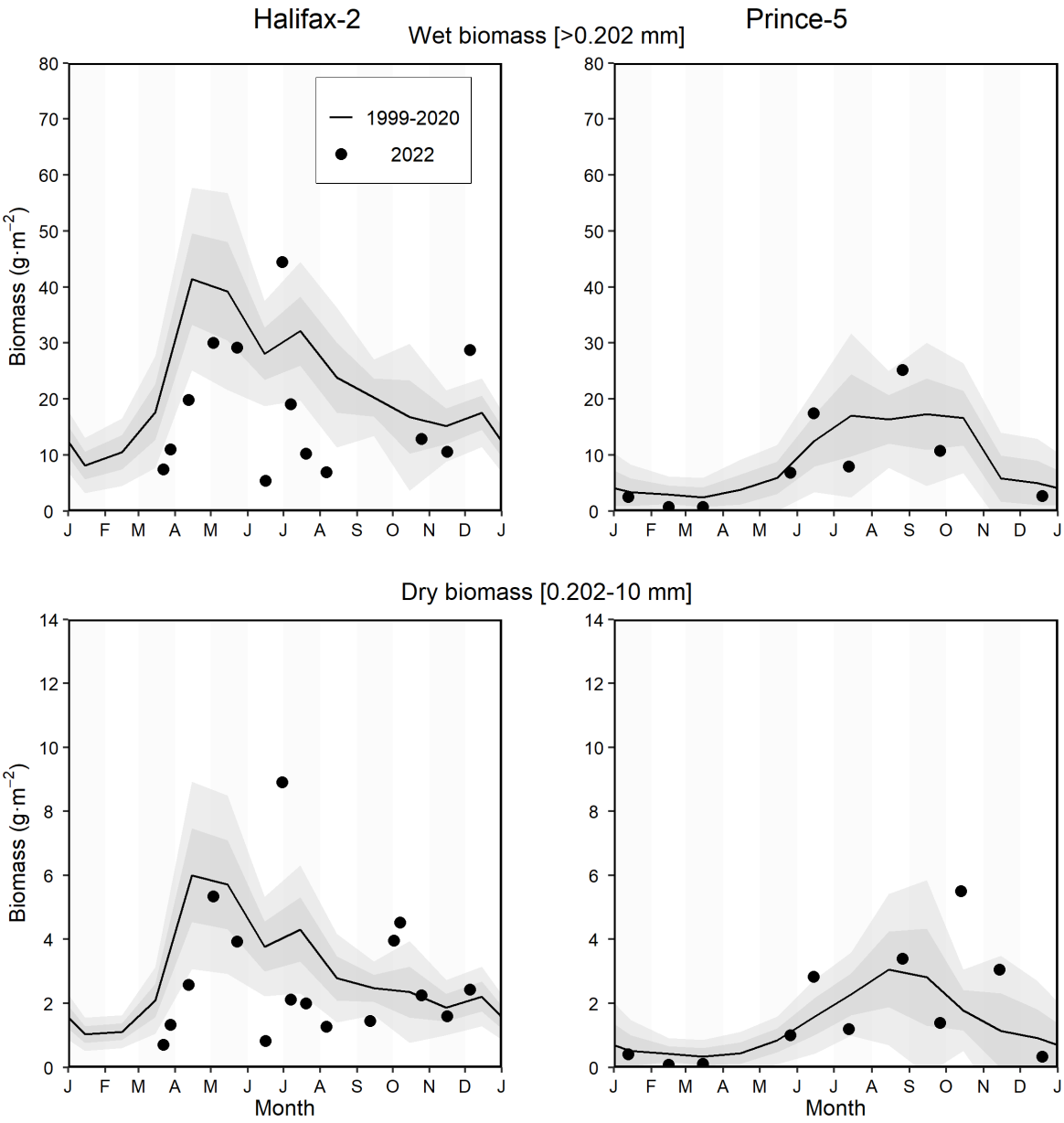

Figure 25. Zooplankton biomass at the Maritimes high-frequency sampling stations. Top panels: Total zooplankton wet biomass. Bottom panels: Mesozooplankton dry biomass. The solid circles represent the 2022 data; the solid line represent the monthly climatological means for the reference period 1999-2020; the gray shaded ribbons represent the standard deviation (±0.5 and ±1 sd) of the monthly means. Tick marks on the horizontal axes indicate the 1st day of the month.

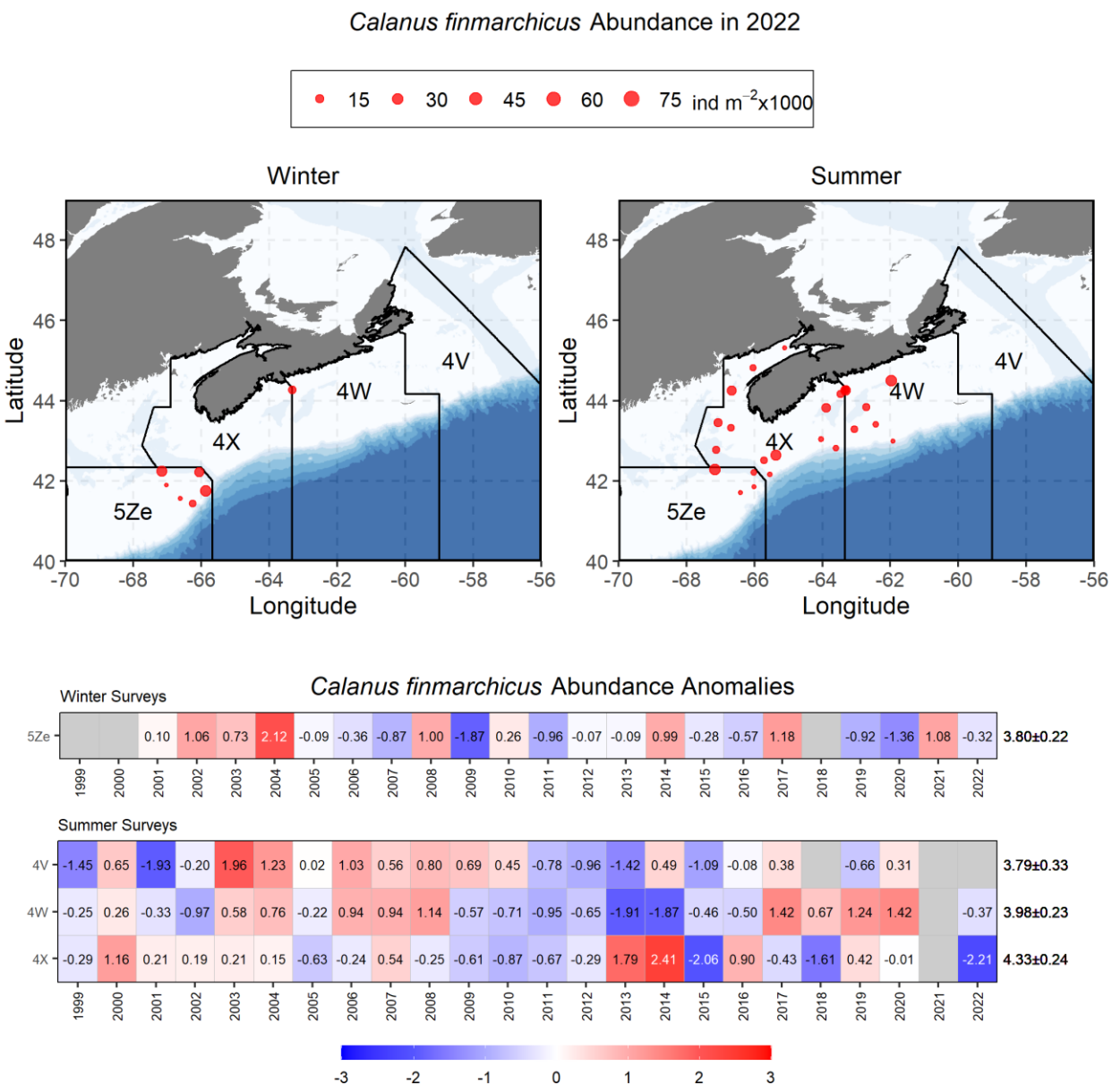

Figure 26. Calanus finmarchicus abundance during the ecosystem trawl surveys. Top panels: Spatial distribution of C. finmarchicus in winter (left) and summer (right) 2022. Middle and bottom panels: Seasonal anomaly scorecards for C. finmarchicus abundance on Georges Bank (5Ze in winter) and the Scotian Shelf and eastern Gulf of Maine (4X, 4W, and 4V in summer); values in each cell are anomalies from the mean for the reference period 1999–2020, in standard deviation (sd) units (mean and sd listed at right in units of $log_{10}(individuals \cdot m^{-2}+1)$). Red (blue) cells indicate higher- (lower-) than-normal abundances. Gray cells indicate missing data.

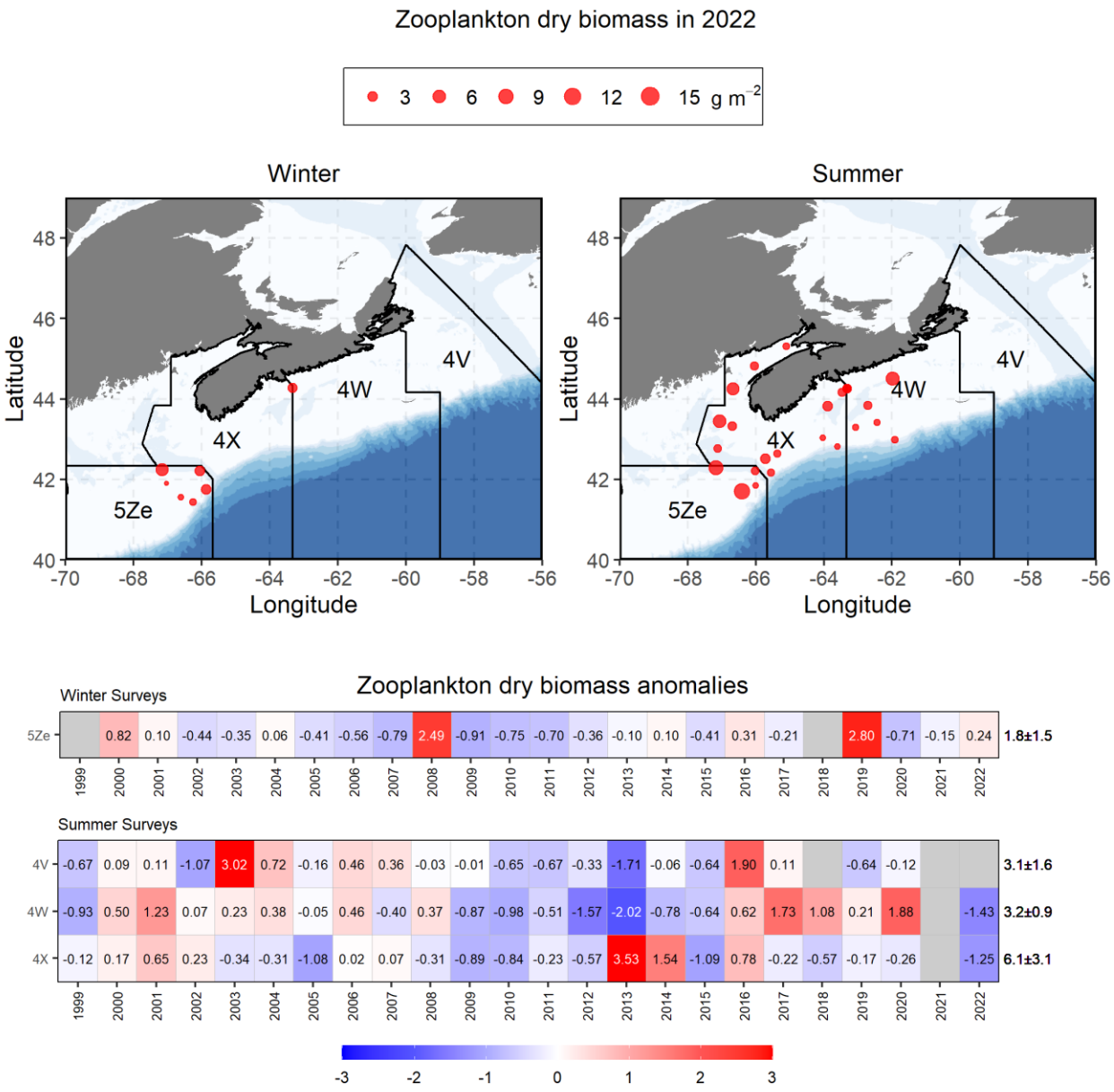

Figure 27. Mesozooplankton dry biomass during the ecosystem trawl surveys. Top panels: Spatial distribution of mesozooplankton dry biomass in winter (left) and summer (right) 2022. Middle and bottom panels: Seasonal anomaly scorecards for mesozooplankton dry biomass on Georges Bank (5Ze in winter) and the Scotian Shelf and eastern Gulf of Maine (4X, 4W, and 4V in summer); values in each cell are anomalies from the mean for the reference period 1999–2020, in standard deviation (sd) units (mean and sd listed at right in units of g·m^{-2}). Red (blue) cells indicate higher- (lower-) than-normal abundances. Gray cells indicate missing data.

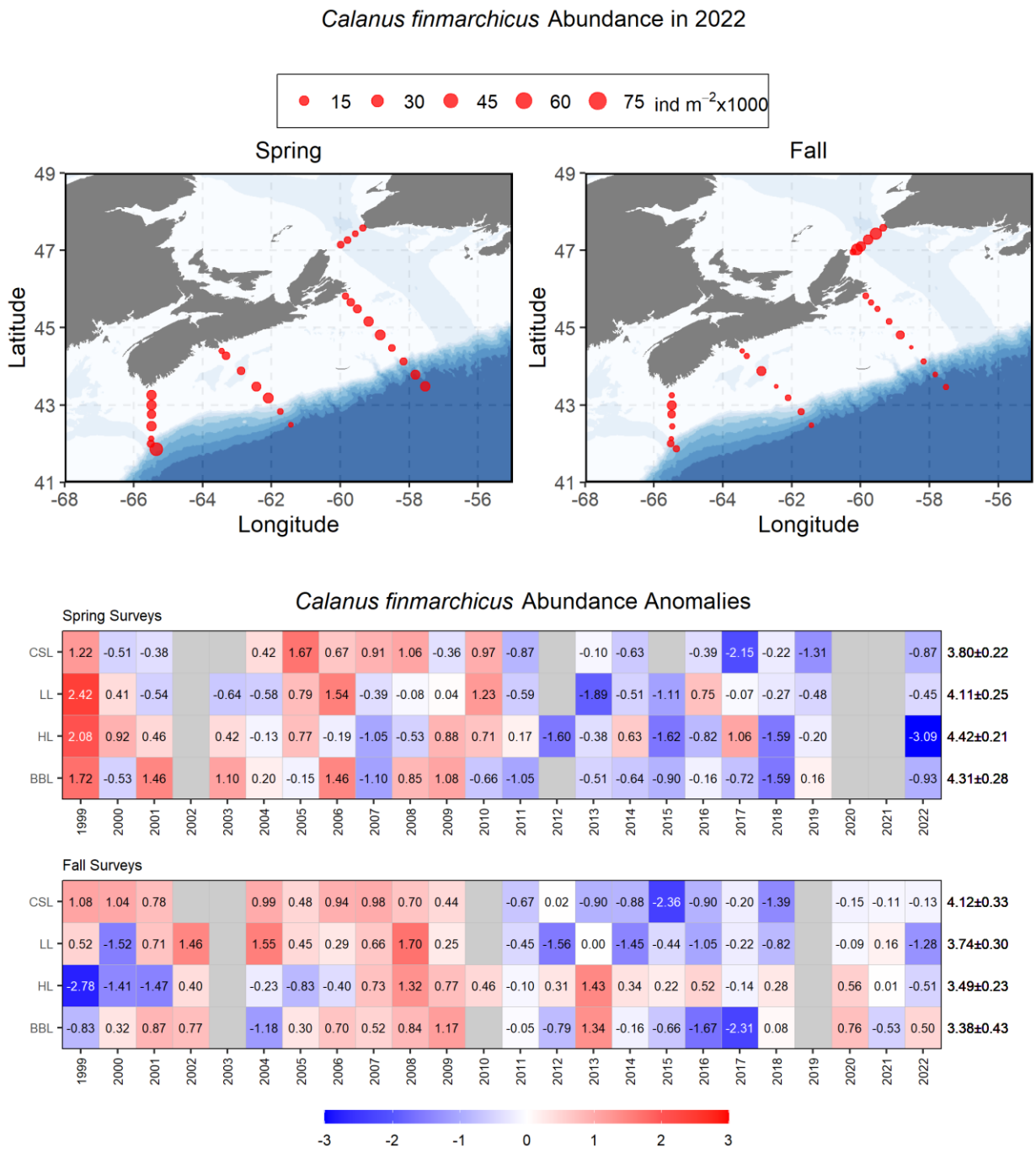

Figure 28. Calanus finmarchicus abundance during the seasonal surveys on the core sections. Top panels: Spatial distribution of C. finmarchicus in spring (left) and fall (right) 2022. Middle and bottom panels: Seasonal anomaly scorecards for C. finmarchicus abundance during spring and fall surveys; values in each cell are anomalies from the mean for the reference period 1999–2020, in standard deviation (sd) units (mean and sd listed at right in units of log_{10}(individuals·m^{-2}+1)). Red (blue) cells indicate higher- (lower-) than-normal abundances. Gray cells indicate missing data.

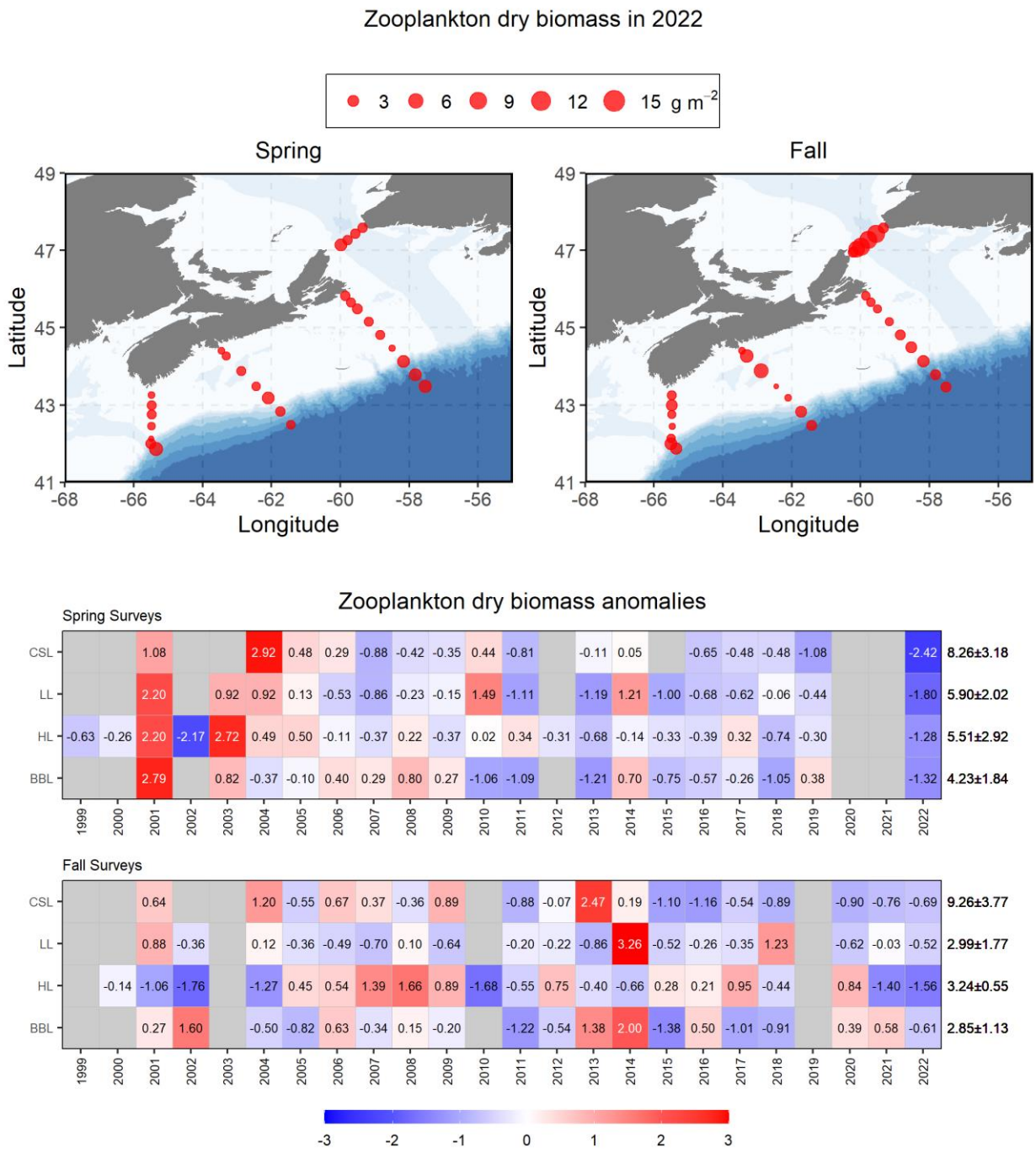

Figure 29. Mesozooplankton dry biomass during the seasonal surveys on the core sections. Top panels: Mesozooplankton dry biomass in spring (left) and fall (right) 2022. Middle and bottom panels: Seasonal anomaly scorecards for mesozooplankton dry biomass during spring and fall surveys; values in each cell are anomalies from the mean for the reference period 1999–2020, in standard deviation (sd) units (mean and sd listed at right in units of g·m^{-2}). Red (blue) cells indicate higher- (lower-) than-normal abundances. Gray cells indicate missing data.

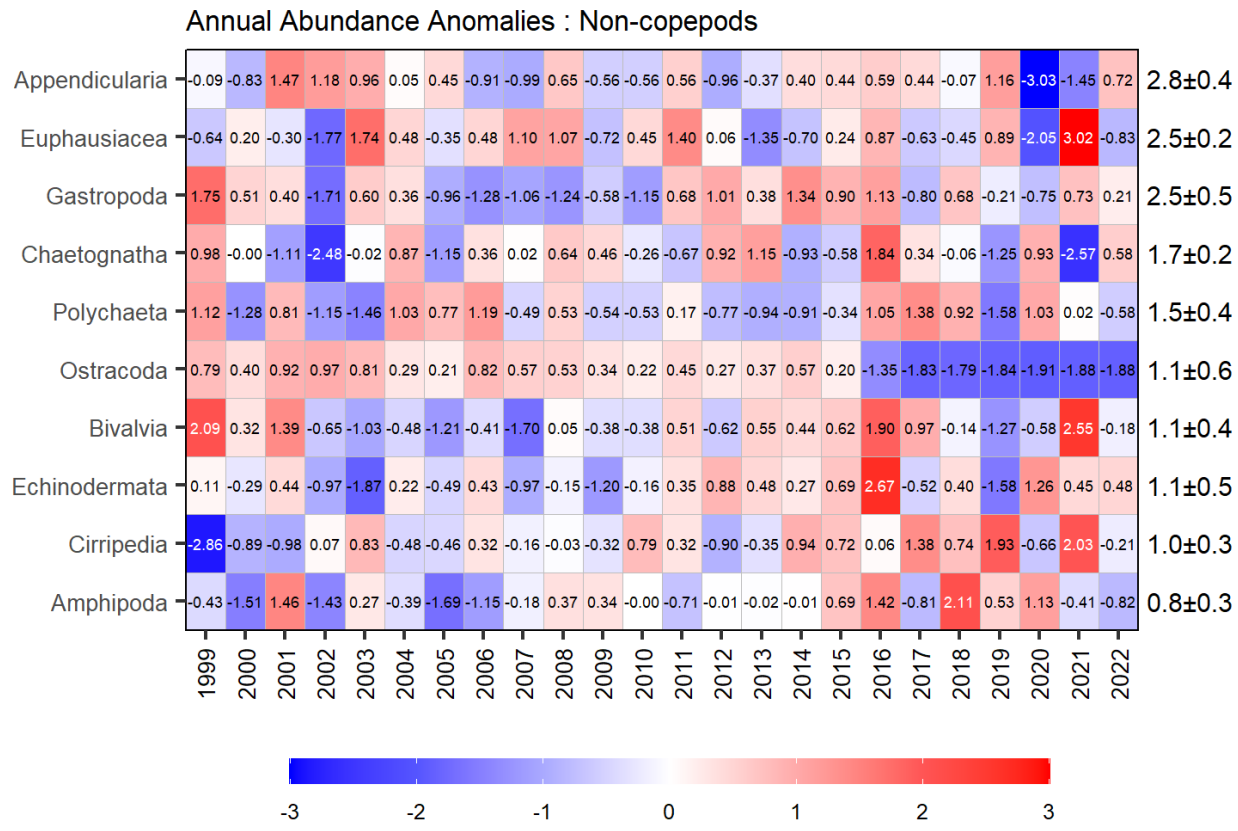

Figure 30. Annual anomaly scorecard for non-copepod groups abundance on the Scotian Shelf sections, ordered from higher to lower abundance. Values in each cell are anomalies from the mean for the reference period 1999–2020, in standard deviation (sd) units (mean and sd listed at right in units of $log_{10}(individuals \cdot m^{-2}+1)$*). Red (blue) cells indicate higher- (lower-) than-normal abundances.*

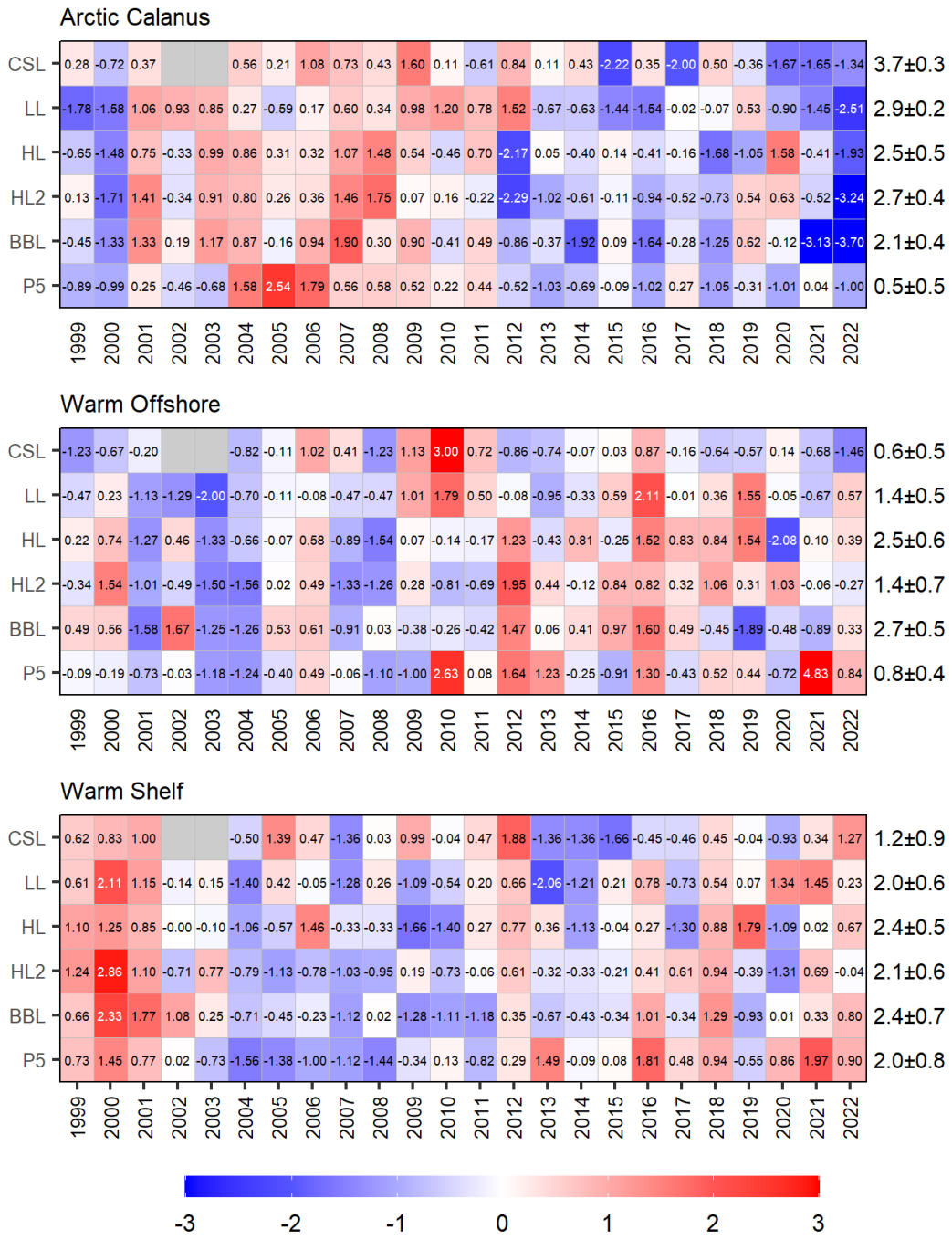

Figure 31. Annual anomaly scorecards for copepod indicator species grouped abundance. Values in each cell are anomalies from the mean for the reference period 1999–2020, in standard deviation (sd) units (mean and sd listed at right in units of log_{10}[individuals·m^{-2}+1]). Red (blue) cells indicate higher- (lower-) than-normal abundances. Gray cells indicate missing data. CSL: Cabot Strait section; LL: Louisbourg section; HL: Halifax section; HL2: Halifax-2; BBL: Browns Bank section; P5: Prince-5.

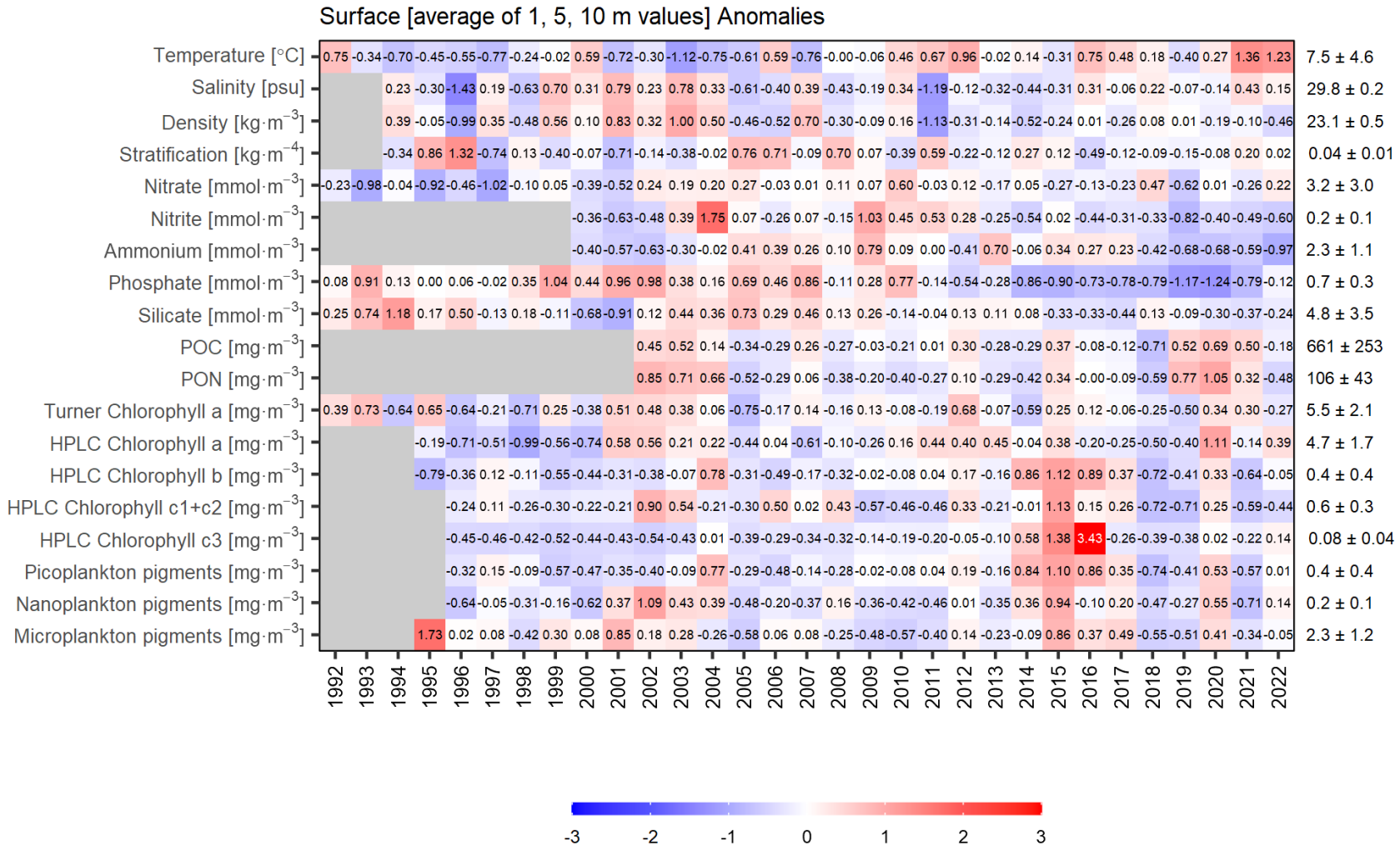

Figure 32. Annual anomaly scorecard for environmental and phytoplankton conditions in the upper water column (1 m, 5 m, and 10 m) in Bedford Basin. Values in each cell are anomalies from the mean for the reference period 1999–2020, in standard deviation (sd) units (mean and sd listed at right). Red (blue) cells indicate higher- (lower-) than-normal levels for a given variable. Gray cells indicate missing data. POC and PON represent particulate organic carbon and nitrogen, respectively.

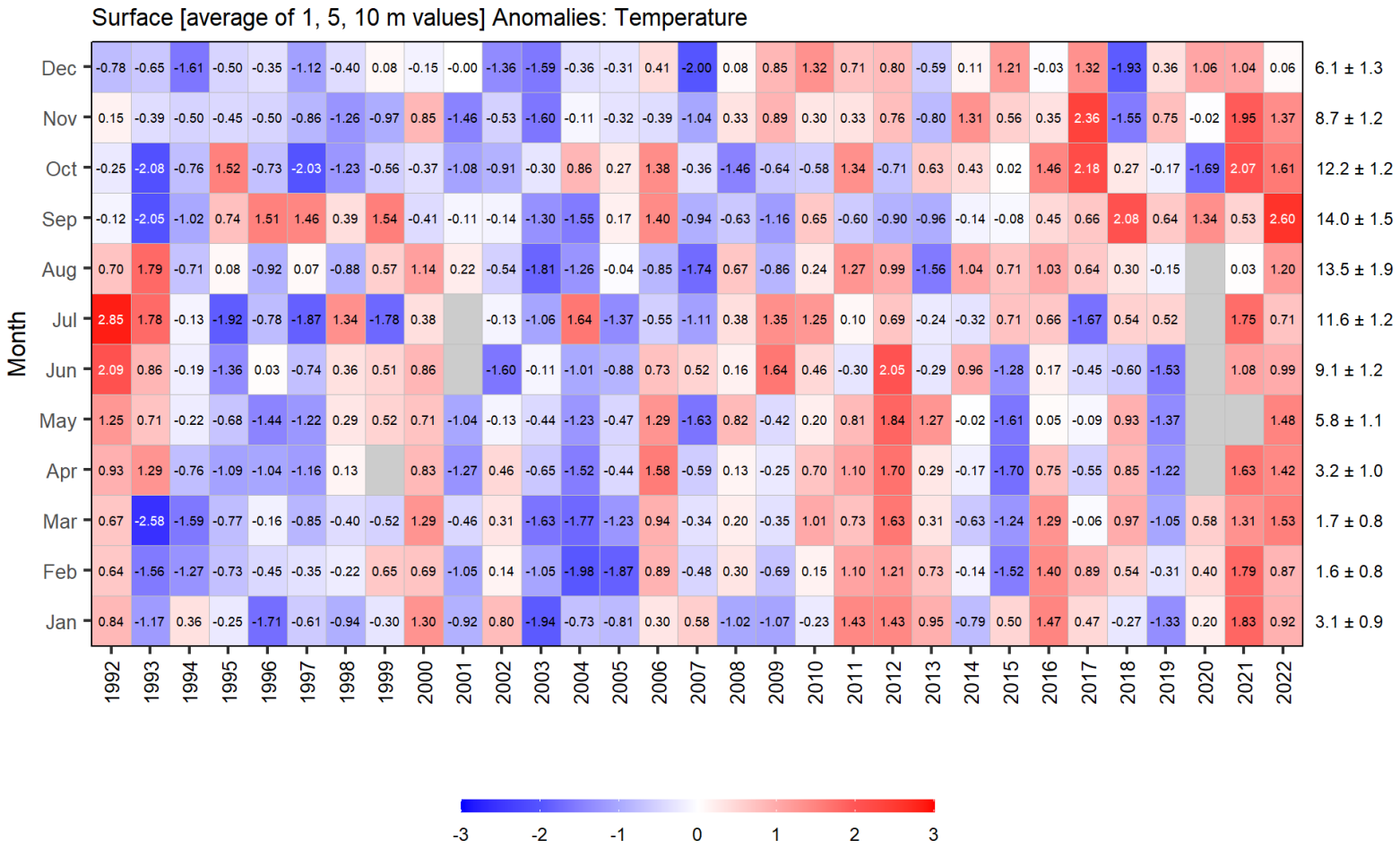

Figure 33. Monthly anomaly scorecard for temperature in the upper water column (1 m, 5 m, and 10 m) in Bedford Basin. Values in each cell are anomalies from the monthly means for the reference period 1999–2020, in standard deviation (sd) units (mean and sd listed at right in units of °C). Red (blue) cells indicate higher- (lower-) than-normal temperature. Gray cells indicate missing data.

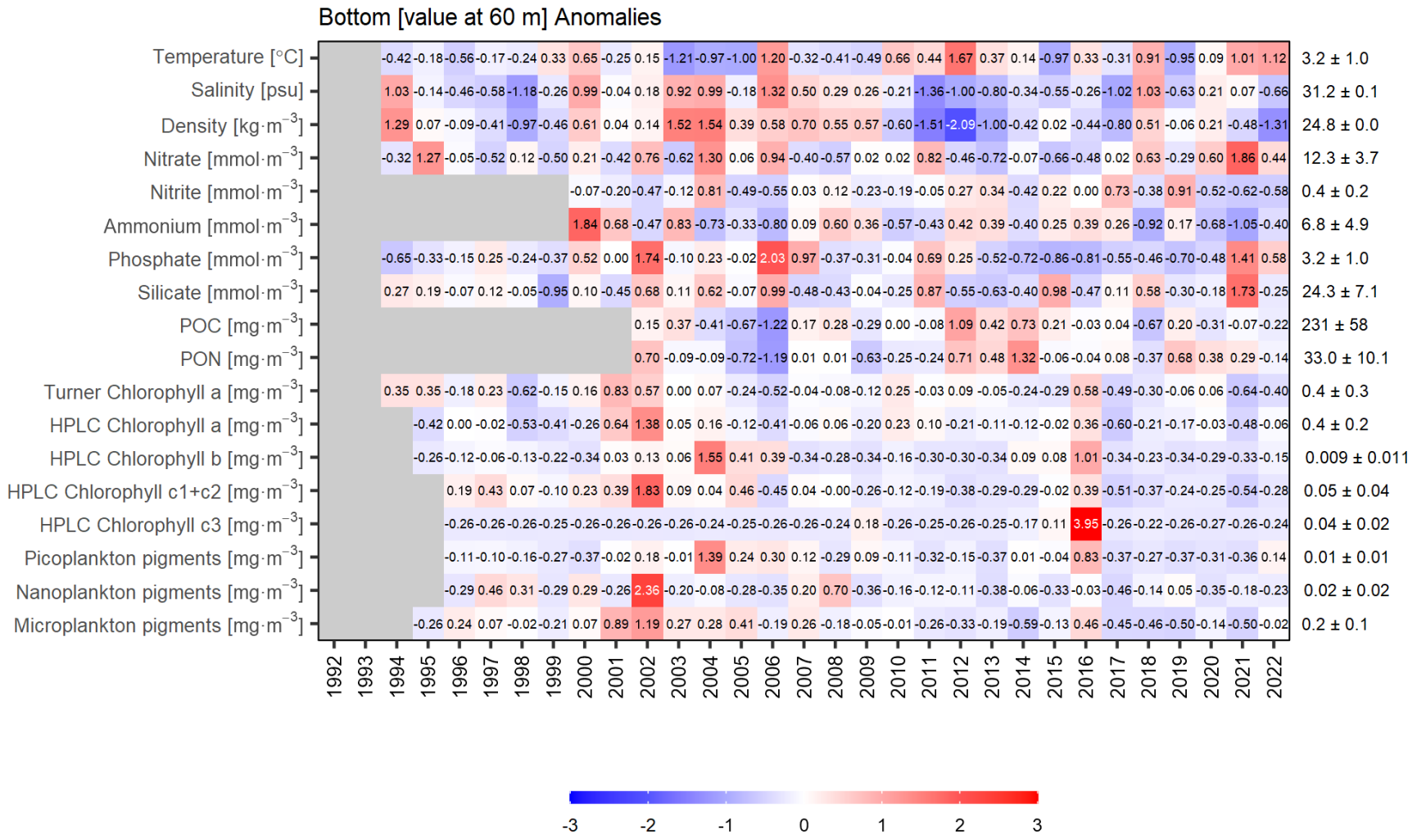

Figure 34. Annual anomaly scorecard for environmental and phytoplankton conditions at 60 m in Bedford Basin. Values in each cell are anomalies from the mean for the reference period 1999–2020, in standard deviation (sd) units (mean and sd listed at right). Red (blue) cells indicate higher- (lower-) than-normal levels for a given variable. Gray cells indicate missing data. POC and PON represent particulate organic carbon and nitrogen, respectively.

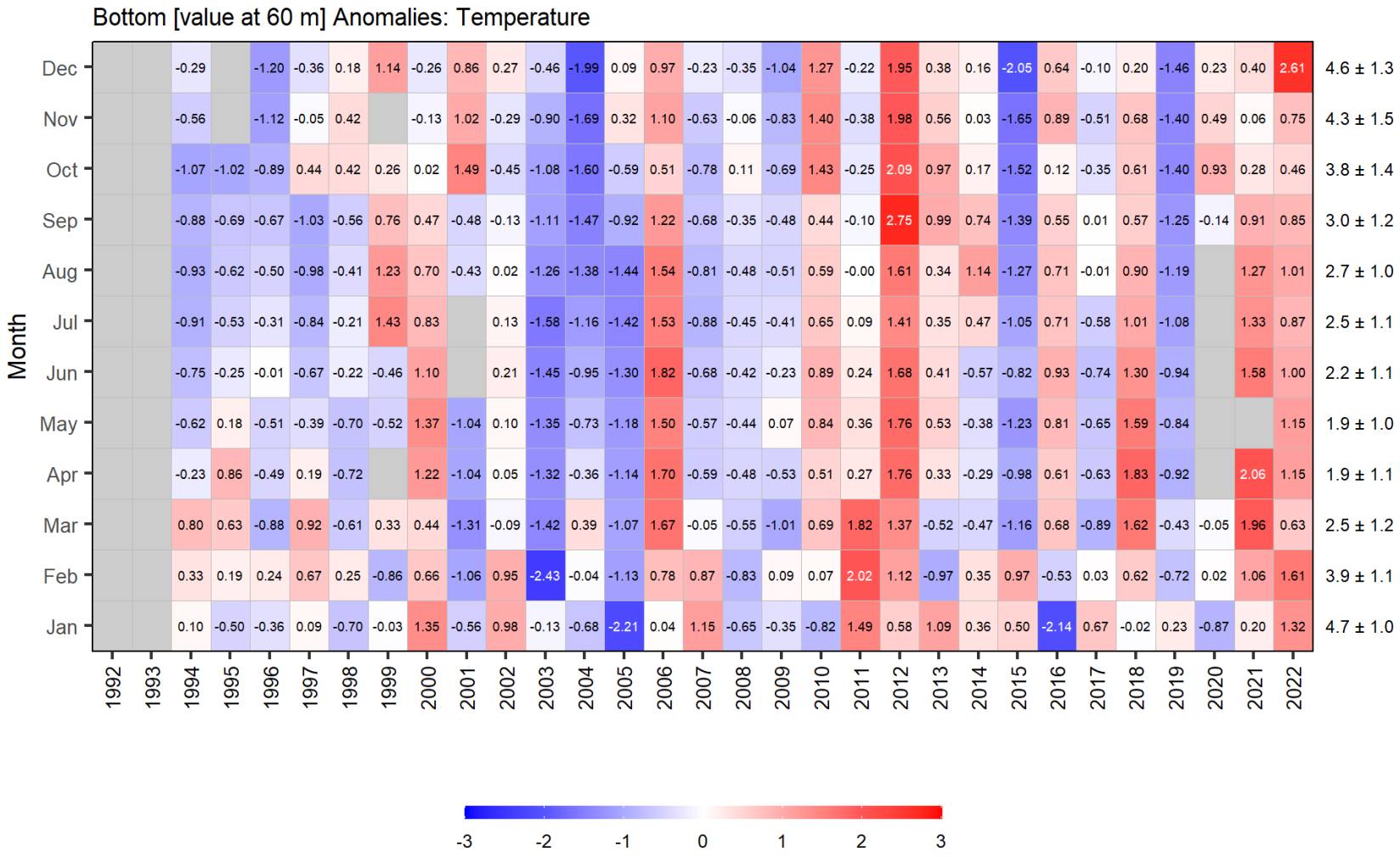

Figure 35. Monthly anomaly scorecard for temperature at 60 m in Bedford Basin. Values in each cell are anomalies from the monthly means for the reference period 1999–2020, in standard deviation (sd) units (mean and sd listed at right in units of °C). Red (blue) cells indicate higher-(lower-) than-normal temperatures. Gray cells indicate missing data.

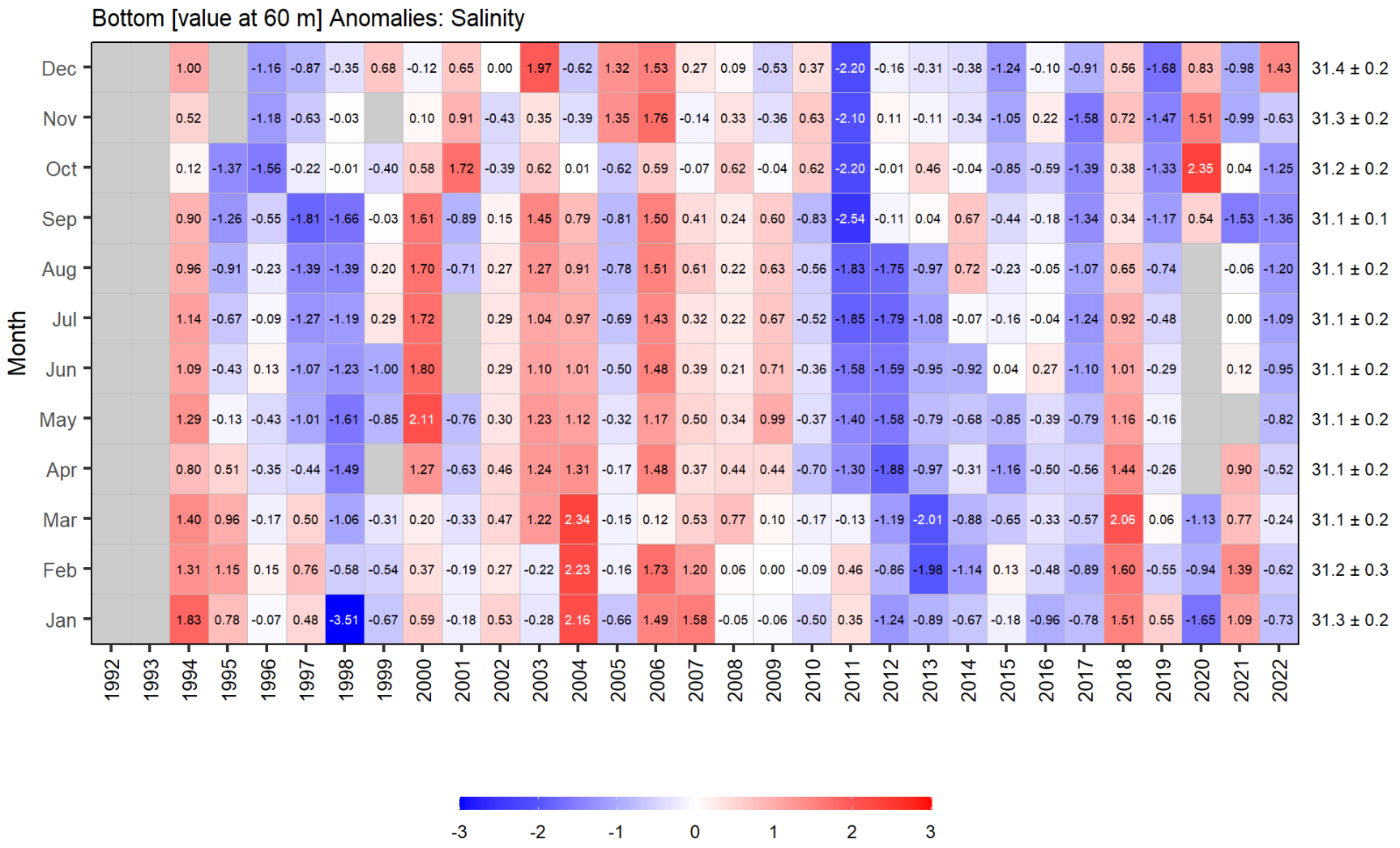

Figure 36. Monthly anomaly scorecard for salinity at 60 m in Bedford Basin. Values in each cell are anomalies from the monthly means for the reference period 1999–2020, in standard deviation (sd) units (mean and sd listed at right in units of psu). Red (blue) cells indicate higher- (lower-) than-normal salinities. Gray cells indicate missing data.

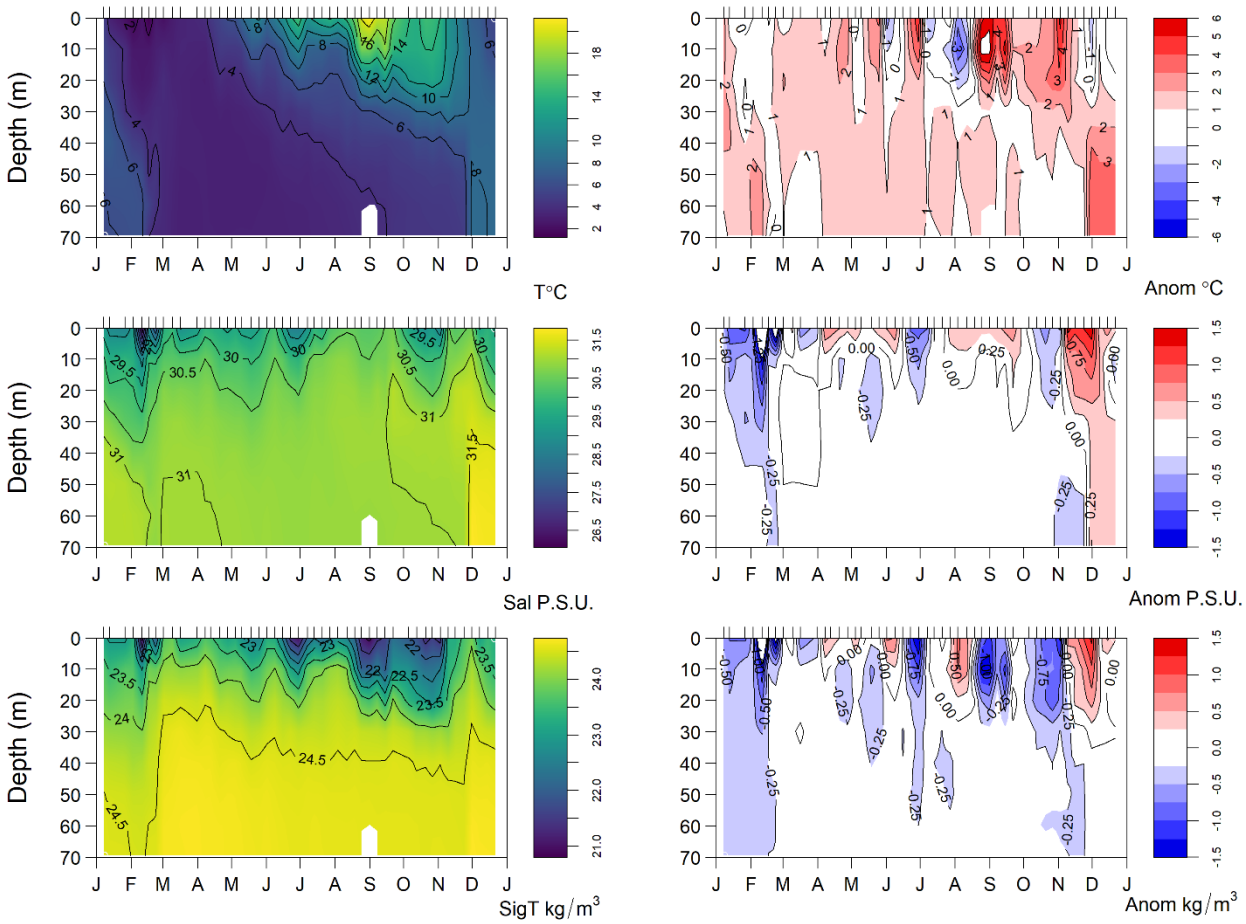

Figure 37. Vertical structure of temperature (top left panel), salinity (middle left panel), and density (bottom left panel) in Bedford Basin in 2022 and their anomalies with respect to 1999–2020 monthly means (right panels). Tick marks on the top horizontal axes indicate sampling dates. Tick marks on the bottom horizontal axes indicate the 1st day of the month.

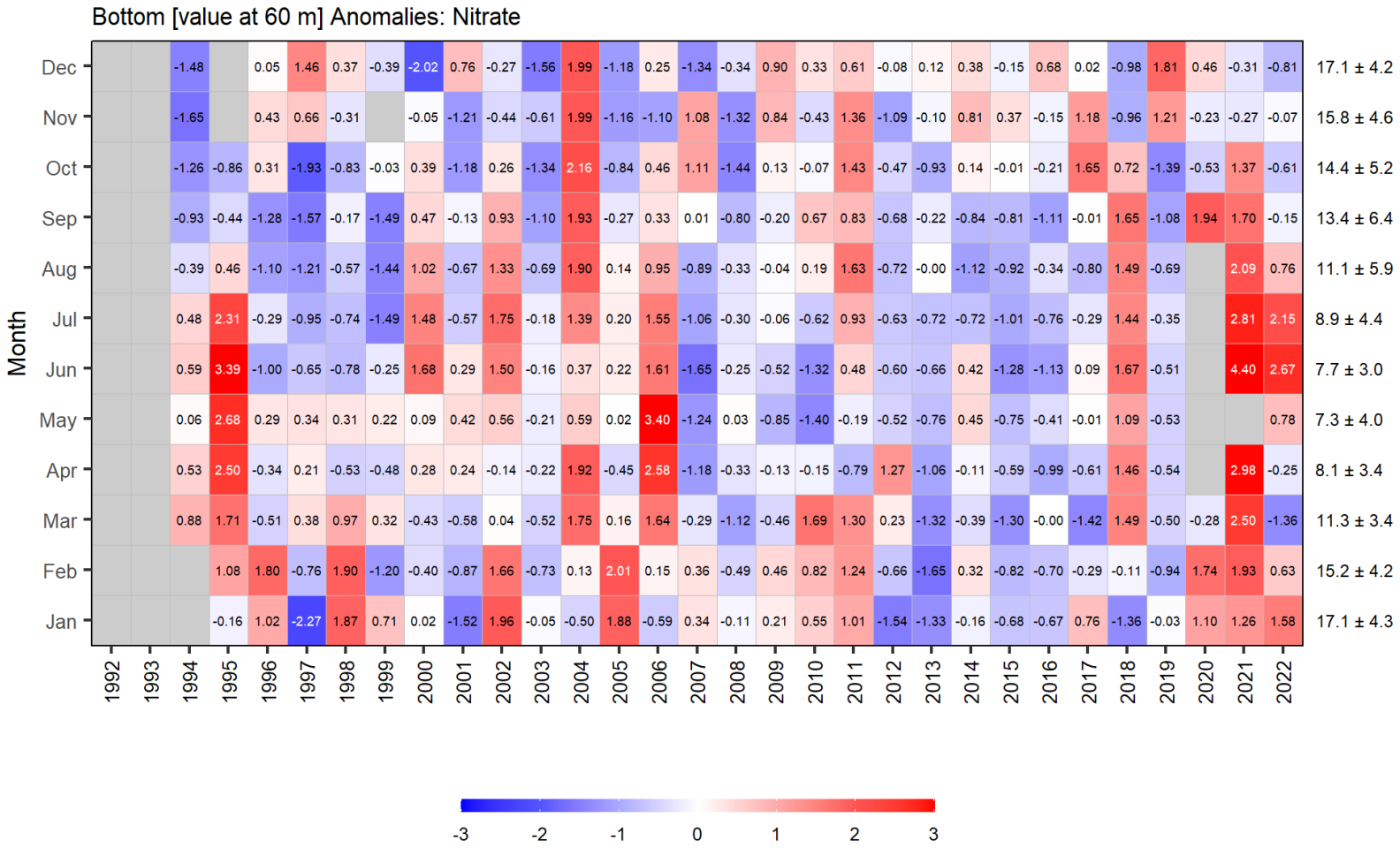

Figure 38. Monthly anomaly scorecard for nitrate at 60 m in Bedford Basin. Values in each cell are anomalies from the monthly means for the reference period 1999–2020, in standard deviation (sd) units (mean and sd listed at right in units of mmol·m^{-3}). Red (blue) cells indicate higher- (lower-) than-normal nitrate concentrations. Gray cells indicate missing data.

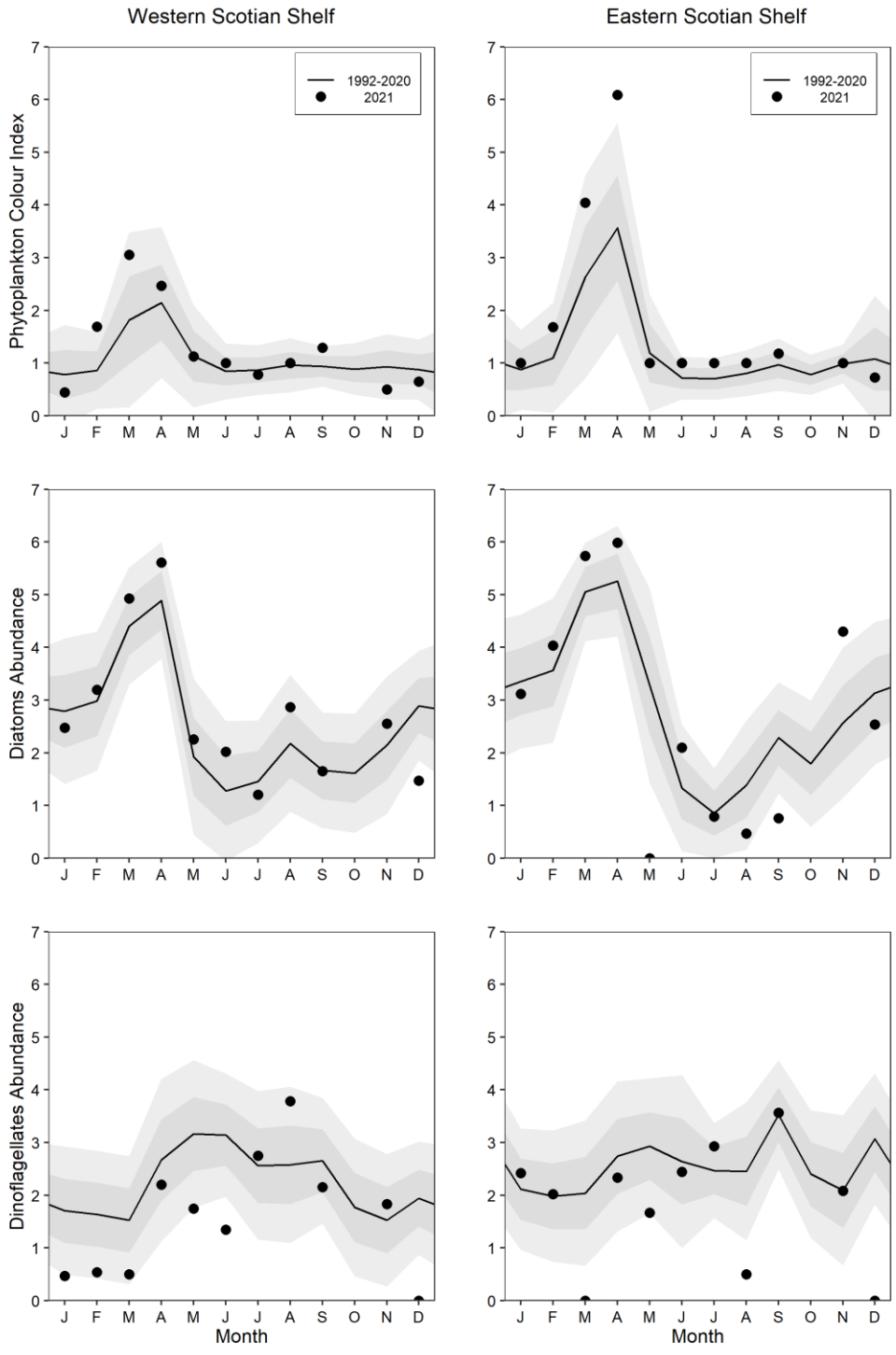

Figure 39. Phytoplankton abundance indices from the Continuous Plankton Recorder surveys on the western (left panels) and eastern (right panels) Scotian Shelf. Top panels: Phytoplankton colour index (PCI). Middle panels: Diatoms abundance. Bottom panels: Dinoflagellates abundance. The solid circles represent the 2021 monthly means; the solid line represent the monthly climatological means for the reference period 1992-2020; the gray shaded ribbons represent the standard deviation (±0.5 and ±1 sd) of the monthly means.

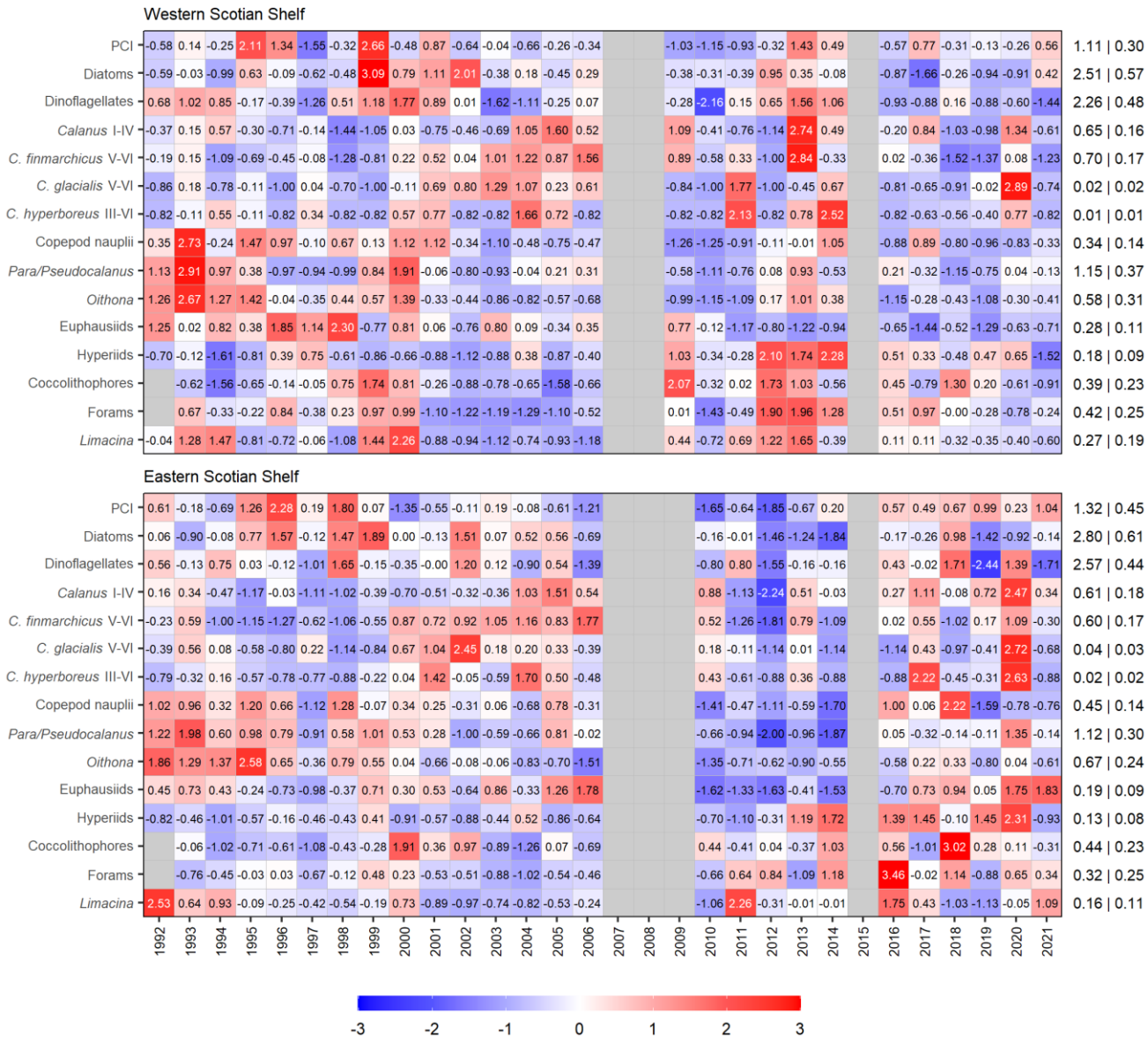

Figure 40. Annual anomaly scorecard for the abundances of phytoplankton and zooplankton taxa observed with the Continuous Plankton Recorder on the eastern Scotian Shelf (top panel) and western Scotian Shelf (bottom panel). Values in each cell are anomalies from the annual means for the reference period 1992–2020, in standard deviation (sd) units (mean and sd listed at right as dimensionless number for PCI and in units of log_{10}(cells·sample^{-1}+1) for phytoplankton abundance and log_{10}(individuals·sample^{-1}+1) for zooplankton abundance). Red (blue) cells indicate higher- (lower-) than-normal abundances. Gray cells correspond to years where either there was sampling in 8 or fewer months, or years where there was a gap in sampling of 3 or more consecutive months.

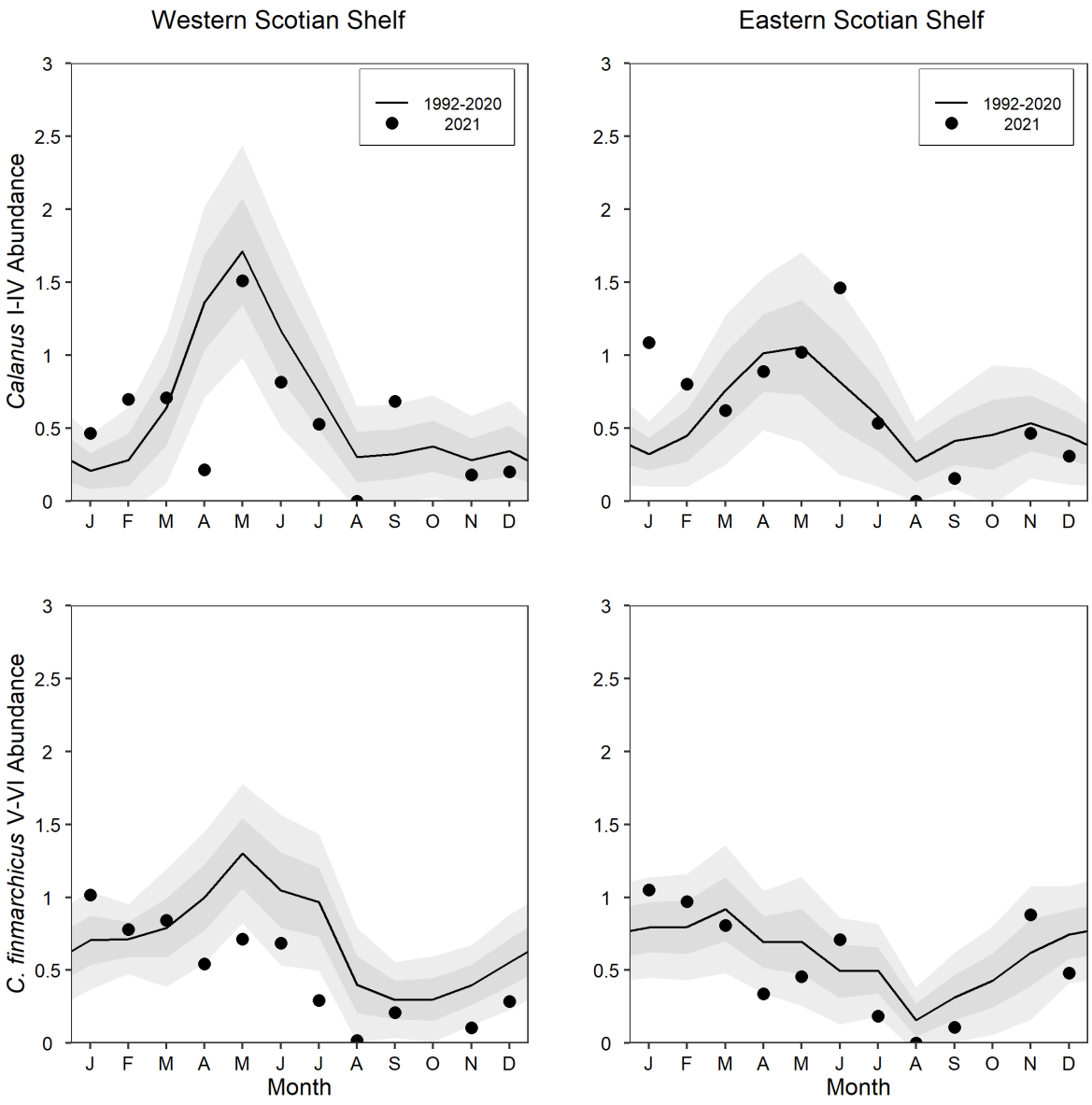

Figure 41. Calanus abundance indices from the Continuous Plankton Recorder surveys on the western (left panels) and eastern (right panels) Scotian Shelf. Top panels: Calanus I-IV abundance. Bottom panels: C. finmarchicus V-VI abundance. The solid circles represent the 2021 monthly means; the solid line represent the monthly climatological means for the reference period 1992-2020; the gray shaded ribbons represent the standard deviation (±0.5 and ±1 sd) of the monthly means.

APPENDIX A: SUPPLEMENTARY FIGURES

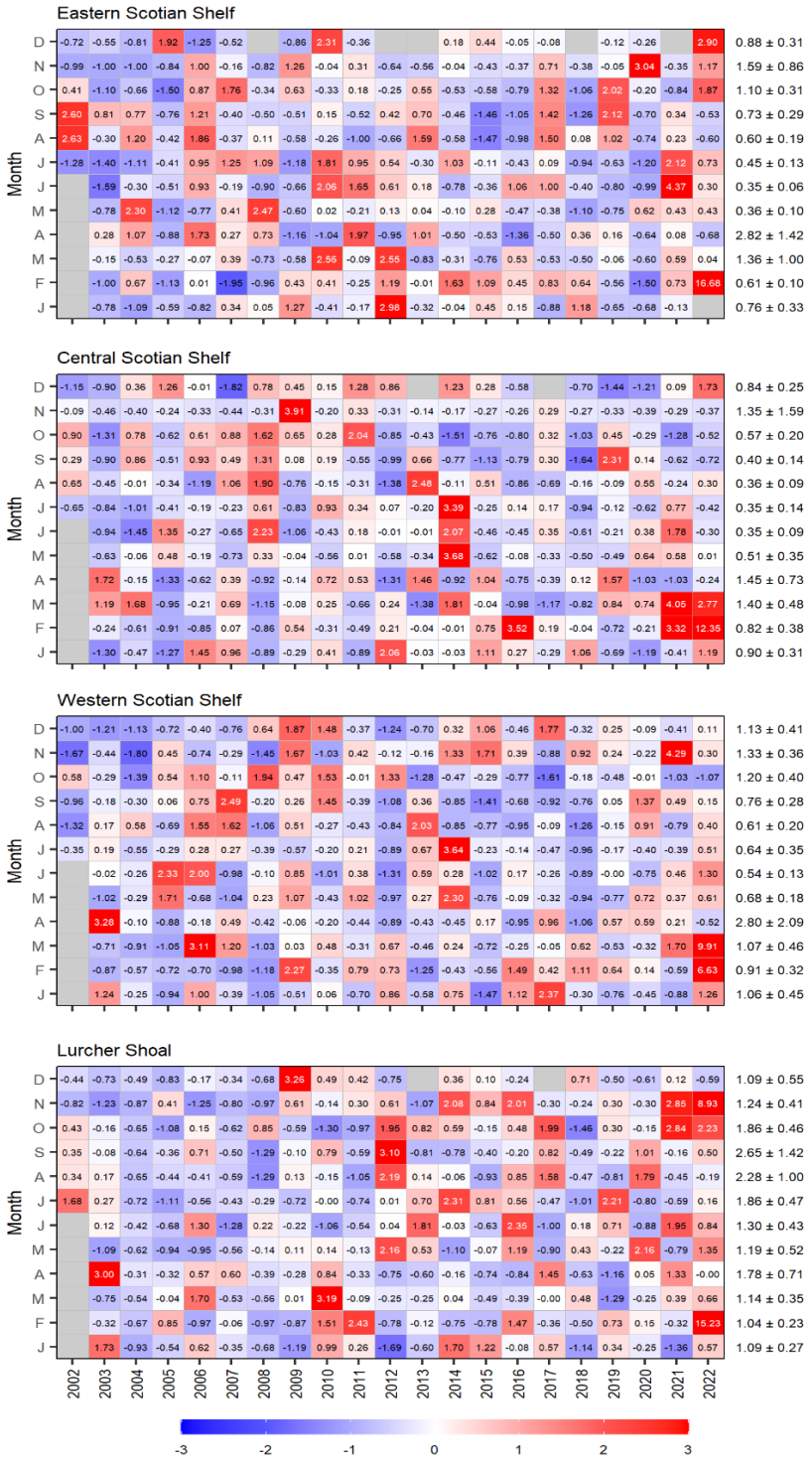

Figure A.1. Monthly anomaly scorecard for surface chlorophyll-a in sub-regions of the Scotian Shelf. Values in each cell are anomalies from the monthly means for the reference period 2003–2020, in standard deviation (sd) units (mean and sd listed at right in units of mg·m^{-3}). Red (blue) cells indicate higher- (lower-) than-normal chlorophyll-a concentrations. Gray cells indicate missing data.

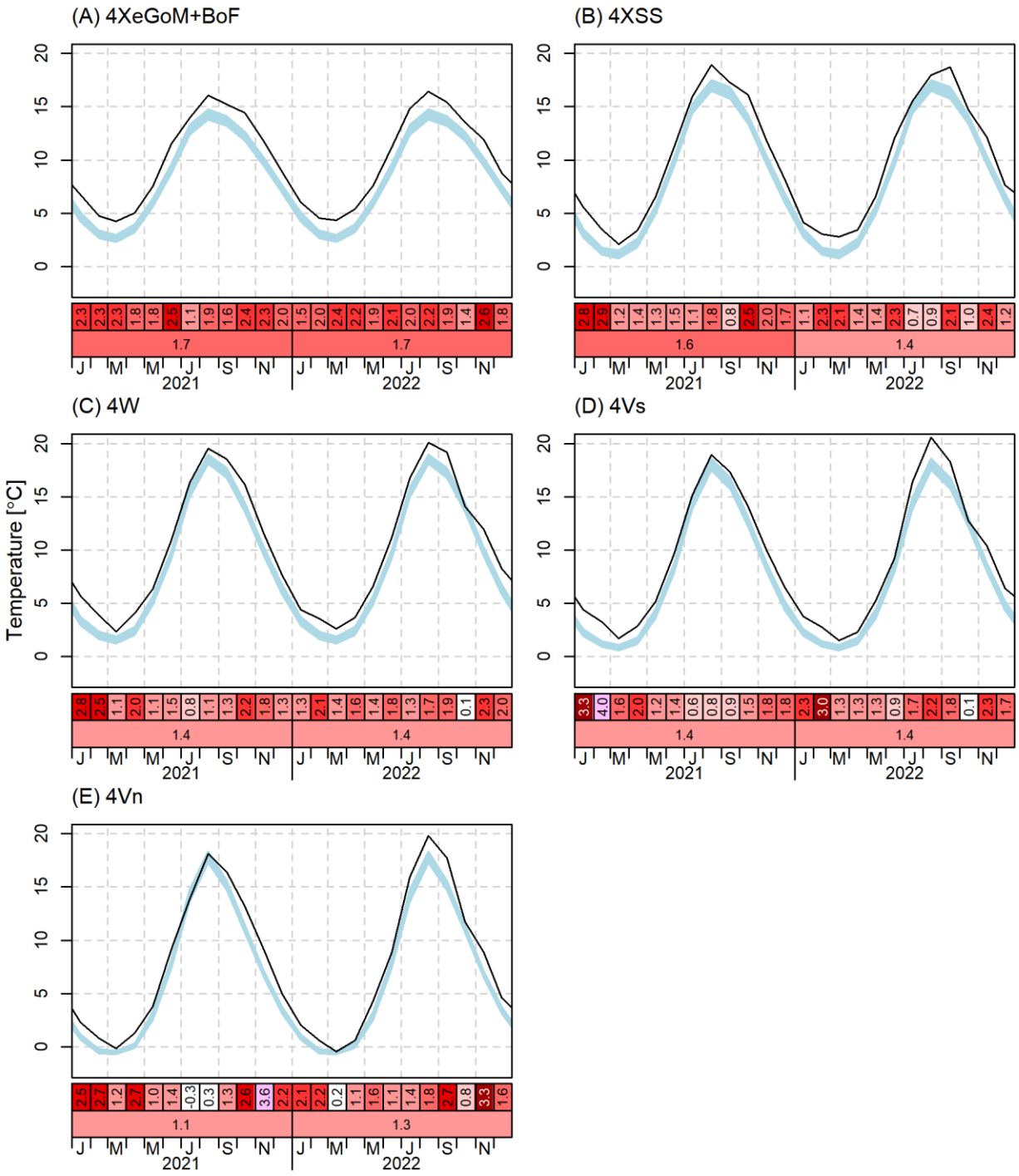

Figure A.2. AVHRR SST monthly and annual averages over the five regions of the Scotian Shelf and Gulf of Maine. The blue area represents the 1991-2020 climatological monthly mean ± 0.5 sd. The scorecards are colour-coded according to the normalized anomalies based on the 1991-2020 climatologies for each month (top row) or for the year (bottom row). Courtesy of Hebert et al. 2023.

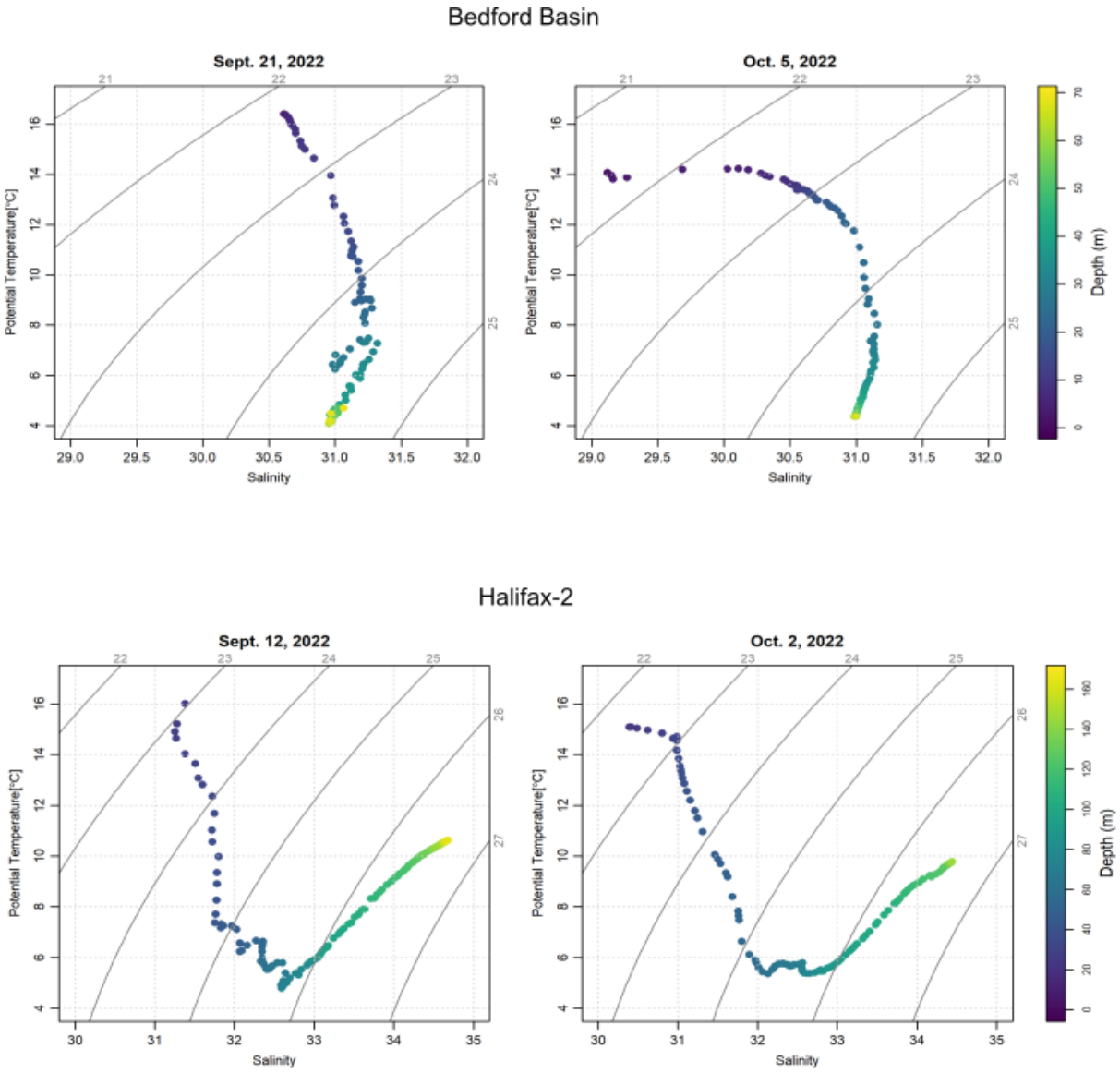

Figure A.3. Temperature-Salinity plots from CTD casts collected in Bedford Basin (upper panels) and at Halifax-2 (lower panels) prior and after the passage of hurricane Fiona on September 24, 2022.